

Anatomical Organization of the Extended Amygdala

by

Michael S. Bienkowski

B.S. in Neuroscience, University of Pittsburgh, 2007

Submitted to the Graduate Faculty of
the Kenneth P. Dietrich Graduate School of
Arts and Sciences in partial fulfillment
of the requirements for the degree of
Doctor of Philosophy

University of Pittsburgh

2012

UNIVERSITY OF PITTSBURGH
DIETRICH SCHOOL OF ARTS AND SCIENCES

This dissertation was presented

by

Michael S. Bienkowski

It was defended on

November 12th, 2012

and approved by

J. Patrick Card, PhD, Professor

Etienne Sibille, PhD, Associate Professor

Peter Strick, PhD, Professor

Alan Sved, PhD, Professor

Gary Aston-Jones, PhD, Professor

Dissertation Advisor: Linda Rinaman, PhD, Professor

Copyright © by Michael S. Bienkowski

2012

ANATOMICAL ORGANIZATION OF THE EXTENDED AMYGDALA

Michael S. Bienkowski, PhD

University of Pittsburgh, 2012

The concept of the extended amygdala proposed by de Olmos and Heimer suggests that the central (CEA) and medial nuclei of the amygdala (MEA) and the bed nucleus of stria terminalis (BST) are parts of a contiguous cellular column of neurons with similar anatomical connectivity and functional output (de Olmos and Heimer 1999). An alternative hypothesis proposed by Larry Swanson suggests that the CEA/MEA and BST are ventral differentiations of the striatum and pallidum, together forming a striatopallidal circuit that participates in a cortical reentrant loop (Swanson and Petrovich 1998, Swanson 2000).

In support of the extended amygdala concept, connections between the amygdala and BST are topographically-organized, suggesting the presence of discrete channels for information processing. Furthermore, results from several studies indicate that lesions of the amygdala or BST often produce experimental results that are quite similar (Zardetto-Smith, Beltz et al. 1994, Newman 1999, Tanimoto, Nakagawa et al. 2003, Nakagawa, Yamamoto et al. 2005, Deyama, Nakagawa et al. 2007). On the other hand, the concept of the extended amygdala has been challenged by results from behavioral studies that suggest a dissociation of CEA and BST functions in mediating behavioral processes associated with fear, anxiety (Walker and Davis 1997, Fendt, Endres et al. 2003, Walker, Toufexis et al. 2003, Sullivan, Apergis et al. 2004), social defeat (Jasnow, Davis et al. 2004), social interaction (Cecchi, Khoshbouei et al. 2002) and ethanol self-administration (Funk, O'Dell et al. 2006).

The studies in this dissertation were designed to test some of the assumptions proposed by the extended amygdala concept by more closely examining the similarities of extended amygdala circuits. In the first study, we tested the hypothesis proposed by de Olmos and Heimer that “all or most of the central extended amygdala would share similar inputs” (de Olmos and Heimer 1999). In the second study, we examined multisynaptic BST circuits that project to CEA and MEA to determine if BST circuits were maintained within topographically-organized channels. Our findings reveal several organizational principles for the anatomical relationship of the amygdala and BST subnuclei and suggest new theories for how extended amygdala circuits process information.

TABLE OF CONTENTS

1.0	GENERAL INTRODUCTION.....	1
1.1	HISTORICAL PERSPECTIVE OF BASAL FOREBRAIN ORGANIZATION.....	1
1.2	NEUROANATOMY OF STRIATOPALLIDAL CIRCUITS.....	3
1.3	EXPERIMENTAL STRATEGIES FOR CIRCUIT MAPPING	8
1.4	HOW ARE EXTENDED AMYGDALA CIRCUITS ORGANIZED?	12
2.0	COMMON AND DISTINCT NEURAL INPUTS TO THE MEDIAL CENTRAL NUCLEUS OF THE AMYGDALA AND ANTERIOR VENTROLATERAL BED NUCLEUS OF STRIA TERMINALIS IN RATS.....	15
2.1	INTRODUCTION	15
2.2	MATERIALS AND METHODS.....	18
2.4	RESULTS.....	23
2.5	DISCUSSION.....	51
3.0	DISTINCT MULTISYNAPTIC CIRCUITS WITHIN THE MEDIAL AND CENTRAL EXTENDED AMYGDALA OF THE RAT	60
3.1	INTRODUCTION	60
3.2	MATERIALS AND METHODS.....	66
3.3	RESULTS	76

3.4	DISCUSSION.....	94
4.0	GENERAL DISCUSSION	100
4.1	SUMMARY AND INTERPRETATION OF EXPERIMENTAL FINDINGS	100
4.2	EXTENDED AMYGDALA VS. STRIATOPALLIDAL MODEL OF THE ANATOMICAL RELATIONSHIP BETWEEN THE AMYGDALA AND BST	102
4.3	THE AMYGDALA AND BST CIRCUITS IN BEHAVIORAL RESPONSES	105
4.3.1	Fear and anxiety	105
4.3.2	Addiction-related behaviors	106
4.3.3	Social and reproductive behaviors.....	109
4.3.4	Impact of the dissertation studies on our understanding of extended amygdala-mediated behavior.....	111
4.4	CONCLUSIONS AND FUTURE DIRECTIONS.....	112
	BIBLIOGRAPHY.....	115

LIST OF TABLES

Table 1. Counts of single- and double-tracer-labeled neurons across brain regions after iontophoretic delivery of tracers to the CEAm and BSTvl.....	27
Table 2. Experimental animals divided into groups based on injection site and tracing approach. Case numbers are listed in the columns.....	75
Table 3. Correlations in retrograde labeling between individual BST subnuclei in CEAm-injected cases.	91
Table 4. Correlation of retrograde labeling between individual BST subnuclei in MEAad-injected cases	92
Table 5. Correlation of retrograde labeling between individual BST subnuclei in MEApd-injected cases.	93

LIST OF FIGURES

Figure 1. Iontophoresis of FG or CTB retrograde tracer into the CEAm.	25
Figure 2. Iontophoresis of FG or CTB retrograde tracer into the BSTvl.....	26
Figure 3. Distribution maps of retrogradely-labeled neurons within the caudal medulla.....	30
Figure 4. Rostrocaudal distribution of retrogradely-labeled NTS neurons.....	31
Figure 5. Distribution maps of retrogradely-labeled pontine neurons	33
Figure 6. Distribution maps of retrogradely-labeled neurons within the caudal midbrain	35
Figure 7. Distribution maps of retrogradely-labeled neurons within the rostral midbrain/caudal forebrain.....	36
Figure 8. Distribution maps of retrogradely-labeled forebrain neurons at the level of the tuberal hypothalamus.	39
Figure 9. Distribution maps of retrogradely-labeled forebrain neurons at the level of the preoptic hypothalamus.	42
Figure 10. Rostrocaudal distribution of retrogradely-labeled neurons within the PVT.....	43
Figure 11. Distribution maps of retrogradely-labeled neurons within the rostral forebrain..	45
Figure 12. Distribution maps of retrogradely-labeled neurons within the temporal cortex/posterior amygdala.....	46

Figure 13. Confocal z-stack images of selected brain regions containing large numbers of CEAm-projecting and BSTvl-projecting neurons and a relatively high incidence of double-labeling.....	49
Figure 14. Schematic representation of the relative incidence of single- and double-tracer-labeled neurons across brain regions projecting to the CEAm and BSTvl.....	50
Figure 15. Structural anatomical model for information processing via CEA and BST circuits	55
Figure 16. Direct connections between the amygdala and BST	64
Figure 17. Anterograde tracing of efferent projections from neurons within individual BST subnuclei reveals robust interconnectivity within the BST network.	65
Figure 18. Sections from Klüver-Barrera-stained BST reference atlas	73
Figure 19. Retrograde and anterograde labeling in the BST after monosynaptic FG/BDA iontophoresis or PRV/CTB co-injection into the CEAm.....	78
Figure 20. Retrograde and anterograde BST labeling after monosynaptic FG/BDA iontophoresis or PRV/CTB co-injection into the MEAad.....	79
Figure 21. Retrograde and anterograde BST labeling after monosynaptic FG/BDA iontophoresis or PRV/CTB co-injection into the MEApd.	80
Figure 22. Average number of retrogradely-labeled BST neurons following tracer delivery into the CEAm, MEAad, and MEApd.	86
Figure 23. Distribution of retrograde labeling within BST subnuclear groups..	87
Figure 24. Distribution of retrograde labeling within individual subnuclei of the algBST.	88
Figure 25. Distribution of retrograde labeling within individual subnuclei of the amgBST.....	89
Figure 26. Distribution of retrograde labeling within individual pBST subnuclei	90

PREFACE

Acknowledgments

The years that I have spent at the University of Pittsburgh as an undergraduate and graduate student have had a tremendous effect on the course of my life. From my first years making friends in the Honors College living community to my later years in the Center for Neuroscience, the University of Pittsburgh has helped me to become who I am today. I would like to thank everyone at the University of Pittsburgh, Department of Neuroscience, Center for Neuroscience, and Center for the Neural Basis of Cognition for creating such a wonderful environment for me to learn and grow.

The work in this dissertation would not have been possible if not for the support and encouragement I received from many individuals. Most of all, I would like to thank my mentor, Linda Rinaman, for believing in me as a young naïve undergraduate. Linda is an excellent scientist and teacher, and her guidance is most responsible for my development as a scientist. She continually encouraged me to set my goals higher and she gave me the freedom to find the answers to my questions. I have always tried to follow her example so that I may be as inspiring to others as she has been to me.

I would like to thank my committee chair, Pat Card, who in many ways was like a second mentor to me. Pat impressed upon me the importance of taking a historical perspective to the

study of neuroanatomy, so that I always understood how and why the field of neuroscience had arrived at the questions I sought to answer. Pat gave me the confidence to believe that I could be a great neuroscientist and I will always appreciate his belief in me.

I would also like to thank the members of my dissertation committee. I would like to thank Etienne Sibille, Alan Sved, and Peter Strick for their advice, support, and guidance throughout the course of my graduate studies. They are all excellent neuroscientists and teachers who I have looked to as role-models for my own career. I would also like to thank my outside examiner, Gary Aston-Jones, for his participation in my dissertation defense. I have always admired his research and it was an honor to have him as a member of my committee.

During my graduate research, I have been fortunate to be surrounded by great people in the Rinaman lab. I would like to thank Li Cai and Vicki Maldovan for their kindness and technical support throughout my career. I would like to thank Layla Banihashemi, my big sister in the lab, for her advice in teaching me how to be a graduate student. Thanks to Jamey Maniscalco, my little brother in the lab, for inspiring me to always work harder. Special thanks to my undergraduate mentee, Elizabeth Wendel, for all her hard work and efforts that were essential to the completion of this dissertation. Thanks also to Deanne Buffalari for her guidance and advice as I begin the next phase of my career.

I would like to thank the staff of the Department of Neuroscience, the Center for Neuroscience at the University of Pittsburgh, and the Center for the Neural Basis of Cognition. I would like to especially thank Joan Blaney, who always took special care of me and always reminded me to turn things in on time.

Finally, I would like to thank my many friends and family who have supported and encouraged me all these years. I would like to thank my best friends, Jesse DiLaura and Chris

Beres, for all of their advice and encouragement. I would like to dedicate this work to my family: my parents, Sigmund and Rose Bienkowski, my sisters, Christine, Cathy, and Diana, my brother-in-laws, Jim, Neil, and Dave, and all of my wonderful nieces and nephews. I would like to thank them all for everything they have done for me. Without their support, none of my achievements would have been possible.

List of Abbreviations

ACBsh	nucleus accumbens, shell division
aco	anterior commissure
AI	agranular insular cortex
amc	amygdalar capsule
AP	area postrema
AStr	amygdala-striatal transition area
Aud	auditory thalamus
BDA	biotinylated dextran amine
BLAp	basolateral amygdalar nucleus, posterior part
BMA	basomedial amygdalar nucleus
BST	bed nucleus of stria terminalis
algBST	anterolateral subnuclear group of the bed nucleus of stria terminalis
angBST	anteromedial subnuclear group of the bed nucleus of stria terminalis
pBST	posterior subnuclear group of the bed nucleus of stria terminalis

BSTal	bed nucleus of stria terminalis, anterolateral subnucleus
BSTam	bed nucleus of stria terminalis, anteromedial subnucleus
BSTdm	bed nucleus of stria terminalis, dorsomedial subnucleus
BSTfu	bed nucleus of stria terminalis, fusiform subnucleus
BSTif	bed nucleus of stria terminalis, interfascicular subnucleus
BSTju	bed nucleus of stria terminalis, juxtacapsular subnucleus
BSTmg	bed nucleus of stria terminalis, magnocellular subnucleus
BSTov	bed nucleus of stria terminalis, oval subnucleus
BSTpr	bed nucleus of stria terminalis, principal subnucleus
BSTrh	bed nucleus of stria terminalis, rhomboid subnucleus
BSTtr	bed nucleus of stria terminalis, transverse subnucleus
BSTv	bed nucleus of stria terminalis, ventral subnucleus
BSTvl	ventrolateral subnuclei group of the bed nucleus of stria terminalis
CA1	field CA1, Ammon's horn
cc	corpus callosum
CEA	central amygdalar nucleus
CEAm	central amygdalar nucleus, medial part
CEAl	central amygdalar nucleus, lateral part
CLI	central linear nucleus raphé
cpd	cerebral peduncle
CRH	corticotrophin-releasing hormone
CTB	cholera toxin subunit B
DI	dysgranular insular cortex

DMX	dorsal motor nucleus of the vagus
DR	dorsal nucleus raphé
dscp	superior cerebellar peduncle decussation
ec	external capsule
FG	Fluorogold
fx	fornix
ILA	infralimbic area
IMD	intermediodorsal nucleus thalamus
IPAC	interstitial nucleus of the posterior limb of the anterior commissure
LHA	lateral hypothalamic area
LS	lateral septal nucleus
mcp	middle cerebellar peduncle
MD	mediodorsal nucleus thalamus
MEA	medial nucleus of the amygdala
MEAad	medial nucleus of the amygdala, anterodorsal subnucleus
MEApd	medial nucleus of the amygdala, posterodorsal subnucleus
ml	medial lemniscus
mlf	medial longitudinal fascicle
mPFC	medial prefrontal cortex
MPO	medial preoptic area
MTN	midline thalamic nuclei
NLOT	nucleus of the lateral olfactory tract
NTS	nucleus of the solitary tract

och	optic chiasm
opt	optic tract
PA	posterior amygdalar nucleus
PAGvl	periaqueductal gray, ventrolateral division
PB	parabrachial nucleus
PBle	parabrachial nucleus, external lateral part
PBlv	parabrachial nucleus, ventral lateral part
PBm	parabrachial nucleus, medial part
PBw	parabrachial nucleus, waist part
PL	prelimbic area
PPN	pedunculopontine nucleus
PRV	pseudorabies virus
PSTN	parasubthalamic nucleus
PVN	paraventricular hypothalamic nucleus
PVT	paraventricular thalamic nucleus
py	pyramid
scp	superior cerebellar peduncle
SI	substantia innominata
sm	stria medullaris
SNc	substantia nigra, compact part
SNr	substantia nigra, reticular part
SPFpm	subparafascicular nucleus thalamus, parvicellular part, medial division
st	stria terminalis

STN	subthalamic nucleus
TR	postpiriform transition area
V4	fourth ventricle
VLM	ventrolateral medulla
VP	ventral pallidum
VPMpc	ventral posteromedial nucleus thalamus, parvicellular part
VTA	ventral tegmental area

1.0 GENERAL INTRODUCTION

1.1 HISTORICAL PERSPECTIVE OF BASAL FOREBRAIN ORGANIZATION

The organization of the basal forebrain has puzzled neuroscientists for decades. In the 1960's, neuroscientists generally believed that non-limbic cortical output was processed through the basal ganglia system, while limbic cortex densely innervated the hypothalamus (Heimer 2003). However, this dichotomy was challenged by the pioneering work of Lennart Heimer (Heimer and Van Hoesen 2006). Heimer's fiber degeneration studies of the olfactory cortex and olfactory tubercle, coupled with evidence of histochemical markers, revealed that the striatum of the basal ganglia extended ventrally to include the olfactory tubercle and part of the SI (substantia innominata), while other parts of the SI were identified as a ventral extension of the pallidum (de Olmos and Heimer 1999). This new ventral striatopallidal circuit was later found to project to the mediodorsal thalamus (MD), revealing a subcortical reentrant loop specifically for limbic cortex.

In creating the concept of the ventral striatopallidal circuit, Heimer and his colleagues found evidence to exclude the amygdala and bed nucleus of stria terminalis (BST) from the other basal forebrain structures. Instead, the amygdala, BST, and rostrocaudally interposed regions of the SI were believed to be constituent parts of a single anatomical structure termed the 'extended amygdala' (Alheid and Heimer 1988). Evidence of this relationship between the amygdala and

BST was first noted by J. B. Johnston in 1923 (Johnston 1923), however the association went unnoticed until resurrected by de Olmos and Heimer (de Olmos and Ingram 1972). De Olmos' development of the cupric silver method demonstrated a continuous cellular column branching the amygdala and BST, which later tracing studies would distinguish as part of two distinct extended amygdala ring structures. The central extended amygdala consists of the central nucleus of the amygdala (CEA), parts of the SI, anterolateral BST, and lateral supracapsular BST. The medial extended amygdala consists of the medial amygdala (MEA), posterior and anteromedial BST, and medial supracapsular BST. The concept of the extended amygdala has proved useful as a model for studies of drug addiction, fear and anxiety, sexual behavior, and appetitive behavior (McGinty 1999), however, the idea of the extended amygdala as a single anatomical structure separate from the striatopallidal system has been contested (Swanson 2003).

The development of more advanced tracing and histochemical methods has provided evidence that the CEA/MEA and BST may share more similarities with the striatum and pallidum than Heimer and colleagues originally thought. The establishment of GABA as a fast inhibitory neurotransmitter and its prominent role in striatopallidal circuitry helped to fuel the debate. Localization of GAD-65 mRNA with *in situ* hybridization revealed that the GABA-ergic medium spiny neuronal populations of the striatum and pallidum were continuous with the CEA/MEA and BST, respectively. Embryological studies further supported that the adult GABA-ergic cell populations of the striatum and CEA are derivatives of the lateral ganglionic eminence, while the pallidum and lateral part of the BST are derivatives of the medial ganglionic eminence, although the origin of the MEA and other parts of the BST is less clear (Medina, Legaz et al. 2004, García-López, Abellán et al. 2008, Soma, Aizawa et al. 2009). Focusing more on the similarities than the differences, Larry Swanson proposed that the CEA/MEA and BST

are ventral differentiations of the striatum and pallidum, whose projections participate in cortical reentrant loops (Swanson and Petrovich 1998, Swanson 2000). Supported by detailed anatomical studies of retrograde and anterograde tracing, Swanson has outlined a putative striatopallidal loop with distinct parts of the cortex, amygdala, BST, and thalamus assuming the roles of the traditional striatopallidal circuitry (called the caudorostral (CR) striatopallidal circuit).

1.2 NEUROANATOMY OF STRIATOPALLIDAL CIRCUITS

Larry Swanson's efforts to characterize the striatopallidal systems are not merely confined to the CR striatopallidal circuit, but to a general theory on the organization of the entire cerebral hemisphere's regulation of motivated behavior (Swanson 2000). Indeed, in evaluating whether the amygdala and BST participate in a striatopallidal circuit, it is important to recognize the similarities and differences that characterize the striatopallidal systems. According to Swanson, in the cerebral hemisphere whatever is not cortex is considered either striatum or pallidum based on evidence of developmental origin, anatomical connectivity, and the preference of glutamate or GABA as the primary fast neurotransmitter. This organization is appealing because it unifies all of the cerebral nuclei and cortical regions into a single structural outline that can be differentiated to suit the function of that circuit. Swanson describes 4 striatopallidal systems: dorsal, ventral, caudorostral, and medial. The dorsal and ventral striatopallidal systems are now widely accepted, while the caudorostral and medial striatopallidal systems are still largely conjectural. The dorsal striatopallidal system is the classic basal ganglia system involving executive and somatomotor cortex and consists of the dorsal striatum (caudate and putamen) and the dorsal pallidum (globus pallidus). The ventral striatopallidal system processes

information from the olfactory cortex and groups the nucleus accumbens, striatal fundus, and olfactory tubercle into a ventral extension of striatum which projects to the ventral pallidum (formerly part of the SI). The caudorostral striatopallidal system considers the CEA and MEA as a caudal extension of striatum and the BST as a rostral extension of the pallidum. The medial striatopallidal system is specialized for hippocampal cortex and defines the lateral septum as striatal and the medial septum/nucleus of the diagonal band as the associated pallidum.

All of these systems share the characteristic of a triple descending projection to the behavioral control columns that generate behavior. Swanson has organized the behavioral control columns into two groups: a rostral group, containing most of the hypothalamus concerned with social behaviors, and a caudal group that regulates exploratory and foraging behavior, including the mammillary bodies, substantia nigra (SN), and ventral tegmental area (VTA). The behavioral control columns are hierarchically-organized and consist of three characteristic regions common to the production of voluntary behavior. At the highest order of the motor system outside the cerebral hemisphere, behavioral controllers are typically located in the hypothalamus and define a baseline level of endogenous activity for the rest of the column. Behavioral controllers project to the motor pattern initiators and generators in the brainstem that determine the series of movements necessary to produce the behavior. Lastly, the motor pattern generators project to the motoneurons in the brainstem and spinal cord that signal the necessary muscle fibers to contract. The cortex, striatum, and pallidum all influence behavior at one or more levels of the column. Cortical projections provide direct excitation to all levels of the behavioral control column via glutamate, while the striatum directly inhibits the hypothalamic behavioral controllers with GABA. However, the striatum also inhibits the GABA-ergic pallidal projections to the motor system, creating a third disinhibitory pathway which removes inhibition

on the motor pattern generators and sends collaterals to the thalamus to complete the subcortical loop. This organization not only allows the striatopallidal network to initiate behaviors, but also gives the network fine control over motor system activity at all levels of the behavioral control column.

In Larry Swanson's organization of the cerebral hemisphere, almost all areas of cortex project to an associated striatal nucleus. The isocortical pyramidal projection neurons are located in layers 3 and 5, but only layer 5 pyramidal neurons send collateral projections to the motor system (corticospinal tract). The cortical inputs to striatum have been shown to be topographically organized in the dorsal, ventral, and medial striatopallidal systems (Groenewegen, Wright et al. 1997), although a cortical region may project to multiple striatal sites. Afferent information to the isocortex is mainly mediated by associated thalamic nuclei that are reciprocally connected to neurons in layer 6 (Herkenham 1980).

The striatum is the primary input structure of a striatopallidal network, typically receiving afferents from 3 main sources: cortex, thalamus, and brainstem. The striatum is topographically organized into functional groups based upon the cortical input to that region. For example, the dorsolateral putamen is associated with motor function, because it receives primary motor and premotor cortex pyramidal fibers. The dorsolateral striatum neurons convey this functional characteristic to the pallidum and SN, where striatal projections are organized in a similar topographical fashion, creating parallel output channels through the striatopallidal circuit. Projections from areas of the ventral striatum that receive input from limbic cortex show similar topography (Groenewegen, Berendse et al. 1993, Maurice, Deniau et al. 1997). These multisynaptic parallel output channels are a defining characteristic of the striatopallidal systems (Alexander, DeLong et al. 1986, Alexander and Crutcher 1990, Hoover and Strick 1993).

However, it should be noted that integration across output channels occurs within each region, such that information is not processed entirely independently (Haber 2003). Overall, the connectivity of the CEA and MEA is highly comparable to other striatal regions, but with a few additional pathways (Zahm, Jensen et al. 1999). The CEA and MEA receive dense input from the medial prefrontal cortex (mPFC), insular cortex (IN), piriform cortex, midline thalamic nuclei, and regions of the brainstem including the parabrachial nucleus (PBN) and nucleus of the solitary tract (NTS) (McDonald, Shammah-Lagnado et al. 1999, Tkacs and Li 1999). However, the CEA and MEA also have connections with areas of the hypothalamus (Petrovich and Swanson 1997). These additional connections with the hypothalamus may be necessary for the suggested role of the caudorostral striatopallidal system in regulating autonomic and endocrine function.

The pallidum is the main output structure of the striatopallidal network. Compared to the striatum, the pallidal projection system is more complex, but the output can generally be divided for two purposes: projections to the behavioral control columns that influence behavior and projections to the thalamic nuclei that feedback onto the cortex. In the dorsal striatopallidal circuit, the globus pallidus can be divided into an external and internal segment (GPe and GPi, the latter referred to as the enteropeduncular nucleus in rats). The striatum innervates both the GPe and GPi, but each nucleus has a very specific output. The GPe is strongly and reciprocally connected to the subthalamic nucleus (STN), which acts as a relay to the GPi. In the rat, but not in primates, evidence suggests that the GPe directly projects to the GPi (Kincaid, Penney Jr et al. 1991), but otherwise the primary role of the GPe involves its relationship with the STN. The GPi sends output to two main regions: thalamic nuclei, including the ventral anterior/ventral lateral thalamus (VA/VL), centromedian thalamus (CM), and lateral habenula, and areas

associated with the behavioral control column (pedunculopontine tegmental nucleus, superior colliculus, periaqueductal gray, parabrachial nucleus, and reticular nucleus) (Takada, Tokuno et al. 1994). The ventral pallidum has similar yet topographically distinct projections to the STN, SN and MD thalamus and has been shown to mediate a disinhibitory circuit similar to the dorsal striatopallidal circuit (Maurice, Deniau et al. 1997).

The BST is a complex group of interconnected nuclei, and characterizing each subnucleus and determining any multisynaptic pathway through the region has proved difficult. In relation to the pallidum, the BST targets many of the same regions but, like the amygdala subnuclei, the BST also projects to the hypothalamus (Dong, Petrovich et al. 2000, Dong, Petrovich et al. 2001, Dong and Swanson 2003, Dong and Swanson 2004, Dong and Swanson 2004, Dong and Swanson 2006, Dong and Swanson 2006). Swanson also includes parts of the SI as part of the caudorostral pallidum and it may be possible that the SI and BST are variations on the GPe and GPi projection systems. Both the SI and BST project to parts of the MD thalamus and midline thalamic nuclei which include the paraventricular nucleus (PVT), CM thalamus, intermediodorsal nucleus (IMD), rhomboid nucleus (Rh), and reunions nucleus (Re).

The thalamus transmits sensory information to the cortex, which striatopallidal circuits can directly modulate at the thalamic nuclei via pallidal efferents. Generally, different thalamic nuclei mediate different output channels of the striatopallidal circuits. Interestingly, when comparing the dorsal, ventral, and caudorostral striatopallidal circuits, the associated thalamic nuclei are topographically organized from lateral to medial. Furthest lateral, the VA/VL thalamic nuclei receive input from the GPi and relay this information back to primary motor and premotor cortex. Just medial to the VA/VL, the MD thalamus receives projections from the ventral pallidum and sends efferents to the mPFC. The BST's projections to the midline

thalamic nuclei present a variety of possible pathways for the existence of a closed striatopallidal loop. However, it is not yet clear which of these nuclei might be involved in any particular output channel. Anatomical evidence has demonstrated that the caudal part of the CM has a distinct projection system from the rostral CM (Van der Werf, Witter et al. 2002). The caudal CM projects densely to the AI, but not the mPFC, suggesting the caudal CM may be involved in an AI functional loop. Similarly, the Rh and Re provide strong projections to the mPFC and not the IN, suggesting that the Rh and Re may play a role in an output channel specific to the mPFC.

1.3 EXPERIMENTAL STRATEGIES FOR CIRCUIT MAPPING

Since the establishment of Ramón y Cajal's functional polarity hypothesis, neuroscientists have been determined to define neural circuits and the direction of information flow within the brain. While Cajal's studies were focused on morphological characteristics in Golgi-stained tissue sections, the development of silver degeneration staining techniques in the 1940-1960's by Nauta, de Olmos, Heimer, and others led to the rapid characterization of neural projection systems throughout the brain (Nauta 1993). These methods reveal anterograde projection systems by lesioning an area of the brain and impregnating tissue sections with silver to label degenerating fibers. However, in the early 1970's a fundamentally different strategy emerged that took advantage of the neural uptake of radioactively-labeled amino acids (Lasek, Joseph et al. 1968), and later the axonal transport of horseradish peroxidase and other plant lectins which act as tracer molecules (Gerfen and Sawchenko 1984). Today, neuroscientists have a plethora of 'classical' tracers such as Fluorogold, cholera toxin subunit B, PHA-L, and biotinylated dextran amine with which to define a brain region's afferents or efferents via

retrograde or anterograde axonal transport. Combinations of classical tracers can be used to identify neurons that send axon collaterals to two brain regions, or to visualize reciprocal connections (Wouterlood 2006). Although classical tracers are excellent tools for revealing monosynaptic projections systems, their ability to define multisynaptic circuits is limited to the overlap of retrogradely-labeled neurons and anterogradely-labeled fibers from two different injections sites (Thompson and Swanson 2010), and additional electron microscopic evidence must be gathered to confirm synaptic contact.

Over the past few decades, neuroscientists have found ways to exploit neurotropic viruses (i.e., herpes simplex virus, rabies virus, pseudorabies virus (PRV)) for the purposes of multisynaptic tract-tracing. Extensive characterization of the viral genes that regulate viral invasiveness, virulence, and transsynaptic passage allowed for the necessary genetic manipulation of specialized strains of viruses which express unique fluorescent reporter genes for localization with brain tissue (Enquist and Card 2003). PRV has become an extremely popular tool because of its effectiveness in a wide range of hosts (Card 1998). However, not all PRV strains are ideal for specific types of viral tracing studies, and selection of a PRV strain is an important factor to consider before conducting experiments. For example, the wild-type strain of PRV, PRV-Becker, can spread in both the anterograde and retrograde direction. Furthermore, a strain of virus that has reduced virulence yet maintains its invasive properties is needed. The Barth strain of PRV (PRV-Bartha) has been shown to transport exclusively in the retrograde direction and displays a marked reduction in viral cytopathic effects on neurons, making PRV-Bartha an ideal tool for identifying multisynaptic pathways in the brain (Card, Levitt et al. 1998).

Understanding the mechanisms by which PRV infects neurons has been important in establishing PRV as a transsynaptic tracer (Flint, Enquist et al. 2008, Card and Enquist 2012). The structure of PRV virions consists of viral DNA encased in a protein capsid, which itself is surrounded by a tegument layer of proteins and a bi-lipid membrane envelope. The outer surface of the lipid envelope contains virally-encoded proteins that are responsible for attachment and receptor-mediated invasion into a target cell. Glycoprotein D is the viral envelope protein most responsible for virion cell attachment through binding to receptors on the target cell such as nectin 1, a cell adhesion molecule expressed in all classes of neurons. While both nectin 1 and glycoprotein D are critical for viral invasion, an envelope protein complex of glycoprotein B, H, and L are required for transsynaptic passage of virions (Favoreel, Van Minnebruggen et al. 2002, Card and Enquist 2012). Virions that do not express this protein complex can infect and reproduce within a host cell, but cannot spread to other cells.

Electron microscopic evidence has revealed the course of cytopathic events inside the cell during PRV infection (Card, Rinaman et al. 1993, Card and Enquist 2012). The appearance of viral capsids inside cell nuclei occurs with characteristic changes in cell morphology including nucleolus dispersion, clumping of chromatin, invaginations of the nuclear envelope. Viral replication and capsid production and assembly are concentrated around intranuclear tubule masses. Mature capsids leave the cell nucleus by budding, in the process acquiring a single membrane envelope. These nucleocapsids traverse the endoplasmic reticulum until de-enveloping upon exit near the trans cisternae of Golgi complexes. Capsids are wrapped with a bilaminar membrane envelope by the Golgi complex to complete virion construction. The recently enveloped virions then transport or diffuse into dendrites where the outer layer of the envelope fuses to the cell membrane, releasing the single-layered virion into the synaptic cleft.

The remaining virion envelope membrane fuses to the presynaptic afferent terminal, thus releasing the naked capsid into the presynaptic neuron to begin the process of viral infection. An important consideration at this timepoint is the possibility that astrocytes with processes near the synapse can become infected, and possibly constitute an additional non-neuronal route for PRV passage through the nervous system. However, electron microscopic evidence reveals that while many of the characteristics of viral replication occur within infected astrocytes, cytoplasmic capsids never acquire the Golgi-derived bilaminar membrane that allows for virions to exit the cell (Card, Rinaman et al. 1993). Thus, rather than constituting a route for cell-to-cell passage, astrocytes buffer the paracrine spread of virions from the synaptic cleft and limit the passage of virions to neuronal synapses.

The use of neurotropic viruses as transsynaptic tracers is not without limitations, and proper controls are necessary for the interpretation of viral labeling. A number of variables must be considered when designing a viral tracing study, including the concentration of the injected virus, the cytoarchitecture of the region being injected, and the post-inoculation time periods (Aston-Jones and Card 2000, Card and Enquist 2012). The minimum viral titer used in a study should be able to produce 100% infectivity in all injected animals. This concentration differs among species, but is approximately 10^5 pfu/ml in rats. Previous studies have also determined that alterations in viral concentration or injection volume influences the number of infected neurons (Card, Enquist et al. 1999). Additionally, the cytoarchitecture of a brain region influences the diffusion of virions at the injection site and the ability to infect a polysynaptic circuit. PRV virions have a high affinity for heparin and chondroitin proteoglycans of the extracellular matrix located in synaptic clefts, which causes most virions to infect neurons via axon terminals. In brain regions with dense neuropil, the high number of synapses restricts the

spread of virions and increases the routes for virus uptake in the region. While the restricted diffusion of virions allows for discrete injection sites, virions are retrogradely transported away from injection sites, which can make identification of the injection site difficult. Finally, temporal analysis is critical to determining the spread of virus from an injection site. Parametric studies should be performed to determine the maximal and intermediate survival times at which the virus infection has progressed. The use of multiple post-inoculation survival times allows for a clear understanding of viral progression through a multisynaptic circuit.

The combination of monosynaptic tracers and viral transsynaptic tracers can help in viral tracing analysis by defining 1st-order neurons and identifying the viral injection site. Previous studies have shown that cholera toxin subunit B can be successfully combined with PRV for circuit analysis although Fluorogold, wheat germ agglutinin-conjugated to horseradish peroxidase coupled to colloidal gold, and rhodamine labeled latex beads have been shown to interfere with viral uptake and/or replication (Chen, Yang et al. 1999, Aston-Jones and Card 2000).

1.4 HOW ARE EXTENDED AMYGDALA CIRCUITS ORGANIZED?

The concept of the extended amygdala suggests that the central and medial nuclei of the amygdala and the BST are parts of a contiguous cellular column of neurons with similar anatomical connectivity and functional output. In support of the extended amygdala concept, amygdala and BST regions appear to receive input and send projections to similar brain regions and results from several studies indicate that lesions of the amygdala often produce experimental results that are quite similar to results obtained after lesions in associated BST regions (Zardetto-

Smith, Beltz et al. 1994, Newman 1999, Tanimoto, Nakagawa et al. 2003, Nakagawa, Yamamoto et al. 2005, Deyama, Nakagawa et al. 2007). On the other hand, the concept of the central extended amygdala has been challenged by results from behavioral studies that suggest a dissociation of CEA and BST functions (Walker and Davis 1997, Fendt, Endres et al. 2003, Walker, Toufexis et al. 2003, Jasnow, Davis et al. 2004, Funk, O'Dell et al. 2006, Walker, Miles et al. 2009). For example, the CEA and lateral BST have been reported to play unique roles in mediating behavioral processes associated with fear, anxiety (Walker and Davis 1997, Fendt, Endres et al. 2003, Walker, Toufexis et al. 2003, Sullivan, Apergis et al. 2004), social defeat (Jasnow, Davis et al. 2004), social interaction (Cecchi, Khoshbouei et al. 2002) and ethanol self-administration (Funk, O'Dell et al. 2006). These differences in amygdala vs. BST function are likely to be mediated by distinct anatomical circuits.

The studies in this dissertation were designed to compare the anatomical relationship of the amygdala and BST. In the first study (section 2.0), we tested the hypothesis proposed by de Olmos and Heimer that “all or most of the central extended amygdala would share similar inputs” (de Olmos and Heimer 1999). We performed dual retrograde tracing of inputs to the medial CEA (CEAm) and ventrolateral BST (BSTvl) and, in one case, mapped the rostrocaudal distribution of CEA and BSTvl afferents throughout the brain. We further examined brain regions which contained dense overlap of retrograde labeling for the extent of collateralized input to the CEA and BSTvl. The second study (section 3.0) uses a combination of monosynaptic and transsynaptic viral tracing approaches to examine the anatomical circuits between the amygdala and BST subnuclei, particularly multisynaptic BST circuits that project to the CEA, anterodorsal MEA (MEAad), and posterodorsal MEA (MEApd). We hypothesized that multisynaptic amygdala-projecting BST circuits would be limited to BST subnuclei within

the topographic boundaries suggested by the direct amygdala/BST connectivity, despite evidence that BST subnuclei are highly interconnected. These studies reveal several organizational principles which define architecture of intrinsic and extrinsic extended amygdala circuits.

2.0 COMMON AND DISTINCT NEURAL INPUTS TO THE MEDIAL CENTRAL NUCLEUS OF THE AMYGDALA AND ANTERIOR VENTROLATERAL BED NUCLEUS OF STRIA TERMINALIS IN RATS

2.1 INTRODUCTION

The central nucleus of the amygdala (CEA) and lateral bed nucleus of stria terminalis (BST) are highly interconnected limbic forebrain regions that form the crux of the integrative functional unit often referred to as the central extended amygdala (de Olmos and Heimer 1999). The original concept of the extended amygdala as proposed by de Olmos and Heimer was based upon observations that extended amygdala structures share similar cytoarchitectural and histochemical characteristics (Alheid and Heimer 1988, de Olmos and Heimer 1999). According to their proposal, the central division of the extended amygdala includes the CEA and the lateral BST, in addition to interposed regions such as the substantia innominata (SI) that bridge the anatomical gap between CEA and lateral BST. De Olmos and Heimer further speculated that “all or most of the central extended amygdala would share similar inputs” (de Olmos and Heimer 1999). Indeed, in addition to robustly innervating each other, the CEA and lateral BST receive inputs from broadly similar brain regions implicated in visceral and somatosensory functions, and send axonal projections to broadly similar regions that maintain homeostasis by modifying behavioral, autonomic, and endocrine outflow (Dong, Petrovich et al. 2001, Dong and Swanson

2003, Dong and Swanson 2004). Results from many studies indicate that CEA lesions often produce experimental results that are quite similar to results obtained after lateral BST lesions (Zaretto-Smith, Beltz et al. 1994, Tanimoto, Nakagawa et al. 2003, Nakagawa, Yamamoto et al. 2005, Deyama, Nakagawa et al. 2007). On the other hand, the concept of the central extended amygdala has been challenged by results from behavioral studies that suggest a dissociation of CEA and BST functions (Walker and Davis 1997, Fendt, Endres et al. 2003, Walker, Toufexis et al. 2003, Jasnow, Davis et al. 2004, Funk, O'Dell et al. 2006, Walker, Miles et al. 2009). For example, the CEA and lateral BST have been reported to play unique roles in mediating behavioral processes associated with fear, anxiety (Walker and Davis 1997, Fendt, Endres et al. 2003, Walker, Toufexis et al. 2003), social defeat (Jasnow, Davis et al. 2004), social interaction (Cecchi, Khoshbouei et al. 2002) and ethanol self-administration (Funk, O'Dell et al. 2006).

The apparent similarities and differences in CEA- and lateral BST-mediated functions may be due, at least in part, to similarities and differences in the connectivity of subregions within each structure. Evidence from retrograde tracing studies indicates that major subdivisions of the lateral BST are interconnected with specific CEA subdivisions that share similar inputs from defined subsets of diencephalic, pontine, and medullary regions (Sun, Roberts et al. 1991). For example, dopaminergic inputs are most heavily concentrated in the lateral CEA (CEAl) and the dorsolateral BST (BSTdl), while noradrenergic (NA) inputs primarily target the medial CEA (CEAm) and ventrolateral BST (BSTvl; distribution of NA fibers shown in Fig. 1d and 2d) (Freedman and Cassell 1994). Thus, even within the “central extended amygdala”, afferent inputs to the CEAl and BSTdl differ to some extent from inputs to the CEA_m and BST_{vl}.

Central afferents to the BST_{vl} in rats have recently been described (Shin, Geerling et al. 2008). Based on its inputs, the BST_{vl} appears to integrate signals that impact emotional and

motivational states such as pain, pleasure, hunger, thirst, and sickness (Gauriau and Bernard 2002, Ciccocioppo, Fedeli et al. 2003, Geerling and Loewy 2006, Gaykema, Chen et al. 2007, Harris and Aston-Jones 2007). Generally, in addition to inputs from the CEAm and other amygdala subregions, the BSTvl receives inputs from the hypothalamus, caudal medulla [including particularly robust input from NA neurons within the caudal nucleus of the solitary tract (NTS) and ventrolateral medulla (VLM)], thalamus, insular cortex, and infralimbic cortex. While most of these regions have also been described as innervating the CEA, the extent to which projections to the BSTvl and CEA arise from the same subregions and, potentially, from the same neurons has been largely unexamined. To date, only the VLM, medial prefrontal cortex, and insular cortex have been reported to contain individual neurons with collateralized axonal inputs to both the CEA and BST (Ciriello, Schultz et al. 1994, Reynolds and Zahm 2005). However, neither study specifically examined inputs to the CEAm and BSTvl, and there has been little experimental effort to discriminate between inputs that target the CEAm vs. the CEAl.

The present study used iontophoretic delivery of two different retrograde neural tracers into the CEAm and BSTvl in order to examine the central distribution and potential overlap of neurons that provide axonal inputs to these specific subregions of the central extended amygdala. We hypothesized that brain regions with relatively large numbers of collateralized inputs to both the CEAm and BSTvl may provide an anatomical substrate for coordinating CEA and lateral BST outflow, while areas with few collateralized inputs may contribute to the unique functions of these two regions.

2.2 MATERIALS AND METHODS

Animals

Adult male Sprague Dawley rats (250-300g BW; Harlan Laboratories, Indianapolis, IN, USA) were individually housed in stainless steel hanging cages in a controlled environment (20-22°C, 12:12 hr light:dark cycle; lights off at 1900 hr) with ad libitum access to water and pelleted chow (Purina 5001). Experimental protocols were approved by the University of Pittsburgh Institutional Animal Care and Use Committee, and were carried out in accordance with the National Institutes of Health Guide for the Care and Use of Laboratory Animals, with efforts to minimize both the number of animals used and their potential discomfort.

Iontophoretic Tracer Delivery

Rats were anesthetized by halothane or isoflurane inhalation (Halocarbon Laboratories, River Edge, NJ; 1-3% in oxygen) and oriented into a Kopf stereotaxic device in the flat skull position. Pulled glass pipette tips (approximately 20 μm outer tip diameter) were attached to the arm of the stereotax. A solution of 1% cholera toxin subunit B (CTB; List Biological Labs, Campbell, CA) in 0.1M phosphate buffer (pH=6.0) or a 1-2% solution of Fluorogold (FG; Fluorochrome, Denver, CO) in 0.1M cacodylic acid was backfilled through the pipette tip using negative pressure, then a wire connected to a current source (Stoelting) was inserted into the tracer solution. During the descent of the glass pipette into the brain, a -0.5 μA retaining current was used to minimize molecular diffusion of tracer from the pipette tip. CTB was unilaterally iontophoresed into the BSTvl (from bregma: -0.3 posterior, +2.8 lateral, -7.0 ventral; 10° angle) or CEAm (from bregma: -2.1 posterior, +3.9 lateral, -7.8 ventral) using a 7s on/off pulsed current of +5 μA for 15 min. Afterward, FG was iontophoresed in the corresponding ipsilateral CEAm or BSTvl using the same pulsed current for 5 min. These iontophoretic parameters were based

on the results of pilot studies to produce comparably sized tracer delivery sites. After the second tracer was delivered, the pipette was withdrawn and the skin closed with stainless steel clips. Rats were injected subcutaneously with 0.5 ml of a mild analgesic (Ketofen) and were returned to their cages after regaining consciousness and full mobility.

One to two weeks after tracer iontophoresis, rats were anesthetized with an overdose of sodium pentobarbital (Nembutal, 100 mg/kg BW, ip) and then transcardially perfused with 0.15M NaCl followed by 500 ml of 4% paraformaldehyde. Brains were postfixed *in situ* overnight at 4°C then removed from the skull and cryoprotected in 20% sucrose solution before sectioning. Brains were sectioned coronally (35 µm) using a freezing microtome. Sections were collected sequentially into 6 adjacent sets and stored in cryopreservant (Watson, Wiegand et al. 1986) at -20°C for later immunocytochemical processing.

Immunocytochemistry

Two sets of tissue sections from each rat (each set containing sections spaced 210 µm apart) were used for single immunoperoxidase localization of FG and CTB to reveal tracer delivery sites and the distribution of afferent inputs to those sites. For this purpose, tissue sections were incubated overnight in buffer (0.1M sodium phosphate, pH 7.4) containing 0.3% Triton-X100, 1% normal donkey serum, and either rabbit anti-FG (1:30,000; Millipore, Temecular, CA) or goat anti-CTB (1:50,000, List Biological Labs, Campbell, CA) antisera. Biotinylated secondary antisera (donkey anti-rabbit or donkey anti-goat IgG; Jackson Immunochemicals, West Grove, PA) were used at a dilution of 1:500. FG or CTB single immunoperoxidase labeling was revealed using Vectastatin ABC Elite reagents (Vector Laboratories, Burlingame, CA) followed by a diaminobenzidine (DAB)-hydrogen peroxidase reaction to produce a brown immunoprecipitate in the cytoplasm of labeled neurons. In selected

cases, additional series of tissue sections were processed for dual immunoperoxidase labeling of either FG or CTB together with the neuronal marker NeuN in order to better define tissue cytoarchitecture. In these cases, FG or CTB immunoperoxidase labeling was revealed by using nickel sulfate in the DAB solution to produce a black immunoprecipitate, followed by a second brown DAB immunoperoxidase reaction after incubating tissue sections in mouse anti-NeuN (1:5000, Millipore, Temecula, CA) and biotinylated donkey anti-mouse IgG (1:500; Jackson Immunochemicals, West Grove, PA), as described above.

A third set of tissue sections from selected cases with well-placed tracer delivery sites into both the CEAm and the BSTvl was processed for dual immunofluorescent localization of both CTB and FG to identify double-labeled neurons. Tissue sections were incubated for 48-72 hr at 4°C in a cocktail of primary antisera at 10 times the concentration used for immunoperoxidase (i.e., FG, 1:3000; CTB, 1:5000). Sections were then rinsed in buffer and incubated overnight (at 4°C) in a cocktail of fluorescently-tagged secondary antisera [Cy3-conjugated donkey anti-rabbit IgG (1:500) and Cy2-conjugated donkey anti-goat IgG (1:300); both from Jackson Immunochemicals]. Fluorescent labeling of dopamine-beta hydroxylase (DBH) shown in Figs. 1c and 2c was performed following a similar protocol on non-experimental rat brain sections using mouse anti-DBH (1:6000; Millipore, Billerica, MA) and Cy3-conjugated donkey anti-mouse IgG (1:300; Jackson Immunochemicals).

Immunoperoxidase- or immunofluorescence-labeled tissue sections were rinsed in buffer and mounted onto Superfrost Plus microscope slides (Fisher Scientific), allowed to dry overnight, dehydrated and defatted in graded ethanols and xylene, and coverslipped using Cytoseal 60 (VWR).

BST Cytoarchitecture and Iontophoresis Delivery Site Analysis

The parcellation and nomenclature of the BST was first described in 1989 by Ju and colleagues based on cyto- and chemoarchitectonic studies of the BST and its surrounding region (Ju and Swanson 1989, Ju, Swanson et al. 1989). Later anterograde tracing studies using discrete injections of PHA-L into each subnucleus led to an updated parcellation and nomenclature (Dong and Swanson 2006). In our study, we attempted to iontophoretically target retrograde tracer to the fusiform subnucleus, which receives particularly dense NA input. However, retrograde tracer iontophoresis in the present study produced larger tracer delivery sites compared to those achieved using PHA-L, and so we describe these delivery sites as encompassing the BSTvl. We refer to the BSTvl as including the fusiform subnucleus and subcommissural part of the anterolateral subnucleus, as described in the Swanson atlas (Swanson 2004). In reference to Paxinos and Watson's atlas, this generally corresponds to the fusiform subnucleus and subcommissural parts of the intermediate, posterior, and ventral subnuclei of the BST's lateral division (Paxinos and Watson 2007). Shin and colleagues (Shin, Geerling et al. 2008) used Ju and colleague's 1989 nomenclature (Ju and Swanson 1989, Ju, Swanson et al. 1989) in their report; thus, their retrograde tracer delivery sites were described as targeted to the fusiform nucleus but diffusing into the anterodorsal and subcommissural subnuclei (comparable to the subcommissural part of the anterolateral subnucleus as defined by Dong and Swanson), the dorsomedial subnucleus, and the parastrial nucleus (part of the preoptic hypothalamus adjacent to the BST). By comparison, the iontophoretic delivery sites in the present study were similarly targeted within the BSTvl, but avoided diffusion into the dorsomedial subnucleus and parastrial nucleus.

Data Plotting and Quantitative Analysis

One selected case with the most accurate CEAm and BSTvl tracer delivery sites was used to fully document the distribution of retrogradely-labeled neurons throughout the rostrocaudal extent of the brain. The distribution of CTB- and FG-positive retrogradely labeled neurons was plotted at 40x magnification using a Nikon light microscope connected to a computerized data acquisition system (Stereoinvestigator; MBF Bioscience). Plots were made using 2 adjacent tissue series separately stained for FG and CTB. First, the distribution of FG-labeled neurons was plotted from one set of sections spaced by 420 μm . Plots of FG-labeled neurons were then matched and aligned to sections from the adjacent CTB-labeled tissue series. CTB-labeled neurons were plotted directly onto the initial FG plots with the digital markers for FG labeling hidden from view to prevent bias while plotting the location of CTB-positive neurons. The composite plots of FG- and CTB-labeled neurons were then overlaid onto corresponding Swanson atlas figures (Swanson 2004) using Adobe Illustrator software.

In the selected plotting case and in two additional cases with the most accurate CEAm and BSTvl tracer delivery sites (see Results), brain regions with overlapping distributions of retrogradely-labeled neurons were further analyzed in dual immunofluorescence-labeled sections to reveal double-labeled neurons. Labeling was visualized and digitally photographed using an Olympus photomicroscope with a 20x objective and filters to visualize Cy2 and Cy3 fluorescence. Counts of single- and double-labeled neurons within each region of interest were derived from images viewed on a computer screen using Adobe Photoshop software, while visualizing retrogradely labeled neurons within red and green color channels. The number of sections through each region that were photographed and used for cell counting, and the approximate bregma levels of quantified sections, are reported in Table 1. Within each afferent

brain region, the percentage of tracer-labeled neurons with collateralized projections was calculated as $[\text{collateralized}/(\text{collateralized} + (\text{CEAm-only and/or BSTvl-only}))] \times 100$. Retrograde labeling was subjected to quantitative analysis only in regions which contained dense overlap of CEA_m-projecting and BST_{vl}-projecting neurons.

Neuroanatomical regions and nomenclature were defined using Swanson's rat brain atlas (Swanson 2004). For each quantified brain region, statistical comparisons of the number of neurons projecting to the CEA_m or BST_{vl} were performed using Student's t-test. Rostrocaudal distribution of retrograde labeling within the NTS and paraventricular thalamus (PVT) was analyzed using two-way ANOVA with rostrocaudal level and tracer target site (CEA_m or BST_{vl}) as independent variables. Differences were considered significant when $P < 0.05$.

2.4 RESULTS

Iontophoretic tracer delivery sites

Three rats (cases 09-133, 09-110, and 10-9) with dual iontophoretic delivery sites that were most accurately targeted and restricted to the CEA_m and BST_{vl} were selected for quantitative analysis of retrograde labeling. In cases 09-110 and 09-133, FG was iontophoresed into the CEA_m (see Fig. 1c) and CTB was iontophoresed into the BST_{vl} (see Fig. 2c). In case 10-9, the tracers delivered into each target were switched (see Figs. 1a and 2a). Retrograde labeling patterns were consistent across these three cases, although the actual numbers of retrogradely-labeled neurons varied (Table 1). Different patterns of retrograde labeling resulted from tracer delivery sites that "missed" the CEA_m and BST_{vl}, and were instead centered in closely adjacent regions. Those findings are presented at the end of the Results section.

Of the three selected cases with the most accurate tracer delivery sites, case 09-133 consistently had the largest number of retrogradely-labeled neurons across quantified brain regions. This representative case was used to digitally plot the distribution of tracer-labeled neurons projecting to the CEAm and BSTvl (see Figs. 3-12).

In general, the large majority of brain regions that contained CEAm-projecting neurons also contained BSTvl-projecting neurons, and vice-versa. However, and as described in more detail in the following sections, some regions projected primarily to the CEAm with comparably less input to the BSTvl (e.g., insular cortex). Some regions displayed the opposite pattern, with relatively more input to the BSTvl compared to the CEAm (e.g., NTS), while some brain regions projected equivalently to both the CEAm and the BSTvl (e.g., PVT). Across all the regions in which retrograde labeling was quantified, double-labeled neurons with axonal projections to both the CEAm and the BSTvl accounted for as little as 2% to as much as 13% of the total population of tracer-labeled neurons (Table 1). The distribution of retrograde labeling is plotted in Figures 3-10, in which red stars represent individual CEAm-projecting neurons, and green circles represent BSTvl-projecting neurons.

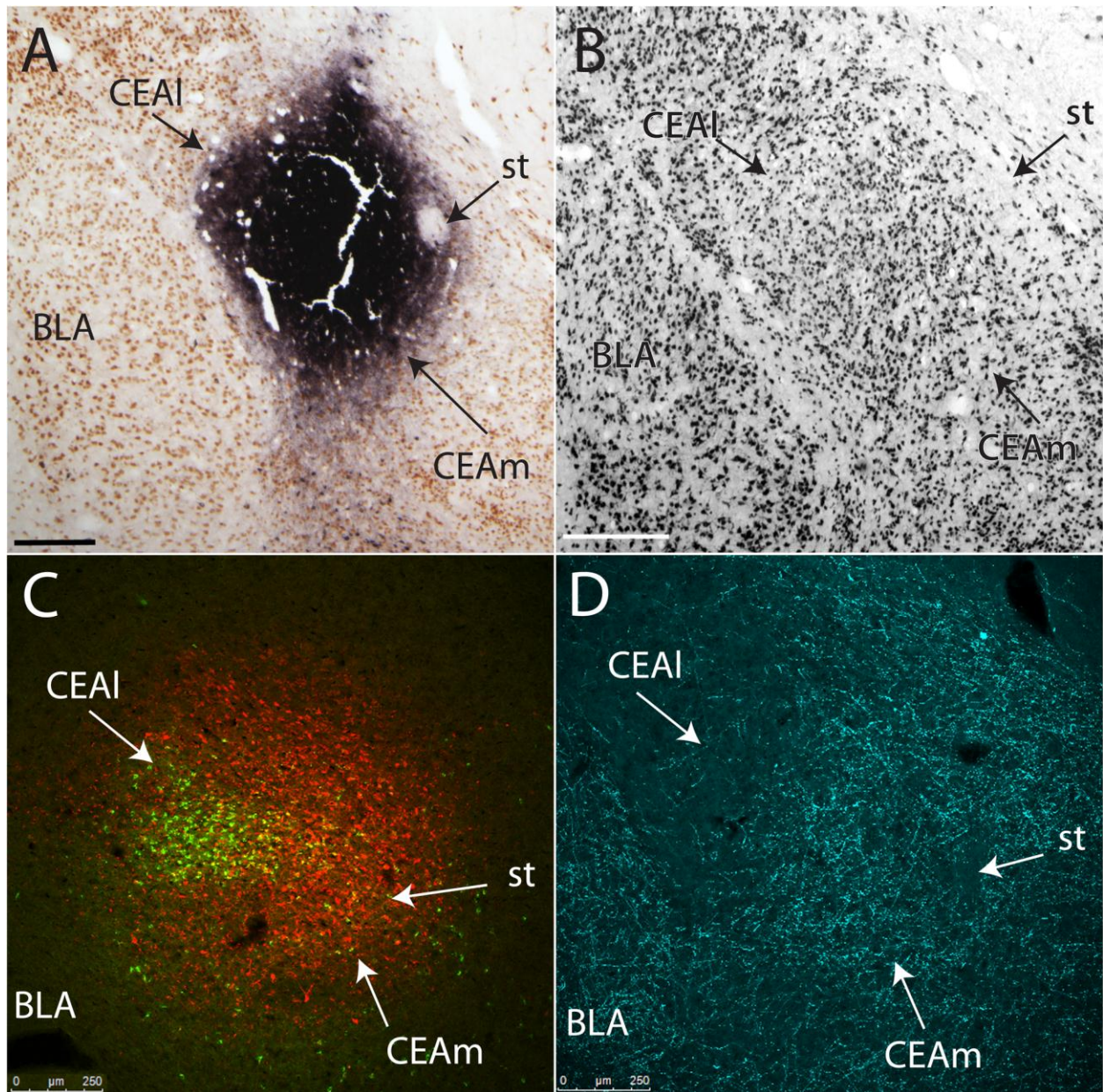


Figure 1. Iontophoresis of FG or CTB retrograde tracer into the CEAm. Medial is to the right. A: In case 10-9, CTB iontophoresis produced a highly localized, dense tracer deposit centered within the CEAm, although robust additional retrograde labeling also is present within the CEAI (CTB immunoperoxidase labeling is black, NeuN immunoperoxidase labeling is brown). B: NeuN immunoperoxidase labeling reveals distinct cytoarchitectural boundaries of the CEA and its subnuclei (similar rostrocaudal level as in panel A). C: In case 09-110, FG iontophoresis produced a spherical tracer delivery site centered within the CEAm (red immunofluorescence), although a larger sphere of tracer diffusion is seen to extend into the CEAI, where retrogradely-labeled BST-projecting neurons (green) are clustered. D: DBH immunofluorescently labeled fibers (cyan) are moderately dense within the CEAm, but much more sparse within the CEAI (similar rostrocaudal level as in panel C, slightly more rostral to the levels shown in panels A and B). Scale bars= 250 μm .

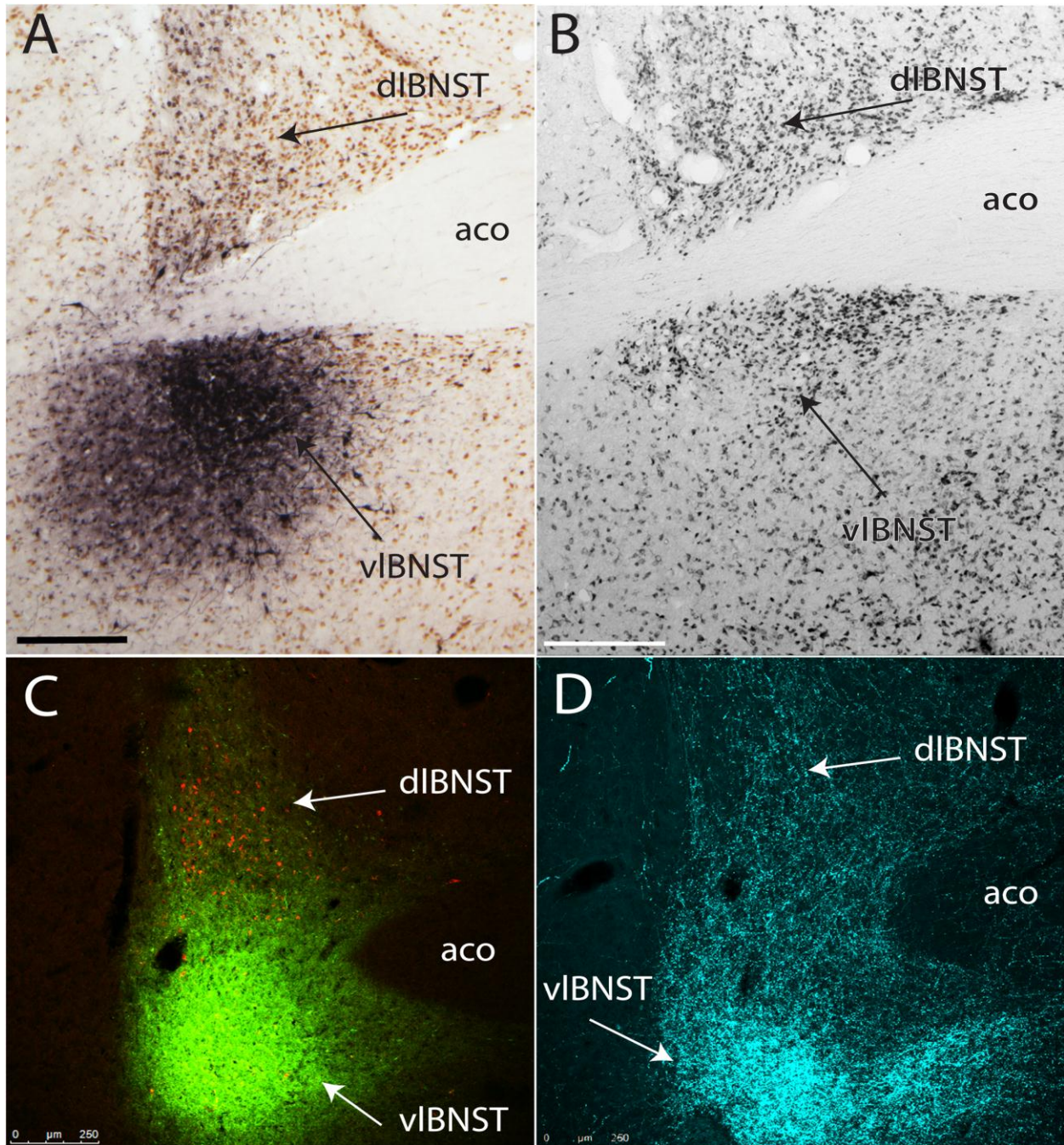


Figure 2. Iontophoresis of FG or CTB retrograde tracer into the BSTvl. Medial is to the right. A: In case 10-9, FG iontophoresis produced a spherical deposit centered close to the lateral border of the BSTvl (FG immunoperoxidase labeling is black, NeuN immunoperoxidase labeling is brown). B: NeuN immunoperoxidase labeling reveals distinct cytoarchitectural boundaries of the BST and its subnuclei (note the fusiform subnucleus is more lightly NeuN-positive compared to other BST subnuclei; similar rostrocaudal level to that shown in panel A). C: In case 09-110, CTB iontophoresis produced a dense tracer deposit (green immunofluorescence) in the BSTvl, overlapping with FG-positive CEAm-projecting neurons (yellow). Additional FG-positive neurons are present within the BSTdl (red). D: DBH immunofluorescently labeled fibers (cyan) form a dense terminal field within the BSTvl, with more moderate labeling observed within the BSTdl (similar rostrocaudal level to that shown in panel C). Scale bars=250 μ m.

Table 1. Counts of single- and double-tracer-labeled neurons across brain regions after iontophoretic delivery of tracers to the CEAm and BSTvl. Retrogradely-labeled neurons were counted in regions that contained overlapping distributions of CEAm- and BSTvl-projecting neurons. For each case (n=3), the number of sections through each region that were used for cell counting is indicated. Within each brain region, the total number of retrogradely-labeled neurons identified as CEAm-projecting, BSTvl-projecting, or collateralized (i.e., double-labeled) are indicated (mean \pm SE). The final two columns indicate collateralized neurons within each brain region expressed as a percentage of all neurons projecting to the CEAm, to the BSTvl, or to either.

Table 1 Counts of single- and double-tracer-labeled neurons across brain regions after iontophoretic delivery of tracers to the CEAm and BSTvl

Region	Bregma levels	Number of sections	mCEAm only	vIBNST only	Collaterals	Coll. % of mCEAm	Coll. % of vIBNST	Coll. % of total
Brainstem								
NTS	-14.36 to -13.44	5	31 \pm 10	121 \pm 2	15 \pm 5	33 \pm 4	11 \pm 4	9 \pm 3
VLM	-14.36 to -13.44	5	6 \pm 4	25 \pm 11	2 \pm 1	21 \pm 11	17 \pm 9	11 \pm 6
Pons								
CLR	-6.85 to -6.50	3	28 \pm 9	34 \pm 6	1 \pm 1	4 \pm 2	3 \pm 2	2 \pm 1
DR	-7.90 to -6.65	4	78 \pm 21	58 \pm 5	7 \pm 1	12 \pm 6	11 \pm 1	6 \pm 2
PBle	-9.50 to -8.85	3	249 \pm 56	81 \pm 19	49 \pm 16	16 \pm 2	39 \pm 12	12 \pm 3
PBlv	-9.80 to -9.50	2	72 \pm 8	23 \pm 5	6 \pm 1	8 \pm 1	22 \pm 4	6 \pm 1
PBm	-9.80 to -9.50	2	133 \pm 25	39 \pm 7	6 \pm 1	4 \pm 1	13 \pm 3	3 \pm 1
PBw	-9.80 to -9.50	2	23 \pm 3	9 \pm 2	3 \pm 1	10 \pm 2	25 \pm 10	8 \pm 2
Forebrain								
AI	-1.08 to +0.45	6	836 \pm 194	70 \pm 32	32 \pm 14	3 \pm 1	31 \pm 1	3 \pm 1
BLAp	-4.45 to -3.90	3	563 \pm 117	262 \pm 47	125 \pm 38	18 \pm 2	32 \pm 6	13 \pm 2
BMA	-2.45 to -2.00	3	791 \pm 287	327 \pm 105	86 \pm 47	8 \pm 2	18 \pm 5	6 \pm 2
ILA	+2.15 to +2.80	3	87 \pm 32	120 \pm 40	9 \pm 5	8 \pm 3	6 \pm 3	3 \pm 2
IPAC	-0.83 to +0.45	6	203 \pm 65	238 \pm 56	24 \pm 8	11 \pm 1	13 \pm 6	5 \pm 1
PSTN	-4.20 to -3.90	3	123 \pm 51	126 \pm 15	10 \pm 4	7 \pm 2	8 \pm 3	4 \pm 2
PVT	-4.20 to -1.08	14	559 \pm 101	588 \pm 29	58 \pm 17	9 \pm 1	9 \pm 2	5 \pm 1
cPVT	-4.20 to -3.50	5	369 \pm 54	212 \pm 13	33 \pm 8	8 \pm 1	13 \pm 2	5 \pm 1
mPVT	-3.25 to -2.00	4	146 \pm 28	141 \pm 5	16 \pm 3	10 \pm 0	10 \pm 1	5 \pm 0
rPVT	-1.90 to -1.08	5	190 \pm 48	376 \pm 21	25 \pm 9	11 \pm 2	6 \pm 2	4 \pm 2
TR	-4.45 to -3.90	3	660 \pm 86	171 \pm 54	21 \pm 9	3 \pm 1	10 \pm 1	2 \pm 1

Medulla

Retrogradely-labeled neurons in the medulla were located primarily within the caudal, visceral portion of the NTS and the caudal VLM ipsilateral to the tracer delivery sites. Significantly more NTS neurons projected to the BSTvl compared to the number of NTS neurons projecting to the CEAm (136 ± 6 vs. 46 ± 15 neurons; $P=0.005$). Rostrocaudal analysis of retrograde labeling patterns revealed a different distribution of BSTvl- vs. CEAm-projecting NTS neurons (Figs. 3, 4). Two-way ANOVA revealed a significant effect of both tracer target site [$F(1, 29) = 90.39, P<0.001$] and rostrocaudal NTS level [$F(4, 29) = 4.26, P<0.05$] on the number of retrogradely labeled NTS neurons, as well as a significant interaction between tracer target site and rostrocaudal level [$F(4, 29) = 6.17, P<0.01$]. At levels caudal to the area postrema (AP), the NTS contained relatively few CEAm-projecting neurons (red stars in Fig. 3a,b). The number of CEAm-projecting NTS neurons increased at more rostral levels, reaching a peak just rostral to the AP (Figs. 3e, 4). Conversely, the number of BSTvl-projecting NTS neurons reached a peak at the mid-AP level (green circles, Figs. 3c, 4). NTS neurons with collateralized projections to both the CEAm and BSTvl were most prevalent in sections just rostral to the AP (Fig. 4). Approximately 9% of all tracer-labeled NTS neurons were double-labeled (Table 1). Overall, $33 \pm 4\%$ of all CEAm-projecting NTS neurons collateralized to also provide input to the BSTvl, whereas only $11 \pm 4\%$ of all BSTvl-projecting NTS neurons collateralized to innervate the CEAm (Table 1).

Retrogradely-labeled VLM neurons were present at the same rostrocaudal levels as retrogradely-labeled NTS neurons (Fig. 3). Quantification of labeling within the VLM revealed a nonsignificant trend towards a greater number of BSTvl-projecting vs. CEAm-projecting neurons (25 ± 11 vs. 8 ± 4 neurons; $P=0.63$). VLM neurons projecting to the CEAm or BSTvl were

distributed uniformly across rostrocaudal levels, and moderate numbers of double-labeled neurons with collateralized projections to both the CEAm and BSTvl were observed (Table 1). Approximately 11% of all tracer-labeled VLM neurons were double-labeled, similar to proportions of double-labeled neurons within the NTS (Table 1).

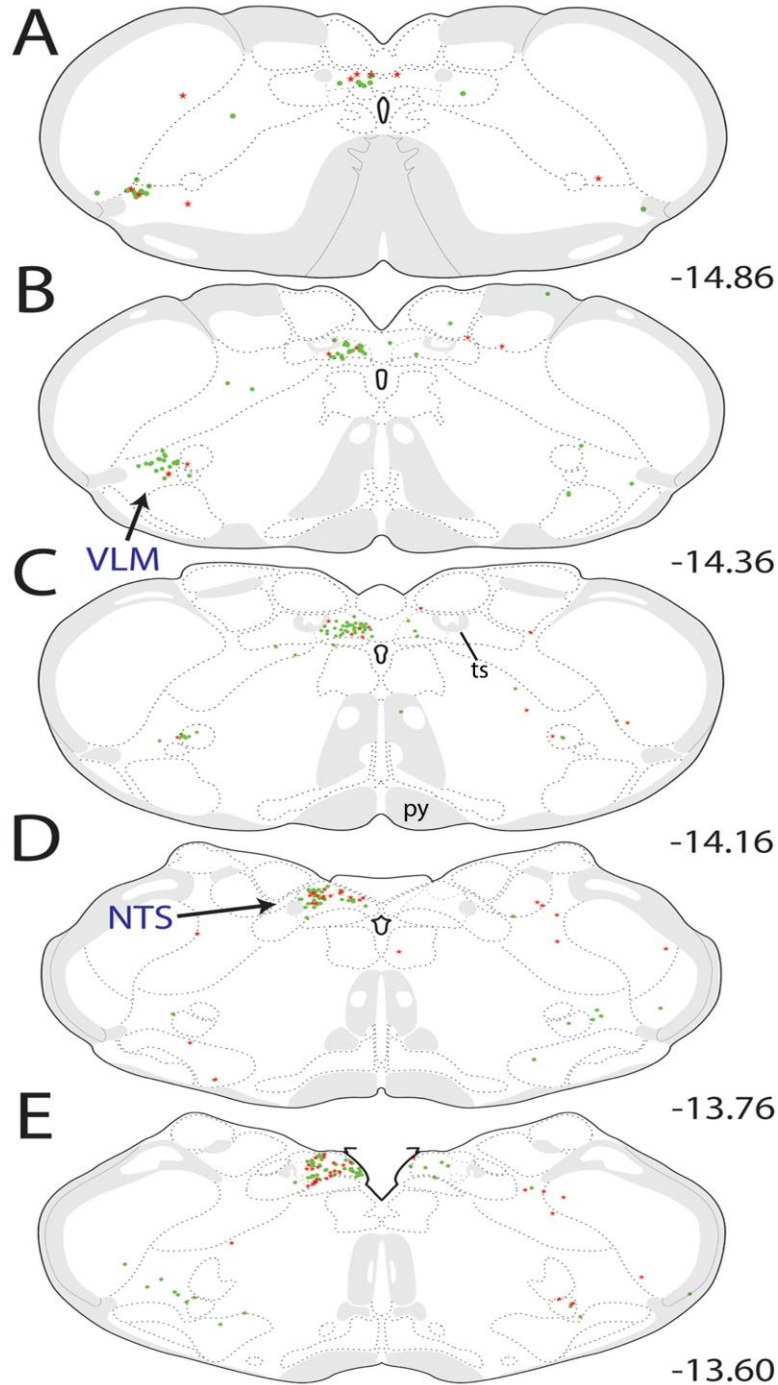


Figure 3. Distribution maps of retrogradely-labeled neurons within the caudal medulla. CEAm- and BSTvl-projecting neurons were located throughout the caudal NTS and VLM, but were most prevalent between bregma levels -14.86 and -13.60 (A-E). The number of BSTvl-projecting NTS neurons (green circles) peaked at the mid-AP level (C; bregma level -14.16) while CEAm-projecting NTS neurons (red stars) were most prevalent at a slightly more rostral level (E; see Fig. 4 for rostrocaudal quantitative data). Within the VLM, the distribution of BSTvl-projecting neurons did not appear to differ across rostrocaudal levels. CEAm-projecting VLM neurons were relatively scarce whereas BSTvl-projecting VLM neurons were more common. See Table 1 for quantification of overall NTS and VLM retrograde labeling and the incidence of double-labeled neurons with collateralized projections to both regions.

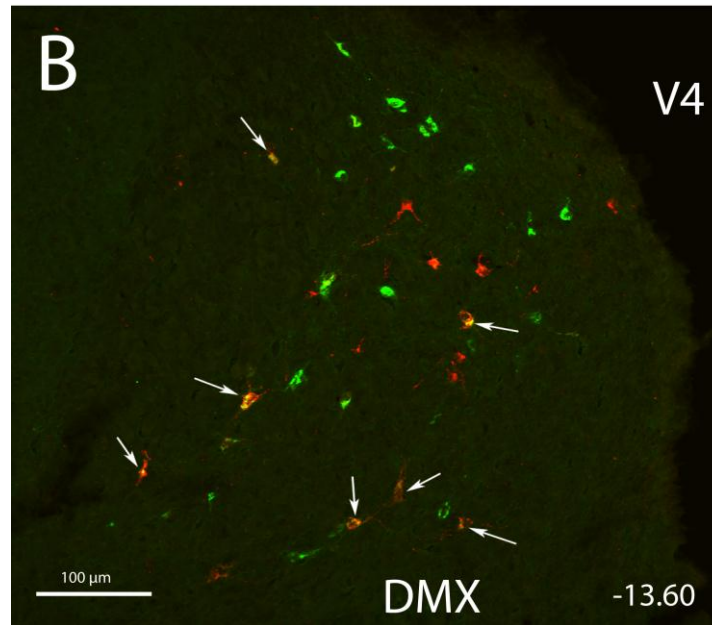
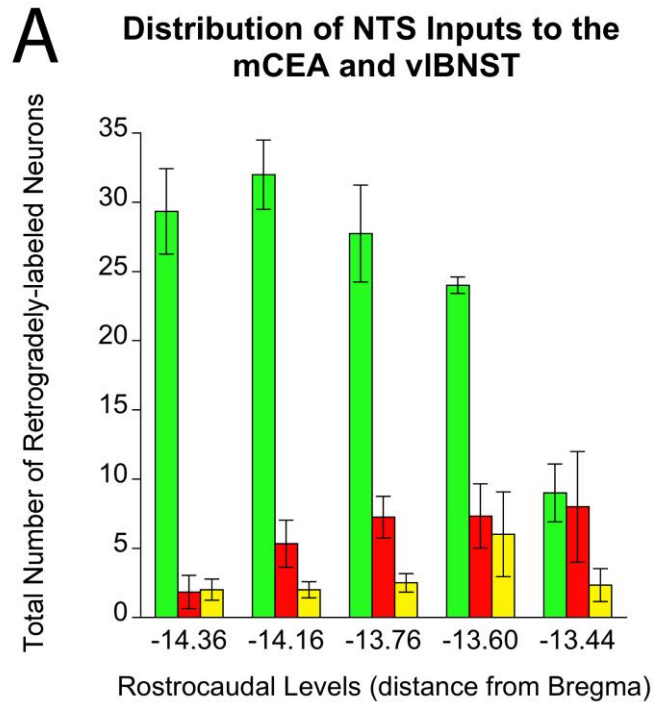


Figure 4. Rostrocaudal distribution of retrogradely-labeled NTS neurons. A: The number of BSTvl-projecting neurons (green) peaked at the mid-AP section level (-14.16 mm from bregma), while smaller numbers of CEA-projecting neurons (red) were distributed somewhat more rostrally, similar to the peak distribution of double-labeled neurons (yellow). B: Confocal z-stack image of the retrograde labeling within the NTS in case 09-133 (bregma level -13.60, see Fig. 3e). FG-positive CEA-projecting neurons are red; CTB-positive BSTvl-projecting neurons are green. White arrows point out several double-labeled neurons whose axons project to both the CEA and BSTvl. Scale bars=250 μ m.

Pons

Pontine input to the CEAm and BSTvl was predominantly confined to the parabrachial nucleus (PB; Fig. 5). The locus coeruleus contained a small number of CEAm- and BSTvl-projecting neurons (i.e., 1-3 neurons per section, data not shown). Retrogradely-labeled neurons were distributed bilaterally within several PB subnuclei, although a strong ipsilateral predominance of labeling was evident (Fig. 5). At the caudal end of the PB (Fig. 5a,b), retrograde labeling within the PB was heavily concentrated within the ventral lateral (PBlv), medial (PBm), and waist subnuclei (PBw). Within these subnuclei, CEAm-projecting neurons significantly outnumbered BSTvl-projecting neurons (PBlv= 79 ± 9 vs. 29 ± 6 neurons; $P=0.01$; PBm= 139 ± 25 vs. 45 ± 7 neurons; $P=0.02$; PBw= 25 ± 4 vs. 11 ± 1 neurons; $P=0.04$). Relatively few (i.e., approximately $6 \pm 1\%$, $3 \pm 1\%$, and $8 \pm 2\%$) of all tracer-labeled neurons within the PBlv, PBm, and PBw were double-labeled (Table 1). More rostral levels of the PB (Fig. 5c) contained larger numbers of CEAm- and BSTvl-projecting neurons that were primarily localized within the external lateral PB subnucleus (PBle; see Fig. 13a), with fewer retrogradely-labeled neurons present within the PBlv, PBm, and PBw. Quantification revealed a nonsignificant trend towards larger numbers of PBle neurons projecting to the CEAm vs. the BSTvl (298 ± 72 vs. 130 ± 9 neurons; $P=0.08$). In contrast to other PB subnuclei, many of the retrogradely-labeled PBle neurons collateralized to innervate both the CEAm and BSTvl: approximately $12 \pm 3\%$ of all tracer-labeled PBle neurons were double-labeled (Table 1). When double-labeled neurons were excluded, significantly more single-labeled PBle neurons projected to the CEAm compared to the number that projected to the BSTvl (Table 1; $P<0.05$).

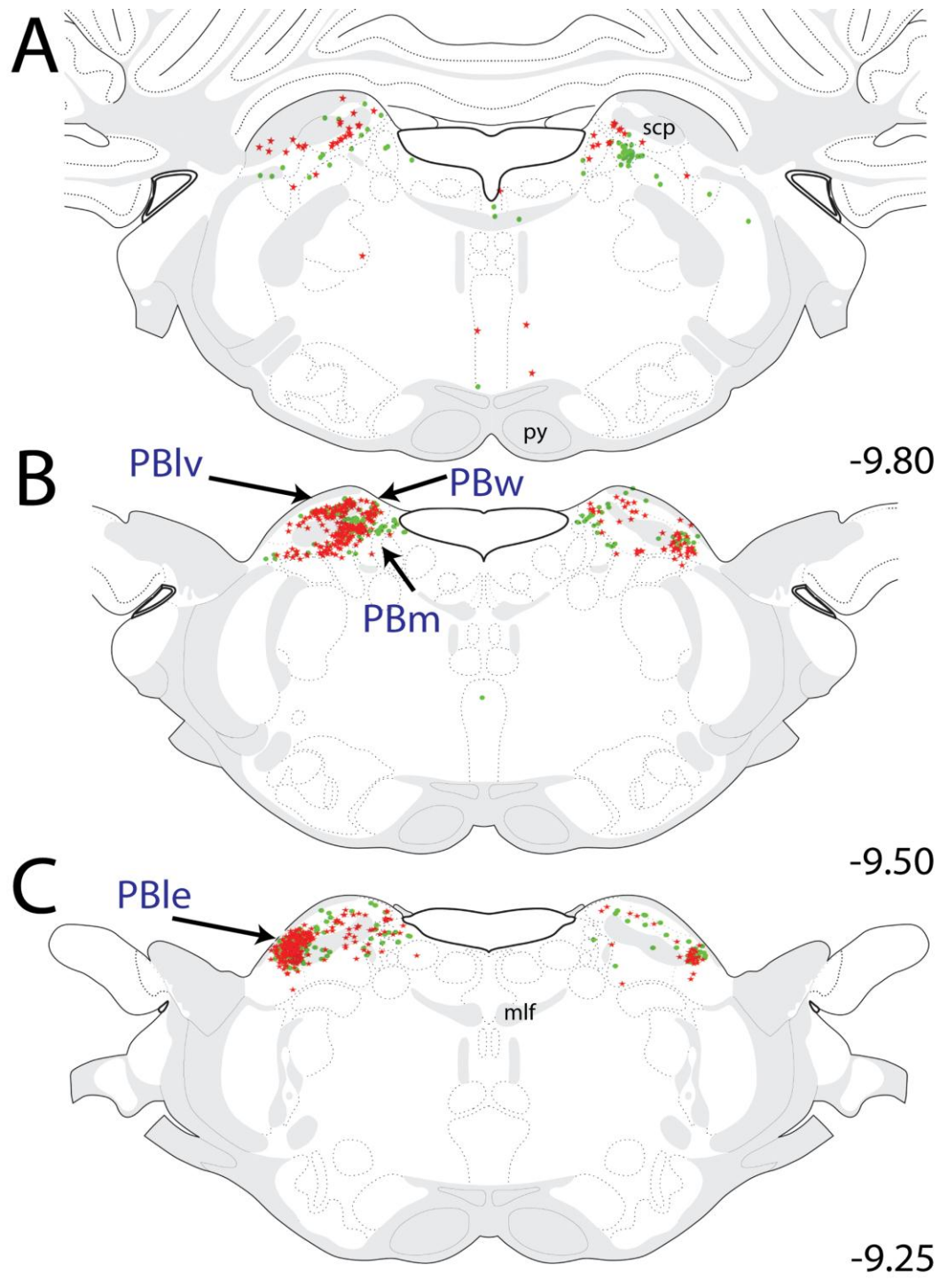


Figure 5. Distribution maps of retrogradely-labeled pontine neurons, which were primarily located in the PB between bregma levels -9.80 and -9.25. Generally, CEAm-projecting PB neurons (red stars) were more prevalent than BSTvl-projecting PB neurons (green circles). At caudal levels (A and B), the majority of retrograde labeling was observed in the PBlv, PBw, and PBm. At more rostral levels (C), large numbers of retrogradely-labeled neurons were located bilaterally within the PBLE. See Table 1 for quantification of overall PB subnuclear retrograde labeling and the incidence of double-labeled neurons with collateralized projections to both the CEAm and BSTvl.

Midbrain

Within the caudal midbrain (Fig. 6a,b,c), CEAm- and BSTvl-projecting neurons were distributed ventral to the central aqueduct, within the pedunclopontine nucleus (PPN), dorsal raphé (DR), and ventral lateral periaqueductal gray (PAGvl). Within the DR, there was no significant difference between the numbers of CEAm- and BSTvl-projecting neurons (77 ± 20 vs. 65 ± 6 neurons; $P= 0.61$), and relatively few tracer-labeled DR neurons (7 ± 1 neurons, $6\pm 2\%$ of total) had collateralized projections to both the CEAm and BSTvl (Table 1). In more rostral midbrain sections, retrograde labeling extended ventrally to include the central linear raphé (CLI; Fig. 6c,d). There was no significant difference between the number of CEAm- and BSTvl-projecting CLI neurons (29 ± 9 vs. 35 ± 6 neurons; $P=0.62$), and there was very little collateralization of individual CLI neurons to both the CEAm and BSTvl (Table 1).

Rostral to the midbrain CLI, CEAm- and/or BSTvl-projecting neurons were located within the ventral tegmental area (VTA; Fig. 7a,b) and the compact portion of the substantia nigra (SNc; Fig. 7c). Retrograde labeling within the VTA was very sparse and was not quantified. The SNc contained a fair number of CEAm-projecting neurons (not quantified, Fig. 7c), but no BSTvl-projecting neurons.

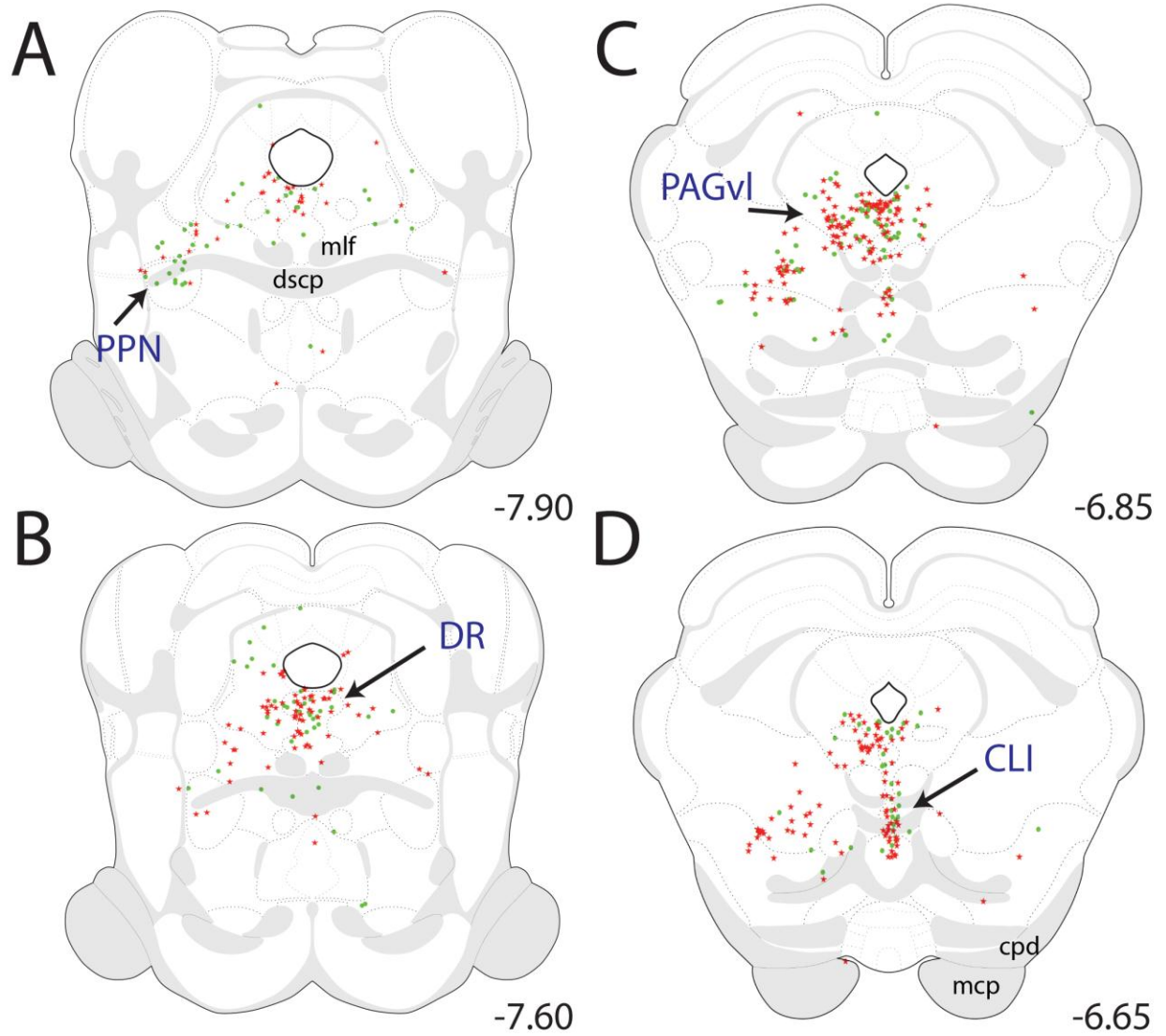


Figure 6. Distribution maps of retrogradely-labeled neurons within the caudal midbrain. Retrogradely-labeled neurons were located within the PPN, DR, PAGvl, and CLI from bregma levels -7.90 to -6.65. A: Within the PPN, most retrogradely-labeled neurons were BSTvl-projecting (green circles) preferentially located near the rostral end of the PPN. At more rostral levels (B and C), large numbers of retrogradely-labeled neurons occupied the region just ventral to the cerebral aqueduct, which includes the DR along the midline and the PAGvl more laterally. Further rostral (D), retrograde labeling extended ventrally along the midline to include neurons within the CLI. Within the DR and CLI, similar numbers of neurons were CEAm-projecting (red stars) and BSTvl-projecting. See Table 1 for quantification of overall PB retrograde labeling within the DR and CLI, and the incidence of double-labeled neurons with collateralized projections to both the CEAm and BSTvl.

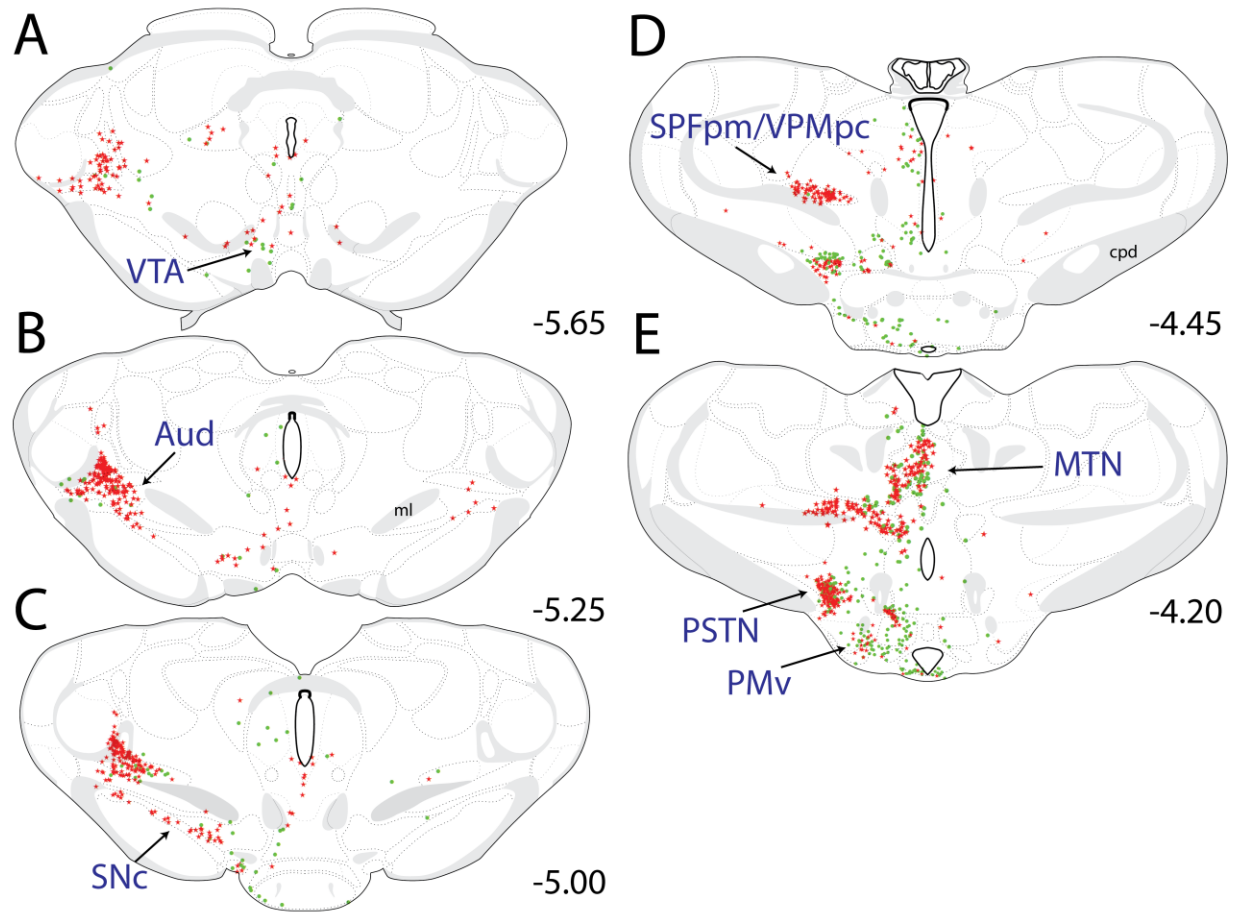


Figure 7. Distribution maps of retrogradely-labeled neurons within the rostral midbrain/caudal forebrain. A-C: Retrogradely-labeled rostral midbrain neurons were located primarily within the SNc and VTA between bregma levels -5.65 and -5.00. Both CEAm-projecting (red stars) and BSTvl-projecting neurons (green circles) were scattered within the VTA (A and B), while only CEAm-projecting neurons were located within the SNc (C). Within the caudal thalamus (A-E), dense clusters of CEAm-projecting neurons were observed within the Aud (A-C), the SPFpm/VPMpc (D), and the MTN (E), with relatively fewer BSTvl-projecting neurons in each region. Within the caudal hypothalamus (C-E), retrogradely-labeled neurons were located within the PSTN and PMv. The PMv contained predominantly BSTvl-projecting neurons and fewer CEAm-projecting neurons, whereas the PSTN contained similar numbers of BSTvl-projecting and CEAm-projecting neurons. See Table 1 for quantification of overall PSTN retrograde labeling, and the incidence of double-labeled neurons with collateralized projections to both the CEAm and BSTvl.

Thalamus

Projections to the CEAm and BSTvl were found throughout the rostrocaudal extent of the thalamus (Figs. 7-9) with large numbers of retrogradely-labeled neurons within more caudally-located thalamic nuclei (Fig. 7a-e). In general, thalamic CEAm-projecting neurons were more prevalent than BSTvl-projecting neurons. At caudal levels, many CEAm-projecting and few BSTvl-projecting neurons were present within the auditory thalamus (Aud; Fig. 7a-c). In more rostral sections (Fig. 7d), primarily CEA-projecting neurons were present within the medial parvicellular subparafascicular nucleus (SPFpm) and the parvicellular ventral posteromedial nucleus (VPMpc). Further rostrally, retrogradely-labeled neurons extended more medially to join the midline thalamic nuclei group (MTN; Fig. 7e), including the central medial nucleus, intermediodorsal nucleus, and the PVT. CEAm- and BSTvl-projecting neurons were distributed throughout the rostrocaudal extent of the MTN (Figs. 7e-8b), but were most numerous within the PVT. When the PVT was considered as a whole, there was no significant difference between the number of CEAm-projecting vs. BSTvl-projecting neurons (618 ± 117 vs. 646 ± 35 neurons; $P=0.83$). Two-way ANOVA revealed a significant effect of PVT rostrocaudal level [$F(1, 83) = 2.75, P < 0.01$] and an interaction between tracer target site and PVT rostrocaudal level [$F(13, 83) = 6.45, P < 0.001$]. When the PVT was divided into three rostrocaudal segments, there was a clear difference in the distribution of CEAm- vs. BSTvl-projecting neurons across the caudal, middle, and rostral thirds of the PVT (cPVT = caudal to bregma level -3.25; mPVT = bregma levels -2.85 through -2.00; rPVT = rostral to bregma level -2.00; Fig. 9). Significantly larger numbers of BSTvl-projecting neurons were located within the rPVT compared to either the mPVT (310 ± 18 vs. 157 ± 7 neurons, $P < 0.005$) or the cPVT (310 ± 18 vs. 179 ± 12 neurons, $P < 0.005$). Conversely, the number of CEAm afferents within the cPVT was significantly

greater than within the mPVT (320 ± 47 vs. 162 ± 31 neurons, $P<0.05$), but was not greater compared to the number of CEAm afferents in the rPVT (320 ± 47 vs. 196 ± 19 neurons, $P=0.72$). Further analysis of retrograde labeling across the three rostrocaudal PVT levels revealed that the cPVT contained significantly greater numbers of CEAm afferents compared to BSTvl afferents (320 ± 47 vs. 179 ± 12 neurons, $P<0.05$), while the rPVT contained a significantly greater number of BSTvl afferents compared to CEAm afferents (310 ± 18 vs. 135 ± 42 neurons, $P=0.02$). The numbers of CEAm and BSTvl afferents within the mPVT were not significantly different (162 ± 31 vs. 157 ± 7 neurons, $P=0.87$).

Hypothalamus

Hypothalamic regions generally contained many BSTvl-projecting neurons and smaller numbers of CEAm-projecting neurons. The hypothalamic distribution of these populations rarely overlapped, and therefore, were plotted (see Figs. 8, 9) but not quantified. The density of BSTvl-projecting neurons in the hypothalamus appeared greatest within the lateral hypothalamic area (LHA; Fig. 8a) and the medial preoptic area (MPO; Fig. 9c). However, one exception to the largely separate hypothalamic distribution of BSTvl- and CEAm-projecting neurons was the parasubthalamic nucleus (PSTN; Fig. 7e, 13b), which contained similar numbers of CEAm- and BSTvl-projecting neurons (133 ± 54 vs. 136 ± 11 neurons, $P=0.96$). Interestingly, despite the dense overlapping distribution of CEAm- and BSTvl-projecting PSTN neurons, relatively few were double-labeled (10 ± 4 neurons, $4\pm 2\%$ of total; Table 1).

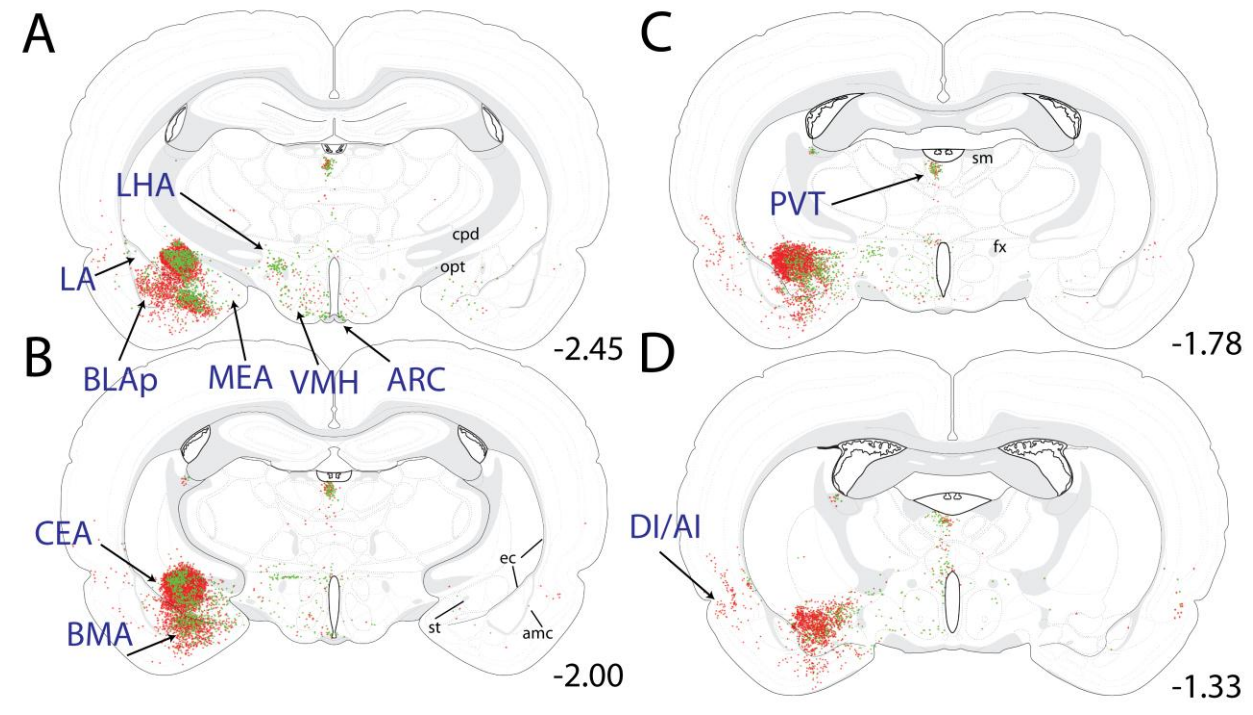


Figure 8. Distribution maps of retrogradely-labeled forebrain neurons at the level of the tuberal hypothalamus. Retrogradely-labeled neurons were located primarily within the CEA, BMA, and BLAp of the amygdala; within the LHA, VMH, and Arc of the hypothalamus; within the PVT of the thalamus; and within the DI/AI region of the cortex. The iontophoretic FG delivery site within the CEA (A-C) labeled large numbers of CEAm-projecting neurons (red stars) whose distribution within the BMA and BLAp overlapped with many BSTvl-projecting neurons (green circles; more caudal sections through the BLAp are shown in Fig. 10). Few retrogradely-labeled neurons were located within the LA or MEA (A). Within the hypothalamus, BSTvl-projecting neurons were prevalent within the LHA, VMH, and ARC, which contained fewer CEAm-projecting neurons (A-D). Retrogradely-labeled thalamic neurons were clustered within the PVT, with smaller numbers of retrogradely-labeled neurons scattered ventrally along the midline (A-D; additional retrograde labeling within the more rostral PVT is shown in Fig. 8). The cortical DI/AI contained large numbers of CEAm-projecting neurons and fewer BSTvl-projecting neurons (A-D; additional retrograde labeling within AI/DI is shown in Figs. 8 and 9). See Table 1 for quantification of overall AI, PVT, BLAp, and BMA retrograde labeling, and the incidence of double-labeled neurons within each region having collateralized projections to both the CEAm and BSTvl.

Basal Forebrain

Within the amygdala, large numbers of CEAm- and BSTvl-projecting neurons were located within the posterior basolateral amygdala (BLAp; Fig. 8a, 12b, 13e) and basomedial amygdala (BMA; Fig. 10a, 13d), while relatively fewer retrogradely-labeled neurons were present within the lateral or medial amygdala (Fig. 10a). There was a non-significant trend towards higher numbers of CEAm-projecting vs. BSTvl-projecting BLAp neurons (689 ± 155 vs. 388 ± 76 neurons; $P=0.16$). Collateralized projections of BLAp neurons to both the CEAm and BSTvl were relatively common. Approximately one third of BSTvl-projecting neurons and 20% of CEAm-projecting neurons within the BLAp were double labeled ($13 \pm 2\%$ of total retrogradely-labeled neurons, Table 1). In contrast, despite similarly large numbers of CEAm- and BSTvl-projecting neurons within the BMA (877 ± 334 vs. 413 ± 151 neurons; $P=0.27$; Table 1), smaller proportions of these neurons were double-labeled as compared to the BLAp ($6 \pm 2\%$ of total retrogradely-labeled neurons, Table 1).

As expected, iontophoresis of retrograde tracer into the CEAm produced abundant retrograde labeling within the BSTvl, and vice versa, as well as retrograde labeling within other regions of the extended amygdala (Figs. 1b, 2b, 8, 9). CEAm-projecting neurons were located throughout the lateral BST, and BSTvl-projecting neurons were found throughout the CEAm and CEAl. Additional CEAm- and BSTvl-projecting neurons were scattered throughout the substantia innominata (SI; Fig. 9a), a region interposed rostrocaudally between the CEA and BST and described as part of the “central extended amygdala” (de Olmos and Heimer 1999). In addition, a dense cluster of CEAm- and BSTvl-projecting neurons was located within a discrete subregion of the SI called the interstitial nucleus of the posterior limb of the anterior commissure (IPAC; Fig. 9b, 13c) (Shammah-Lagnado, Alheid et al. 2001). Quantification of retrogradely-

labeled IPAC neurons revealed no significant difference between the number of CEAm and BSTvl afferents (227 ± 73 vs. 262 ± 48 neurons; $P=0.71$). A moderate proportion of IPAC neurons projected axons to both the CEAm and BSTvl (Table 1). The caudal part of the nucleus accumbens shell (ACBsh), particularly its dorsal medial tip, contained large numbers of BSTvl-projecting neurons but relatively few CEAm-projecting neurons (Fig. 11a).

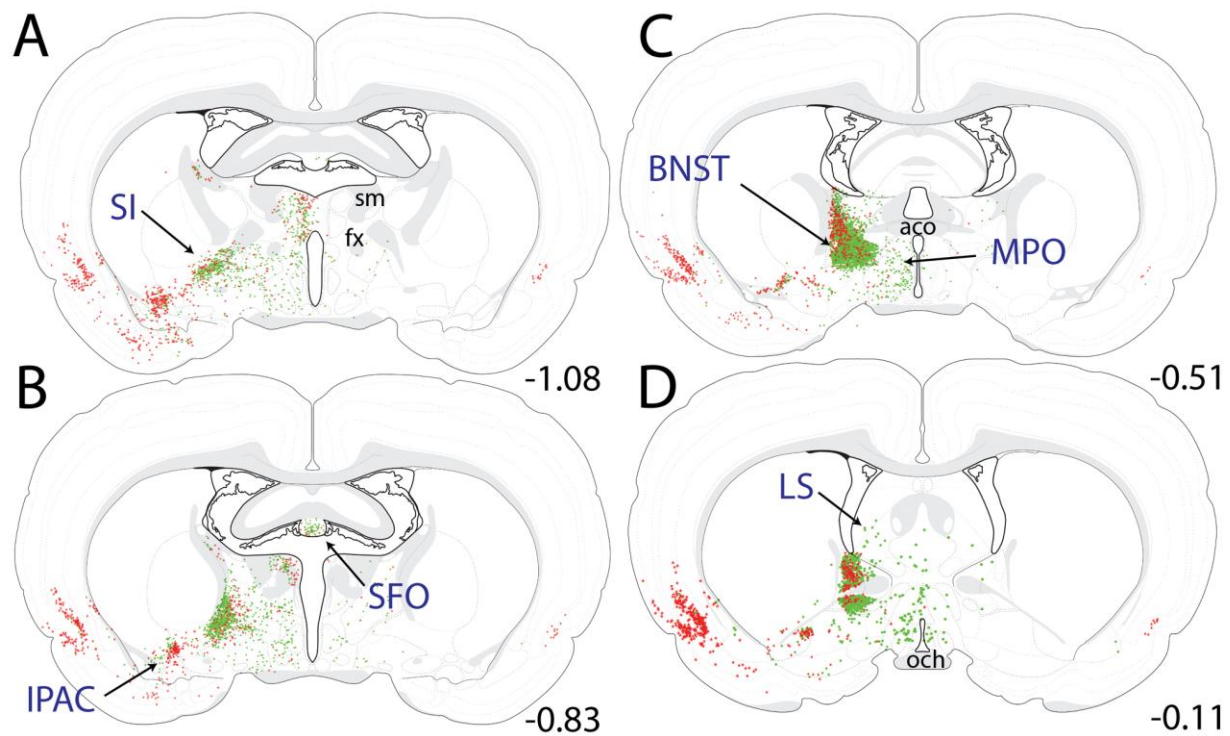


Figure 9. Distribution maps of retrogradely-labeled forebrain neurons at the level of the preoptic hypothalamus. Retrogradely-labeled neurons were located within the SI, IPAC, BST, SFO, and LS of the basal forebrain; the MPO of the hypothalamus, and the DI/AI region of the cortex. Iontophoretic CTB delivery produced a spherical deposit centered within the BSTvl that retrogradely labeled many neurons within the BSTdl (C, D). CEAm-projecting (red stars) and BSTvl-projecting neurons (green circles) were scattered throughout the SI, but formed a dense cluster within the IPAC (A-D). The SFO (B), MPO (A-D), and LS (D) contained many BSTvl-projecting neurons and fewer CEAm-projecting neurons (retrograde labeling within the more rostral LS is shown in Fig. 9). See Table 1 for quantification of overall AI and IPAC retrograde labeling, and the incidence of double-labeled neurons within each region having collateralized projections to both the CEAm and BSTvl.

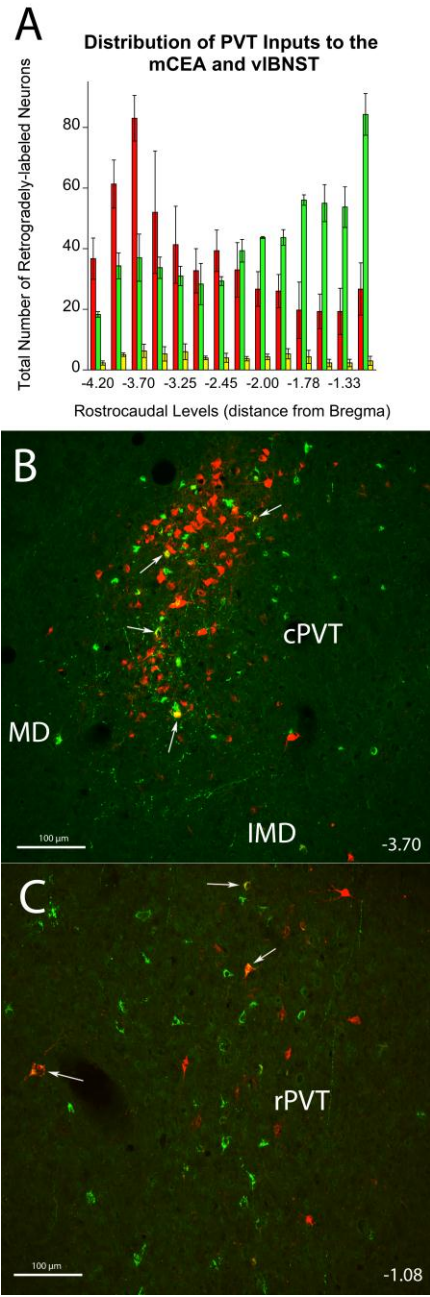


Figure 10. Rostrocaudal distribution of retrogradely-labeled neurons within the PVT. A: Larger numbers of CEAm-projecting neurons (red) were located within the cPVT (-4.20 to -3.50), while larger numbers of BSTvl-projecting neurons (green) were located within the rPVT (-1.90 to -1.08). Similar numbers of CEAm-projecting and BSTvl-projecting neurons were present in the mPVT (-3.25 to -2.00). Double-labeled neurons with collateralized axonal projections to both the CEAm and BSTvl (yellow) were distributed relatively evenly across rostrocaudal levels (see also Table 1). B: Confocal z-stack image of retrogradely-labeled neurons within the cPVT in case 09-133 (bregma level -3.70). FG-positive CEAm-projecting neurons (red) were significantly more prevalent than CTB-positive BSTvl-projecting neurons (green) within the cPVT (B). Double-labeled neurons are identified by white arrows. C: Confocal z-stack image of retrogradely-labeled neurons within the rPVT in the same case (09-133; bregma level -1.08). CTB-positive BSTvl-projecting neurons (green) were significantly more prevalent than FG-positive CEAm-projecting neurons (red) within the rPVT. Double-labeled neurons are identified by white arrows. Scale bars for B and C= 200 μ m.

Cerebral Cortex

Three major regions of the cerebral cortex contained CEAm- and BSTvl-projecting neurons. The densest cortical input to the CEAm and BSTvl arose from a region situated near the rhinal sulcus, including the agranular and dysgranular insular cortex (AI and DI, respectively; Figs. 8, 9, 11). Within the AI, significantly greater numbers of retrogradely-labeled neurons projected to the CEAm vs. the BSTvl (868 ± 208 vs. 102 ± 45 neurons; $P=0.02$). More than 30% of BSTvl-projecting AI neurons also projected to the CEA (i.e., were double-labeled), whereas double-labeled neurons comprised only 3% of all AI input to the CEAm (Table 1).

A dense overlap of CEAm- and BSTvl-projecting neurons was observed within deep layers of the caudal infralimbic cortex (ILA; Fig. 11d, 13f), with only a few scattered cells observed in the more dorsally situated prelimbic cortex (PL; Fig. 11d, 13f). Quantification of retrogradely-labeled neurons within the ILA revealed similar numbers of CEAm- and BSTvl-projecting neurons (96 ± 37 vs. 129 ± 43 neurons; $P=0.6$). Despite their overlapping distributions, BSTvl- and CEAm-projecting neurons within the ILA rarely collateralized to both the CEAm and BSTvl ($3 \pm 2\%$ of total retrogradely-labeled neurons; Table 1).

Within the ventral cerebral cortex, dense retrograde labeling was located within the postpiriform transition area (TR, sometimes referred to as the amygdala-piriform transition area; Fig. 12b, 13e), with fewer retrogradely-labeled neurons scattered throughout the more medially situated posterior amygdala (PA), and also within area CA1 of the ventral hippocampus (Fig. 12a). Quantification of retrogradely-labeled TR neurons revealed a significantly greater number of CEAm-projecting vs. BSTvl-projecting neurons (682 ± 94 vs. 192 ± 63 neurons; $P=0.01$). Relatively few TR neurons collateralized to innervate both the CEAm and BSTvl ($2 \pm 1\%$ of total retrogradely-labeled neurons; Table 1).

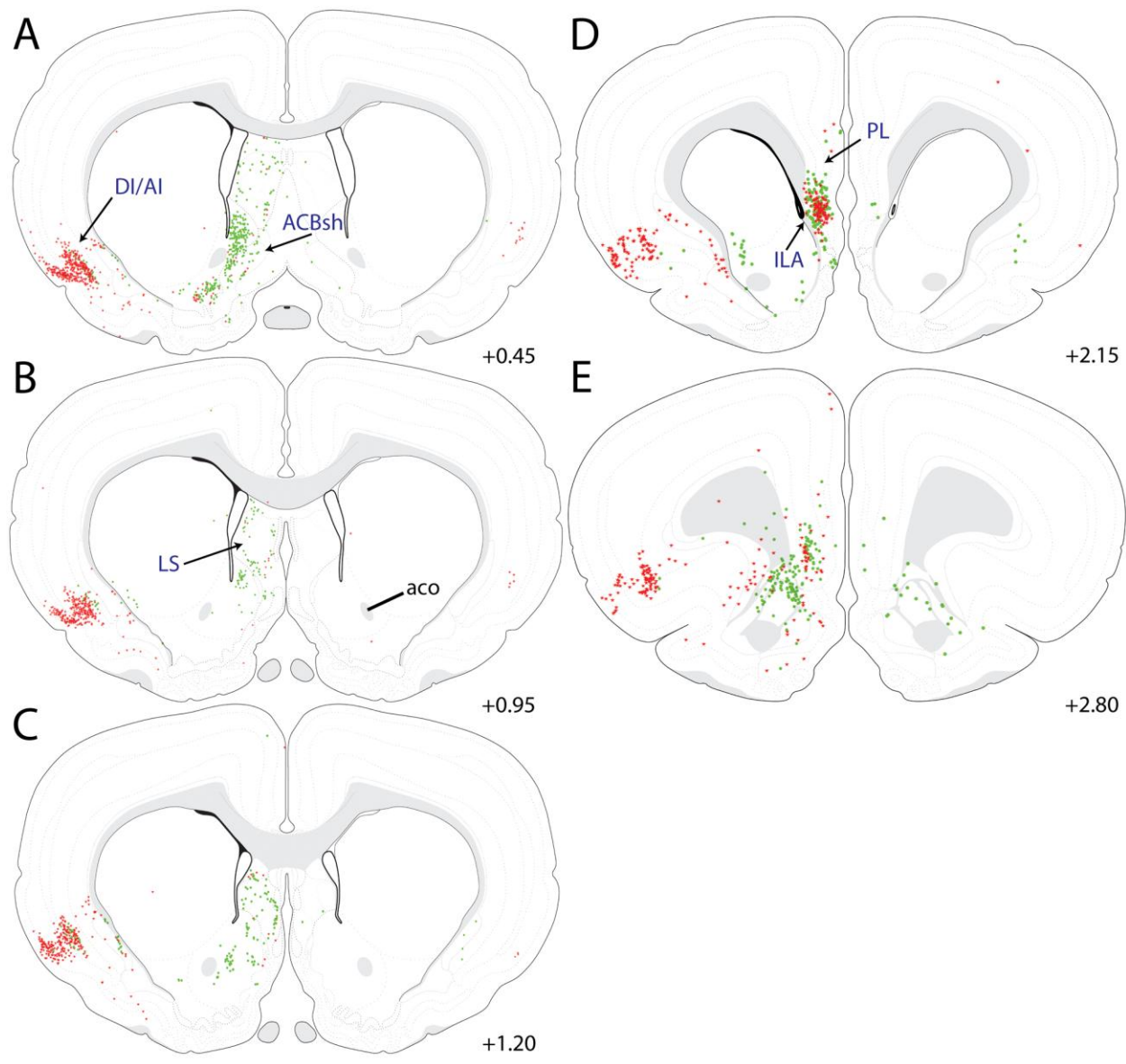


Figure 11. Distribution maps of retrogradely-labeled neurons within the rostral forebrain. Retrograde labeling within the basal forebrain was located primarily within the ACBsh and LS, and cortical labeling was located within DI/AI and ILA. The ACBsh and LS contained primarily BSTvl-projecting neurons (green circles), while the DI/AI contained predominantly CEAm-projecting neurons (red stars). Large numbers of both CEAm-projecting and BSTvl-projecting neurons were located within the ILA of the medial prefrontal cortex, whereas retrograde labeling within PL was much more sparse (D). See Table 1 for quantification of overall AI and ILA retrograde labeling, and the incidence of double-labeled neurons within each region having collateralized projections to both the CEAm and BSTvl.

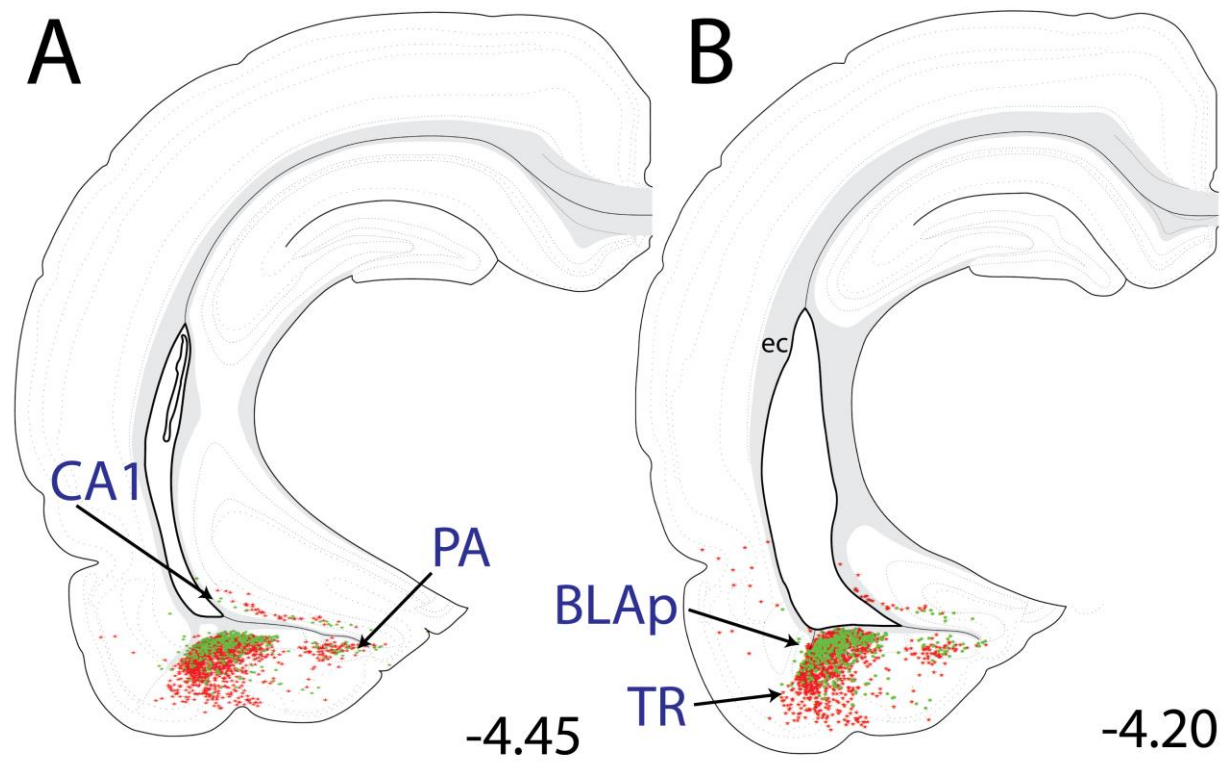


Figure 12. Distribution maps of retrogradely-labeled neurons within the temporal cortex/posterior amygdala. Large numbers of retrogradely-labeled neurons were present within the BLAp and PA of the amygdala, TR of the cortex, and CA1 region of the ventral hippocampus. Large numbers of CEAm-projecting neurons (red stars) were located within both the BLAp and TR, while the BLAp contained predominantly BSTvl-projecting neurons (green circles). Smaller numbers of CEAm-projecting and BSTvl-projecting neurons were present within the PA and CA1 region. See Table 1 for quantification of overall BLAp retrograde labeling, and the incidence of double-labeled BLAp neurons with collateralized projections to both the CEAm and BSTvl.

Retrograde labeling patterns after tracer iontophoresis into regions adjacent to CEAm and BSTvl

The goal of this study was to target specific subregions of the central extended amygdala, i.e., the BSTvl and the CEAm, for retrograde tracing of their afferent inputs. This clearly is a challenging task, given the relatively small size of each structure. Thus, we sought to determine whether tracer delivery sites that were viewed as “accurately centered” and relatively confined to the BSTvl or CEAm produced retrograde labeling that was distinct from labeling produced by tracer delivery centered in adjacent “incorrect” regions. “Incorrect” tracer delivery sites located adjacent to the BSTvl included the ventral pallidum (VP, lateral to the BST) and the posterior BST (pBST). Iontophoretic delivery of tracer into the VP produced abundant retrograde labeling in the medial subthalamic nucleus (STN), whereas accurate BSTvl iontophoretic delivery produced retrogradely-labeled neurons in the adjacent PSTN with no labeling in the STN. Iontophoretic delivery of tracer into the pBST produced dense retrograde labeling within the MEA, whereas MEA labeling was much more sparse after accurate tracer placement in the BSTvl. Tracer delivery into the VP or pBST also produced little or no retrograde labeling within other brain regions that contained labeled neurons after accurate BSTvl tracer delivery, including the NTS, VLM, BLAp, TR, and PSTN.

“Incorrect” tracer delivery sites adjacent to the CEAm included the dorsally situated amygdala-striatal transition area (AStr), the CEAl, and/or the BLA. In contrast to labeling produced by accurate CEAm-targeted sites, iontophoretic delivery of tracer into the BLA produced substantially more retrograde labeling within the pontine locus coeruleus (Asan 1998), and bilateral retrograde labeling of neurons within layer 3 of the nucleus of the lateral olfactory tract, consistent with previous findings (Santiago and Shammah-Lagnado 2004). Tracer delivery into the AStr retrogradely labeled neurons within secondary somatosensory cortex, which does

not project to the CEA (Shammah-Lagnado, Alheid et al. 1999). This cortical region was not labeled in rats with accurate CEAm tracer delivery sites in the present study. Cases in which the center of the iontophoretic delivery site was located within the CEAI rather than the CEAm produced little or no retrograde labeling within the NTS or VLM, in contrast to results following CEAm-centered tracer delivery, and consistent with the preferential distribution of NA fibers within the CEAm as compared to the CEAI (shown in Fig. 1d). NA inputs to the CEA arise primarily from the caudal medulla, and the large majority of NTS and VLM neurons that project to the CEA are NA neurons (Myers and Rinaman 2002).

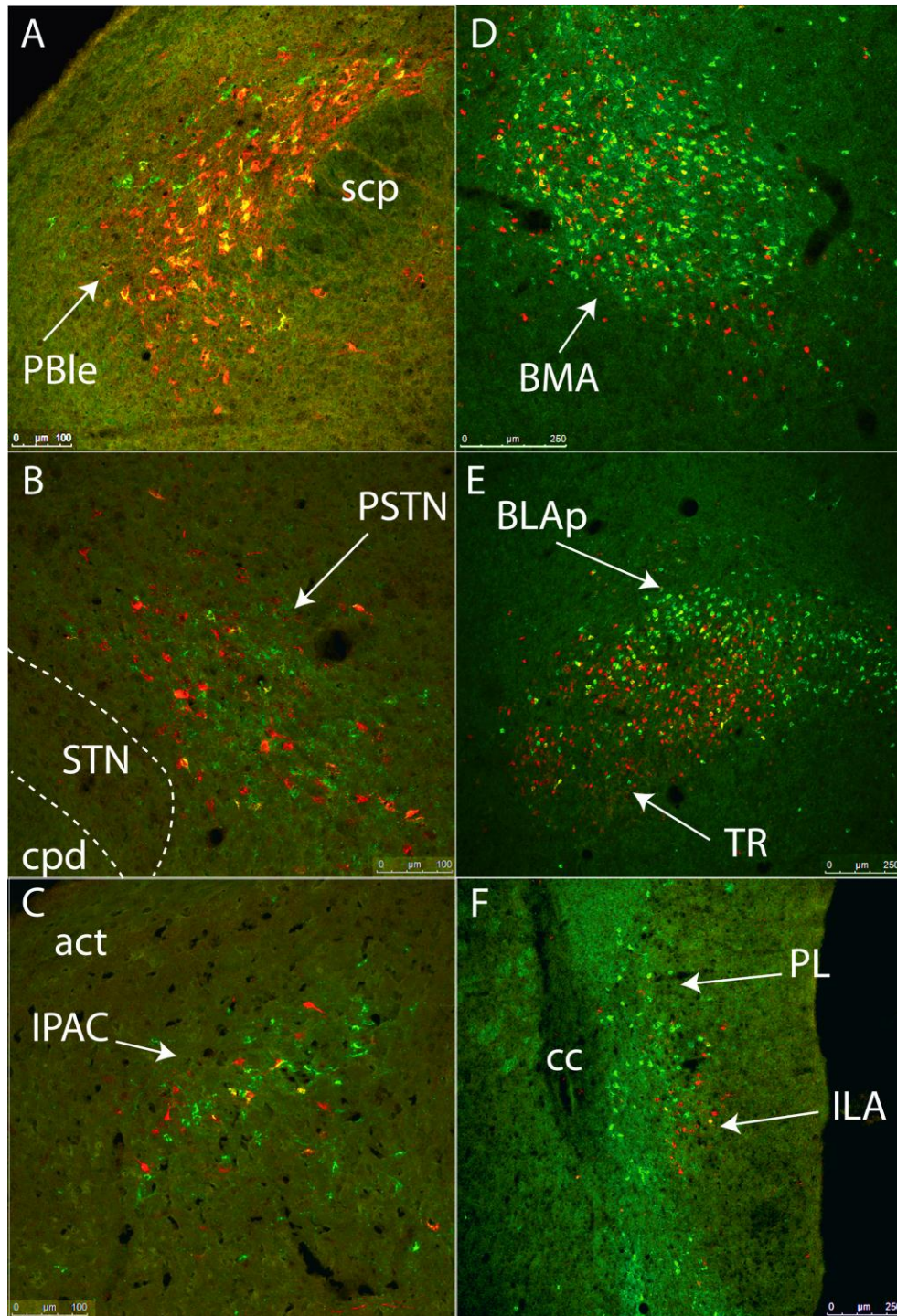


Figure 13. Confocal z-stack images of selected brain regions containing large numbers of CEAm-projecting and BSTvl-projecting neurons and a relatively high incidence of double-labeling: PBlc (A, compare to Fig. 5c), BMA (D, compare to Fig. 8b), and BLAp (E, compare to Fig. 12b). Conversely, despite the presence of large numbers of retrogradely labeled neurons projecting to the CEAm or BSTvl, relatively few double-labeled neurons were observed within the PSTN (B, compare to Fig. 7e), IPAC (C, compare to Fig. 9b), or ILA (F, compare to Fig. 11d). See Table 1 for quantitative data. Scale bars = 100μm in A-C, 250μm for D-F.

Predominance of Individual Brain Region's Input to the mCEA vs vIBNST

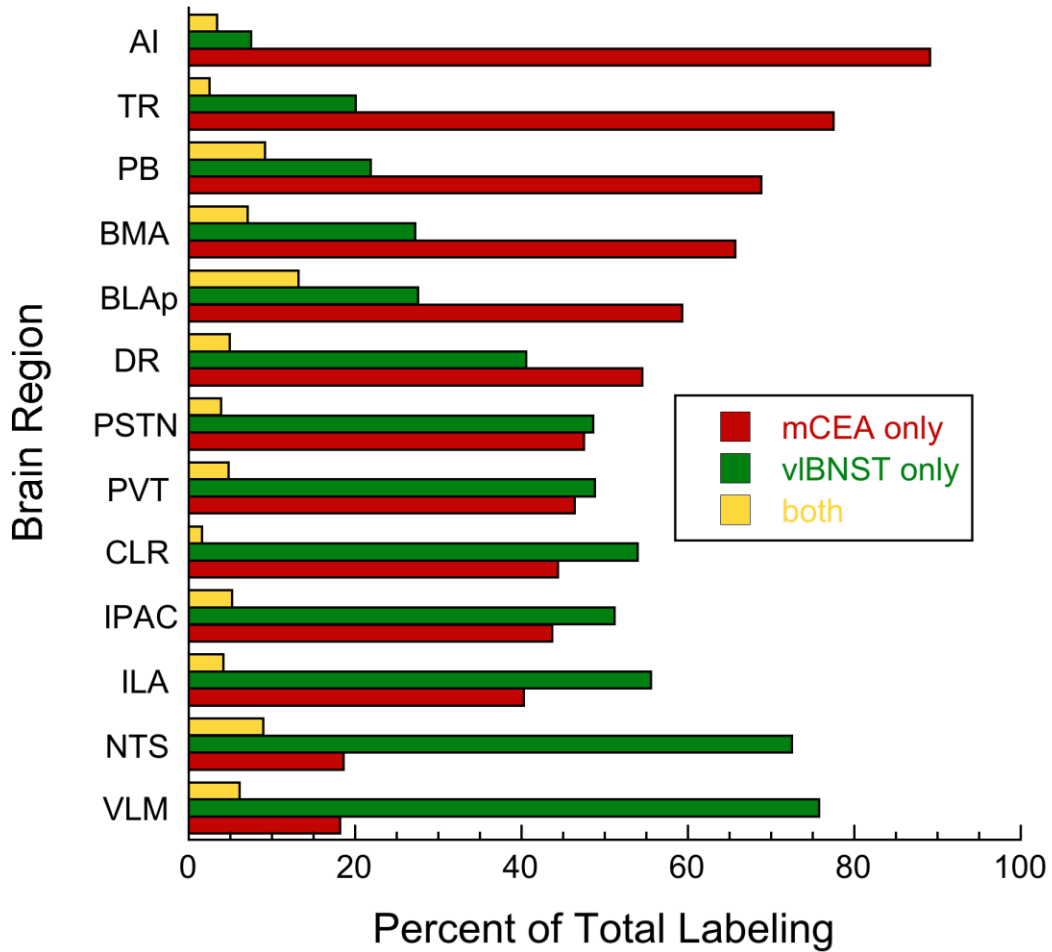


Figure 14. Schematic representation of the relative incidence of single- and double-tracer-labeled neurons across brain regions projecting to the CEAm and BSTvl. All regions in which labeling was quantified projected to both the CEAm and BSTvl, although each region contributed varying degrees of input to the CEAm vs. the BSTvl. The proportion of double-labeled neurons projecting to both the CEAm and BSTvl was generally similar across brain regions.

2.5 DISCUSSION

The present report is the first to fully map and compare the anatomical distribution of neurons projecting to the CEA and lateral BST, the two major components of the central extended amygdala. Our results are specifically focused on central neural inputs to CEAm and BSTvl subregions of the central extended amygdala. Although VLM and cortical neurons have been reported to provide collateralized axonal input to the CEA and BST (Roder and Ciriello 1994, Reynolds and Zahm 2005), previous studies did not investigate inputs that specifically target the CEAm and BSTvl. The present study reveals three patterns of retrograde labeling among brain regions that innervate the CEAm and BSTvl: high numbers of CEAm afferents with fewer BSTvl afferents, high numbers of BSTvl afferents with fewer CEAm afferents, or relatively even numbers of CEAm and BSTvl afferents (Fig. 14). Interestingly, neurons with collateralized inputs to both the CEAm and BSTvl exist within most of the CNS regions that project to either target, although the incidence of collateralization varies among regions (Fig. 14). These results generally support De Olmos and Heimer's proposal that "all or most of the central extended amygdala would share similar inputs" in the sense that the CEAm and BSTvl receive inputs from the same brain regions (de Olmos and Heimer 1999). Indeed, the SNc appears to be the only brain region that provides input to the CEAm but not to the BSTvl. However, our new findings reveal that inputs from cortical and sensory-related regions appear to preferentially target the CEAm, while inputs from motor-related "behavioral control columns" ((Swanson 2000); see following section) appear to preferentially target the BSTvl.

General principles for the organization of neural inputs to the central extended amygdala

In addition to considering our results as they pertain to the concept of the “central extended amygdala”, another way to interpret these findings arises from Larry Swanson’s descriptive model of how the brain regulates motivated behavior (Swanson 2000). Generally speaking, behaviorally-relevant information from widespread regions of the cerebral cortex reaches motor output systems through a triple descending projection to hierarchically-organized behavioral control columns, with each column dedicated to the production of a specific category of behavioral output (i.e., social, defensive, reproductive, or exploratory). Each column contains three levels of control that are common to the production of motivated behavioral output. The highest-order level of behavioral control is located within specific subregions of the hypothalamus and other rostral brainstem nuclei. This upper level of control defines an endogenous baseline activity level for specific subsets of brainstem motor pattern initiators and generators in order to regulate the series of movements that are necessary to produce organized behavior by controlling specific sets of brainstem and spinal motor neurons that initiate muscle contraction.

Overall, brain regions that contained larger numbers of neurons projecting to the CEAm vs. the BSTvl (Fig. 14) are associated with cortical or sensory systems (e.g., AI, BLAp, BMA, PB, TR, cPVT, Aud, SPFpm/VPMpc), while brain regions that contained larger numbers of neurons projecting to the BSTvl vs. the CEAm include striatal-like regions and areas associated with Swanson’s behavioral control columns (e.g., most of the hypothalamus, NTS, VLM, ACBsh, LS, PPN). When incorporated with anatomical data from the literature detailing CEA and BST efferent projections (Dong, Petrovich et al. 2001, Dong and Swanson 2003, Dong and Swanson 2004, Dong and Swanson 2006, Dong and Swanson 2006), these new findings support

an organizational hypothesis for two primary pathways through which behaviorally-relevant information is processed by the CEA and BST. First, similar to Swanson's model, we propose that cortical and sensory information necessary for initiating behaviors converges primarily within the CEA, including the CEAm, which then presumably recruits BST neurons that project to effectors in the motor system's top-down behavioral control columns (see Fig. 15a) (Dong, Petrovich et al. 2000, Swanson 2000, Dong, Petrovich et al. 2001, Dong and Swanson 2003, Dong and Swanson 2004). Secondly, we propose that bottom-up feedback about ongoing behavior is initially received and processed primarily by the BST, including the BSTvl, which then relays the information to the CEA in order to modulate ongoing motor outflow (see Fig. 15b). These top-down and bottom-up pathways may represent parallel but separate anatomical circuits within the CEA and BST, or may facilitate a bidirectional flow of information through the same circuit nodes.

In contrast to the "central extended amygdala" concept, Larry Swanson has noted that the network architecture of the CEA and BST shares many similarities to basal ganglia striatopallidal loop networks (Swanson 2000). He has suggested that the CEA is a caudal extension of the striatum and the BST is a rostral extension of the pallidum that together form a caudorostral striatopallidal circuit that is specially differentiated to regulate autonomic, neuroendocrine, and somatomotor output (Swanson 2000). Our results demonstrating differences in the organization of inputs to the CEAm and BSTvl lend supporting evidence for a striatopallidal-like organization of the CEAm and BSTvl. However, whereas motor feedback to the globus pallidus and ventral pallidum arises from brain regions involved in somatomotor control such as the STN, SNr, and the PPN (DeVito, Anderson et al. 1980), the pallidal-like BSTvl receives more robust direct input from regions involved in somatomotor and visceromotor

control, including the hypothalamus and pontine and medullary regions that receive and process visceral sensory inputs. Thus, the BSTvl (and the CEAm, to a lesser extent) receives moment-to-moment feedback about the physiological consequences of behavior, including autonomic and endocrine adjustments, consistent with evidence that changes in visceral and endocrine outflow can occur with little or no ongoing control by cortical structures. Given this abundant feedback, the CEA and BST are well-positioned to adjust somatomotor, autonomic, and neuroendocrine outflow as necessary to support ongoing and anticipated behavioral responses.

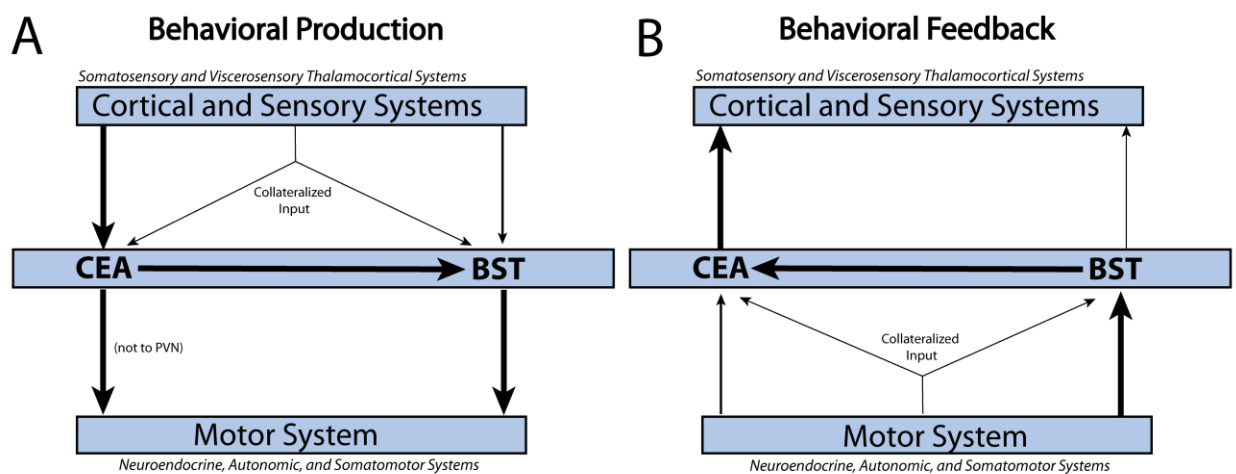


Figure 15. Structural anatomical model for information processing via CEA and BST circuits, based on published literature and results from the present study (schematic inspired by (Dong, Petrovich et al. 2001)). A: Cortical and sensory (i.e., thalamic) regions project predominantly to the CEA, with less robust direct input to the lateral BST. The CEA can directly or indirectly (via the BST) send information to hypothalamic and brainstem motor systems that generate neuroendocrine, autonomic, and somatomotor behavioral responses. B: Interoceptive feedback from motor systems regarding executed neuroendocrine, autonomic, and somatomotor outflow is received primarily by the lateral BST, with additional direct and relayed feedback to the CEA. The CEA is proposed to relay this feedback to the cortex and sensory thalamus. Thus, the CEA and BST are proposed to serve as an interface between cortical and motor systems. Bifurcating arrows represent collateralized projections from individual neurons that target both the CEA and BST, although these were minor compared to separate direct projections.

Collateralized inputs to the CEAm and BSTvl

Individual neurons with collateralized axonal inputs to the CEAm and BSTvl were observed in nearly every brain region that contained retrogradely-labeled neurons, although the incidence of collateralized projection neurons differed among regions. The largest proportions of retrogradely-labeled neurons that were double-labeled were found within the IPBN, BLAp, and NTS (Fig. 14), suggesting that information transfer from these regions to the CEAm and BSTvl is more highly coordinated as compared to inputs from other brain regions. Previous work has demonstrated that BLA-driven neural responses within the CEA and BST are temporally synchronized in order to simultaneously activate target neurons within the brainstem, providing evidence for cooperative output of the extended amygdala (Nagy and Pare 2008). Interestingly, the BLAp, IPBN, and NTS are critical structures for acquisition in aversive learning paradigms (Sakai and Yamamoto 1998, Fanselow and LeDoux 1999, Fendt and Fanselow 1999, Reilly 1999), and the relatively high degree of collateralized input to the CEAm and BSTvl from these regions may contribute to the acquisition of newly learned behaviors through synchronized activity.

The PSTN and ILA stood out as having relatively few collateralized inputs to the CEAm and BSTvl, despite abundant retrograde labeling from both target regions. The PSTN and ILA are strongly implicated in providing descending control over autonomic functions (Hurley, Herbert et al. 1991, Fisk and Wyss 2000, Heidbreder and Groenewegen 2003, Goto and Swanson 2004, Ciriello, Solano-Flores et al. 2008). Transneuronal viral tracing of preautonomic circuits has revealed distinct parallel descending projections to specific visceral targets (Sved, Cano et al. 2001). The presence of relatively few collateralized inputs from the PSTN and ILA to the

CEAm and BSTvl suggests that neurons in these regions may contribute to differential control over autonomic output to different visceral targets.

Rostrocaudal distribution of CEA_m- and BST_{vl}-projecting neurons within the NTS and PVT

Although the NTS and PVT contained overlapping distributions of CEA_m- and BST_{vl}-projecting neurons, rostrocaudal analysis revealed differing distributions of where these neurons were located within each nucleus. Within the NTS, BST_{vl}-projecting neurons were most prevalent at the level of the area postrema, while the largest number of CEA_m-projecting neurons peaked just rostral to the area postrema (Fig. 3a), which also contained the largest number of neurons with collateralized axons to both the CEA_m and BST_{vl}. Because vagal sensory inputs to the NTS terminate in a generally viscerotopic pattern (Kalia and Sullivan 1982, Altschuler, Bao et al. 1989), our findings of differing distributions of CEA_m- vs. BST_{vl}-projecting NTS neurons suggests differences in the type of viscerosensory feedback that may be relayed to the CEA_m vs. the BST_{vl}.

Within the PVT, BST_{vl}-projecting neurons were significantly more prevalent within the rPVT compared to the cPVT, consistent with a previous qualitative report of the distribution of BST_{vl}-projecting neurons within the PVT (Shin, Geerling et al. 2008). Conversely, CEA_m-projecting neurons were significantly more prevalent in the cPVT than the rPVT (Fig. 10a). Interestingly, the cPVT also provides dense axonal input to corticotrophin-releasing factor (CRF) neurons of the CEAl and BSTdl (Li and Kirouac 2008). A series of experiments have found that cPVT lesions affect behavioral and endocrine responses to chronic stress (Bhatnagar and Dallman 1998, Bhatnagar, Huber et al. 2002, Bhatnagar, Huber et al. 2003, Jaferi, Nowak et al. 2003), while the rPVT appears to play a role in light-induced entrainment of circadian rhythms

(Salazar-Juárez, Escobar et al. 2002). Further investigation of the differential PVT input to the CEAm and BSTvl is needed to understand how these inputs may contribute to unique functions of the two limbic regions.

Medial prefrontal cortical projections to the BSTvl

Lesion studies of the medial prefrontal cortex (mPFC) have revealed contrasting functional roles for the PL vs. ILA in regulating the hypothalamic-pituitary-adrenal (HPA) neuroendocrine stress axis, suggesting that the ILA promotes HPA axis activity while the PL suppresses it (Radley, Arias et al. 2006). Two recent reports have directed focus on the BST as a relay for PL cortical inhibitory influence over the HPA axis (Radley, Gosselink et al. 2009, Radley and Sawchenko 2011). Within the BSTvl, the fusiform and dorsomedial BST subnuclei contain GABA-ergic neurons that innervate neuroendocrine neurons within the medial parvocellular subregion of the paraventricular nucleus of the hypothalamus (PVN) (Cullinan, Herman et al. 1993, Cullinan, Ziegler et al. 2008). In the present study, however, almost all of the mPFC neurons that project to the BSTvl were located within the ILA, in agreement with a previous retrograde tracing study of BSTvl inputs (Shin, Geerling et al. 2008) and anterograde tracing studies of neural projections from the ILA and PL (Sesack, Deutch et al. 1989, Hurley, Herbert et al. 1991, Chiba, Kayahara et al. 2001, Vertes 2004).

Conclusions

The CEA and lateral BST have been described as constituent parts of an anatomical-functional macrosystem known as the ‘central extended amygdala’ (de Olmos and Heimer 1999). Our new findings challenge this view by revealing the anatomical organization of common and distinct sets of neural inputs to two discrete subregions of this proposed macrosystem, the CEAm

and BSTvl. Cortical and sensory systems primarily target the CEAm, while input from behaviorally-relevant motor systems and viscerosensory nuclei relaying interoceptive feedback from the body primarily target the BSTvl. Neurons with collateralized axonal inputs to both the CEAm and BSTvl are located within nearly all of the brainstem and forebrain regions that provide axonal input to either structure. The incidence of collateralization varies across brain regions, but is relatively minor compared to the number of neurons that provided distinct input to either the CEAm or BSTvl. Taken together, our new findings suggest an anatomical framework for information processing that may contribute to a better understanding of how CEA and BST circuits participate in organizing complex behavioral responses to cognitive and physiological challenges.

3.0 DISTINCT MULTISYNAPTIC CIRCUITS WITHIN THE MEDIAL AND CENTRAL EXTENDED AMYGDALA OF THE RAT

3.1 INTRODUCTION

The bed nucleus of the stria terminalis (BST) is a heterogeneous limbic forebrain structure comprising 12 subnuclei with distinct cytoarchitecture and anatomical connectivity. The BST has become a primary focus of research on the neural substrates of anxiety, due to its expression of anxiogenic neuropeptides (i.e., calcitonin gene-related peptide and corticotrophin-releasing hormone, CRH), and its anatomical connectivity with stress-responsive brain regions, particularly the amygdala (Lungwitz, Molosh et al. , Dong, Petrovich et al. 2001, Walker, Toufexis et al. 2003, Duvarci, Bauer et al. 2009, Hammack, Guo et al. 2009, Walker, Miles et al. 2009, Sink, Walker et al. 2011, Sink, Walker et al. 2012, Yassa, Hazlett et al. 2012). The amygdala and BST are densely interconnected, and have been considered by some to be distributed parts of the same structure, termed the ‘extended amygdala’ (Alheid and Heimer 1988, de Olmos and Heimer 1999, Zahm 2006). The concept of the extended amygdala has generated interest in unraveling the complex neuroanatomy and subnuclear connectivity of the amygdala and BST in order to better understand their structural and functional relationship.

The efferent projections of various amygdalar and BST subnuclei have been examined by Dong and colleagues in a series of PHA-L anterograde tracing studies (Dong, Petrovich et al.

2000, Dong, Petrovich et al. 2001, Dong and Swanson 2003, Dong and Swanson 2004, Dong and Swanson 2004, Dong and Swanson 2006, Dong and Swanson 2006). In general, connections between the amygdala and BST are topographically organized such that the anterolateral group of BST subnuclei (algBST) is reciprocally connected with the central nucleus of the amygdala (CEA), and the anteromedial (amgBST) and posterior (pBST) groups of BST subnuclei are reciprocally connected with the medial nucleus of the amygdala (MEA; Fig. 16). These topographically organized, reciprocal connections suggest the presence of discrete channels for information processing between specific subregions of the amygdala and BST. However, the algBST, amgBST, and pBST are interconnected with each other in a complex manner (Fig. 17; summarized from (Dong, Petrovich et al. 2000, Dong, Petrovich et al. 2001, Dong and Swanson 2003, Dong and Swanson 2004, Dong and Swanson 2004, Dong and Swanson 2006, Dong and Swanson 2006)), making it both possible and likely that BST subnuclei directly connected with the CEA also exert indirect influence over the MEA, and vice-versa, via circuits within the BST. Indeed, several BST subnuclei have projections that cross the topographical border that separates those that innervate the CEA from those that innervate the MEA (red/blue border in Fig. 17). Thus, all BST subnuclei might contribute either directly or indirectly to the activity of neurons within both the MEA and CEA. To determine whether individual BST subnuclei provide direct and/or indirect input to the MEA and CEA, a multisynaptic tracing approach is needed.

Traditional monosynaptic retrograde and anterograde tracers have limited utility for defining multisynaptic sequential connections among 3 or more regions. In addition, in order to confirm the presence of synaptic connections between 2 brain regions, traditional tracers must be combined with electron microscopy to identify synaptic contacts between labeled profiles. A powerful alternative approach involves the use of neurotropic viral tracers, such as pseudorabies

virus (PRV), which self-amplify and transport across synapses within multisynaptic circuits (Card 1998, Card 1998, Card, Enquist et al. 1999, Aston-Jones and Card 2000, Aston-Jones, Chen et al. 2001, Card and Enquist 2001, Enquist and Card 2003, Aston-Jones, Zhu et al. 2004). The attenuated Bartha strain of PRV (PRV-Bartha) is especially useful for transsynaptic tracing due to its reduced virulence and its restricted transsynaptic transport in the retrograde direction.

Interpreting the synaptic connectivity of neurons within distributed circuits based on transneuronal viral labeling patterns is facilitated by examining the spread of viral infection across several post-inoculation intervals (Card 1998, Aston-Jones and Card 2000). However, after moderate to long post-inoculation intervals during which time the virus has undergone several rounds of replication and transsynaptic transport, it can become difficult to interpret the origin of viral labeling for any given brain region. In addition, the rapid uptake and transport of virions away from the central injection site can make it difficult to accurately identify these sites in fixed tissue sections. Previous studies have demonstrated that the retrograde tracer cholera toxin subunit B (CTB) can be successfully combined with PRV to discriminate neurons with direct (i.e., first-order) inputs to central injection sites from 2nd- or 3rd-order, transsynaptically infected neurons, and CTB also facilitates accurate assessment of the viral injection site (Chen, Yang et al. 1999, Aston-Jones and Card 2000). When used together, monosynaptic tracers and transsynaptic viral tracers can identify neurons that are directly or indirectly connected to a given brain region through direct and multisynaptic pathways.

Experiments described in the present report use both monosynaptic and transsynaptic tracers to quantitatively dissect the distinct multisynaptic BST circuits that provide input to the medial CEA (CEAm) vs. the anterodorsal (MEAad) or posterodorsal MEA (MEApd). In the first set of experiments, we iontophoresed a cocktail of monosynaptic anterograde and retrograde

neural tracers (i.e., biotinylated dextran amine, BDA, and Fluorogold, FG, respectively) into the CEAm, MEAd, or MEApd of adult male rats to confirm previous reports of topographically-organized reciprocal direct connections between the amygdala and BST. Additionally, quantification of retrograde labeling will determine the distribution of first-order inputs within each BST subnucleus. In the second set of experiments, we injected PRV or a mixture of PRV and CTB into the same three amygdala subnuclei. Rats were sacrificed either 48 or 60 hours post-inoculation to determine the distribution and number of first- or second/third-order infected neurons in each BST subnucleus. Data-based statistical correlations and network analyses revealed distinct multisynaptic BST circuits that provide input to the CEAm, MEAd, and/or MEApd, and subnuclear differences in the relative strength of intra-BST connections.

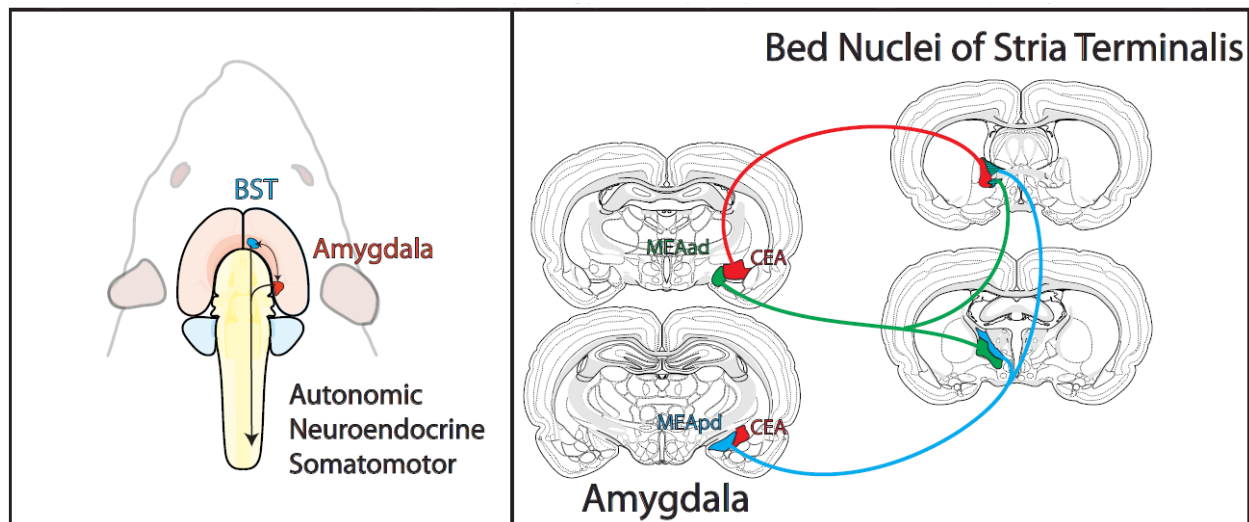


Figure 16. The amygdala and BST coordinate autonomic, neuroendocrine, and somatomotor responses to psychological and physiological stressors (left). Results from anterograde tracing studies support the existence of topographically-organized reciprocal connections between amygdalar and BST subnuclei (right). The CEA is reciprocally connected to the anterolateral group of BST subnuclei (algBST), while the MEAd and MEApd are bidirectionally connected to complementary subregions of the posterior BST (pBST) and the anteromedial BST subnuclei group (amgBST).

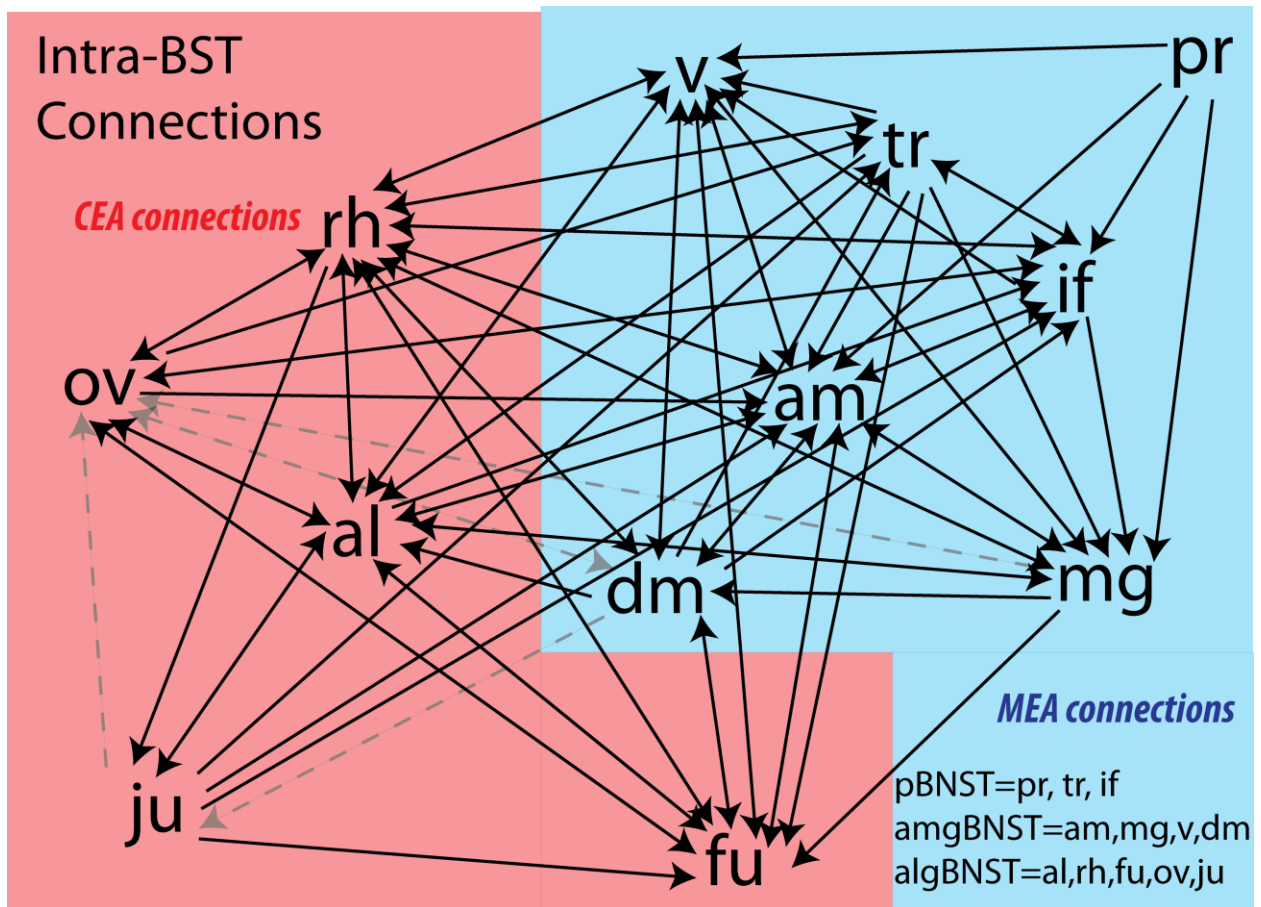


Figure 17. Anterograde tracing of efferent projections from neurons within individual BST subnuclei reveals robust interconnectivity within the BST network. BST subnuclei with inputs to the CEA are shown on a red background, whereas BST subnuclei with inputs to the MEA are shown on a blue background (data summarized from Dong and Swanson, summarized from (Dong, Petrovich et al. 2000, Dong, Petrovich et al. 2001, Dong and Swanson 2003, Dong and Swanson 2004, Dong and Swanson 2004, Dong and Swanson 2006, Dong and Swanson 2006)). While the discrete topographic connections of the BST with separate amygdalar subregions suggest the presence of separate pathways for information processing (Fig. 16), the rich intra-BST connectivity suggests that integration may occur across these boundaries, as indicated by connection lines that cross the red/blue border). Grey dashed lines indicate connections which were sparse or the presence of boutons was unclear.

3.2 MATERIALS AND METHODS

Animals

Adult male Sprague Dawley rats (225-250g BW; Harlan Laboratories, Indianapolis, IN, USA) were individually housed in a controlled environment (20-22°C, 12:12 hr light:dark cycle; lights off at 1900 hr) with *ad libitum* access to water and pelleted chow (Purina 5001). Viral tracing experiments were performed in an approved Biosafety Level 2+ facility, where virally-infected rats remained after surgery. All experiments were conducted in accordance with the NIH *Guide for the Care and Use of Laboratory Animals* and were approved by the University of Pittsburgh IACUC, Recombinant DNA Committee, and Division of Environmental Health and Safety.

Iontophoretic Delivery of Monosynaptic Tracers

Rats were anesthetized by isoflurane inhalation (Halocarbon Laboratories, River Edge, NJ; 1-3% in oxygen) and positioned into a Kopf stereotaxic device. A pulled glass micropipette tip (approximately 1 mm in length with 20 μm outer tip diameter) containing a 1:1 tracer cocktail of 1% Fluorogold (FG; Fluorochrome, Denver, CO) in 0.1M cacodylic acid and 5% biotinylated dextran amine (BDA; MW 10,000; Invitrogen) in 0.9% saline was prepared and connected to a current source (Stoelting) via a copper conductance wire. The glass pipette tip was lowered into the brain at coordinates targeting either the CEAm (mm from bregma: 2.1 posterior, 3.9 lateral, 8.0 ventral), MEAad (mm from bregma: 1.8 posterior, 2.8 lateral, 8.8 ventral), or MEApd (mm from bregma: 2.4 posterior, 3.5 lateral, 8.4 ventral). During the descent of the glass pipette into the brain, a -1.5 μA retaining current was used to minimize molecular diffusion of tracer. When the tip of the pipette reached the target site, the retaining current was turned off and the tracer cocktail was iontophoresed using a 7s on/off pulsed current of +5 μA for 10 min. After tracer

delivery, the pipette was withdrawn and the skin closed with stainless steel clips. Rats were injected subcutaneously with 0.5 ml of a mild analgesic (Ketofen; 2 mg/kg) and were returned to their cages after regaining consciousness and full mobility.

Multisynaptic Viral Tracing using Pseudorabies Virus (PRV)

Rats were anesthetized by isoflurane inhalation (Halocarbon Laboratories, River Edge, NJ; 1-3% in oxygen) and positioned into a Kopf stereotaxic device. A pulled glass pipette tip was attached to the stereotaxic arm and the back end of the glass pipette was soldered to a polyethylene tube connected to a PicoPump (World Precision Instruments, Sarasota, FL). The glass pipette was back-filled with solution containing PRV-263 (3.4×10^8 pfu / mL) or a 3:1 mixture of PRV-263 and 0.25% solution of cholera toxin subunit B (CTB; List Biological Labs, Campbell, CA, USA) diluted in deionized water. PRV-263 is a recombinant strain of pseudorabies virus carrying the Brainbow 1.0L cassette with similar infection time course to its parent strain, PRV-Bartha. PRV-263's recombinant properties (Card, Kobiler et al. 2011, Card, Kobiler et al. 2011) were not utilized in the present study. After loading, the glass pipette was immediately lowered into the brain targeting the same coordinates used in iontophoresis experiments. The pipette tip was left in place for 3 min at the target site before injecting 100nl of PRV-263 or PRV-263/CTB over 10 min (10 nl/min). Following the injection, the pipette was left in place for 3 min before being removed from the brain. The incision was closed with stainless steel clips and rats were injected subcutaneously with 0.5 ml of Ketofen before being returned to their home cages in the BSL 2 laboratory where they remained for the rest of the experiment.

Histology

After an appropriate survival time (one week after tracer iontophoresis; 48 or 60 hr after PRV injections), rats were anesthetized with an overdose of sodium pentobarbital (Vortech Pharmaceuticals, Dearborn, MI) and then transcardially perfused with 0.15M NaCl followed by 500 ml of fixative solution containing 4% paraformaldehyde, 1.4% lysine, and 0.2% sodium metaperiodate in 0.1 M phosphate buffer. Brains were post-fixed *in situ* overnight at 4°C, and then removed from the skull and cryoprotected in 20% sucrose solution before sectioning. A freezing stage microtome was used to cut coronal brain sections with a thickness of 35 µm. Sections were collected sequentially into 6 adjacent sets (sections spaced 210 µm apart) and stored in cryopreservant (Watson, Wiegand et al. 1986) at -20°C for later immunohistochemical processing.

Immunohistochemistry

Tissue sections from rats that received dual iontophoretic delivery of tracers (FG/BDA or PRV/CTB) were processed for triple immunofluorescence to localize both tracers as well as calbindin 28k, expressed by a subpopulation of GABA neurons within the BST. Following treatment with 0.5% sodium borohydride, tissue sections from cases labeled with FG/BDA were incubated for 48 hr in buffer (0.1M sodium phosphate, pH 7.4) containing 0.3% Triton-X100, 1% normal donkey serum, rabbit anti-FG (1:3,000; Millipore, Temecular, CA), and mouse anti-calbindin 28k (1:250; Sigma-Aldrich, St. Louis, MO). Next, tissue sections were rinsed and then incubated for 24 hr in a mixture of Alexa Fluor 647-conjugated donkey anti-rabbit IgG, Alexa Fluor 488-conjugated donkey anti-mouse IgG, and Cy3-conjugated streptavidin (1:500 each; Jackson Immunochemicals, West Grove, PA).

Tissue sections from rats co-injected with PRV/CTB were processed for triple immunofluorescence following a protocol similar to that described above. Sections were incubated in a primary antibody cocktail comprising rabbit anti-PRV (either Rb132 or Rb133, 1:2000), goat anti-CTB (1:5,000, List Biological Labs, Campbell, CA), and mouse anti-calbindin 28k. Rb132 and Rb133 antibodies were generated against acetone-inactivated virus and specifically recognize viral epitopes present within infected neuronal nuclei and somatodendritic compartments (Card and Enquist 2001). After rinsing, sections were incubated in a cocktail of fluorescently tagged secondary antisera (1:500 each, Jackson Immunochemicals; Cy3-conjugated donkey anti-goat IgG; Alexa Fluor 488-conjugated donkey anti-mouse IgG, and Alexa Fluor 647-conjugated donkey anti-rabbit IgG).

Cases injected with PRV only were processed for dual immunoperoxidase labeling of PRV and the neuroanatomical marker NeuN, in order to plot the distribution of infected (i.e., PRV-positive) BST neurons using Stereoinvestigator mapping software. Sections were treated with 0.5% sodium borohydride and 30% hydrogen peroxide and subsequently incubated overnight in Rb132 or Rb133 (1:20,000). Immunoperoxidase labeling of virally-infected neurons was achieved using biotinylated donkey anti-rabbit IgG (1:500; Jackson Immunochemicals, West Grove, PA) followed by Vectastain ABC Elite reagents (Vector Laboratories, Burlingame, CA) and a nickel-intensified diaminobenzidine (DAB)-hydrogen peroxidase reaction to produce a black immunoprecipitate identifying infected neurons. NeuN immunoreactivity was subsequently revealed after sequentially incubating sections in mouse anti-NeuN (1:5000, Millipore, Temecula, CA), biotinylated donkey anti-mouse IgG (1:500; Jackson Immunochemicals, West Grove, PA), and Vectastain ABC Elite reagents, followed by a non-intensified brown DAB immunoperoxidase reaction to reveal NeuN labeling.

Immunoperoxidase- or immunofluorescence-labeled tissue sections were rinsed in buffer and mounted onto Superfrost Plus microscope slides (Fisher Scientific), allowed to dry overnight, dehydrated and defatted in graded ethanols and xylene, and coverslipped using Cytoseal 60 (VWR).

Identification of BST Subnuclei

A critical aspect of this study is the identification and parcellation of the BST subnuclei. The BST nomenclature we use are delineated within the Swanson rat brain atlas (Swanson 2004) and defined by anterograde tracing studies using discrete injections of PHA-L into each BST subnucleus (Dong and Swanson 2006) that are built upon the foundation of prior cyto- and chemo-architectonic studies of the BST and its surrounding region (Ju and Swanson 1989, Ju, Swanson et al. 1989). However, the BST sections represented within the Swanson atlas are too infrequent (50-320 μm between sections, 40 μm section thickness) to match experimental tissue sections and identify BST subnuclei rostrocaudally. To more reliably identify BST subnuclei when analyzing experimental tissue sections, we generated a BST reference atlas using a series of Klüver-Barrera-stained paraffin-embedded tissue sections (12 μm section thickness, 60 μm apart) generated by Dr. J. Patrick Card to reveal BST cytoarchitecture and myelinated fiber pathways (Fig. 18). Due to the high section frequency of this reference atlas, experimental tissue sections can be closely matched to the appropriate rostrocaudal level in the atlas. The determination of BST boundaries were guided by the most closely matching reference atlas section, and adjusted as needed based on the interpretation of either the NeuN cytoarchitecture in peroxidase-labeled tissue sections or the distribution of calbindin 28k (in immunofluorescent tissue sections). Calbindin 28k expression is a useful marker of BST boundaries, as it is highly

expressed within regions adjacent to the BST (i.e. ventrolateral septum, parastrial nucleus, ventromedial striatum) as well as specific BST subnuclei (BSTpr and BSTju).

Imaging and Quantitative Data Analysis

Cases with accurate tracer delivery sites were analyzed to determine the number of retrogradely-labeled neurons within individual BST subnuclei. Tissue series labeled for NeuN and PRV immunoperoxidase were used to create maps of the rostrocaudal distribution of infected BST neurons. The borders of the BST subnuclei were determined by comparing cytoarchitecture revealed by NeuN labeling to the Klüver-Barrera-stained tissue sections previously discussed. The distribution of infected neurons across 6 BST sections was plotted at 40x magnification using a Nikon light microscope connected to a computerized data acquisition system (StereoInvestigator; MBF Bioscience).

Tissue sections processed for triple immunofluorescent labeling (from both tracer iontophoresis and PRV experiments) were digitally photographed using an Olympus photomicroscope equipped with a Hamamatsu digital camera (Hamamatsu Photonics, Hamamatsu, Japan) and filters to visualize Cy2, Cy3, and Cy5 fluorescence in the green, red, and blue color channels, respectively. Using a 10x objective, photographs of the entire BST in each of 6 rostrocaudal sections were obtained by taking overlapping images (6-21 images depending on the size of the BST region). Images were transferred to a computer and merged into one high-resolution panoramic image using Adobe Photoshop software. With reference to the Klüver-Barrera-stained set of sections referred to above, the borders of the BST and its subnuclei were drawn onto the Photoshop image. Single- (PRV-positive) and double-labeled (PRV/CTB-positive) neurons within each subnucleus were visualized separately using the red and blue color channels, and were marked and quantified using Photoshop's count tool.

The number of FG-positive or PRV-positive and PRV/CT-positive neurons within each individual BST subnucleus was totaled across all 6 BST sections. Within each case, the proportion of labeling within each BST subnucleus was calculated using the formula $[(\text{number of labeled-neurons within a BST subnucleus}) / (\text{the number of labeled neurons in the entire BST}) * 100]$ to normalize between-animal experimental variability in tracer injection site size and tracer uptake. Since the distribution of retrogradely-labeled neurons generated by iontophoretic delivery of FG was not significantly different from CTB-labeled neurons produced from PRV/CTB so-injection, CTB labeling data was treated as independent cases and grouped with FG cases as ‘monosynaptic labeling’ (discussed in Results section). Statistical comparisons of the mean proportion of labeling within BST subnuclei for each injection site (CEAm, MEAad, and MEApd) were performed using one-way ANOVA with transsynaptic passage of the tracer (monosynaptic labeling vs. 48 hr vs. 60 hr. viral labeling) as the independent variable, followed by post-hoc t tests. Within each experimental injection site group, cross correlation analyses were performed to determine the relationship of retrograde labeling between individual BST subnuclei at each step of transsynaptic passage of the tracer. Differences were considered significant when $P < 0.05$.

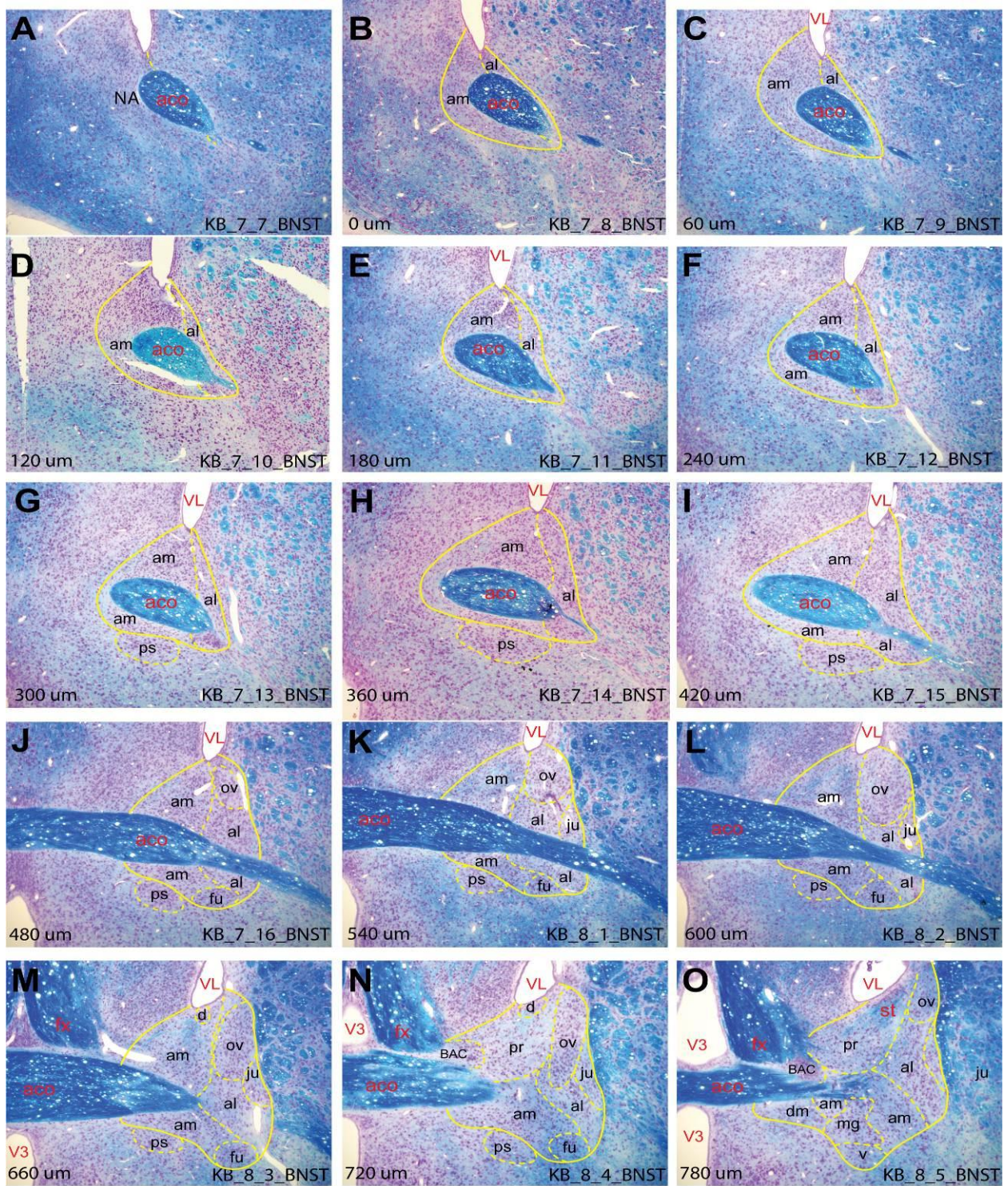
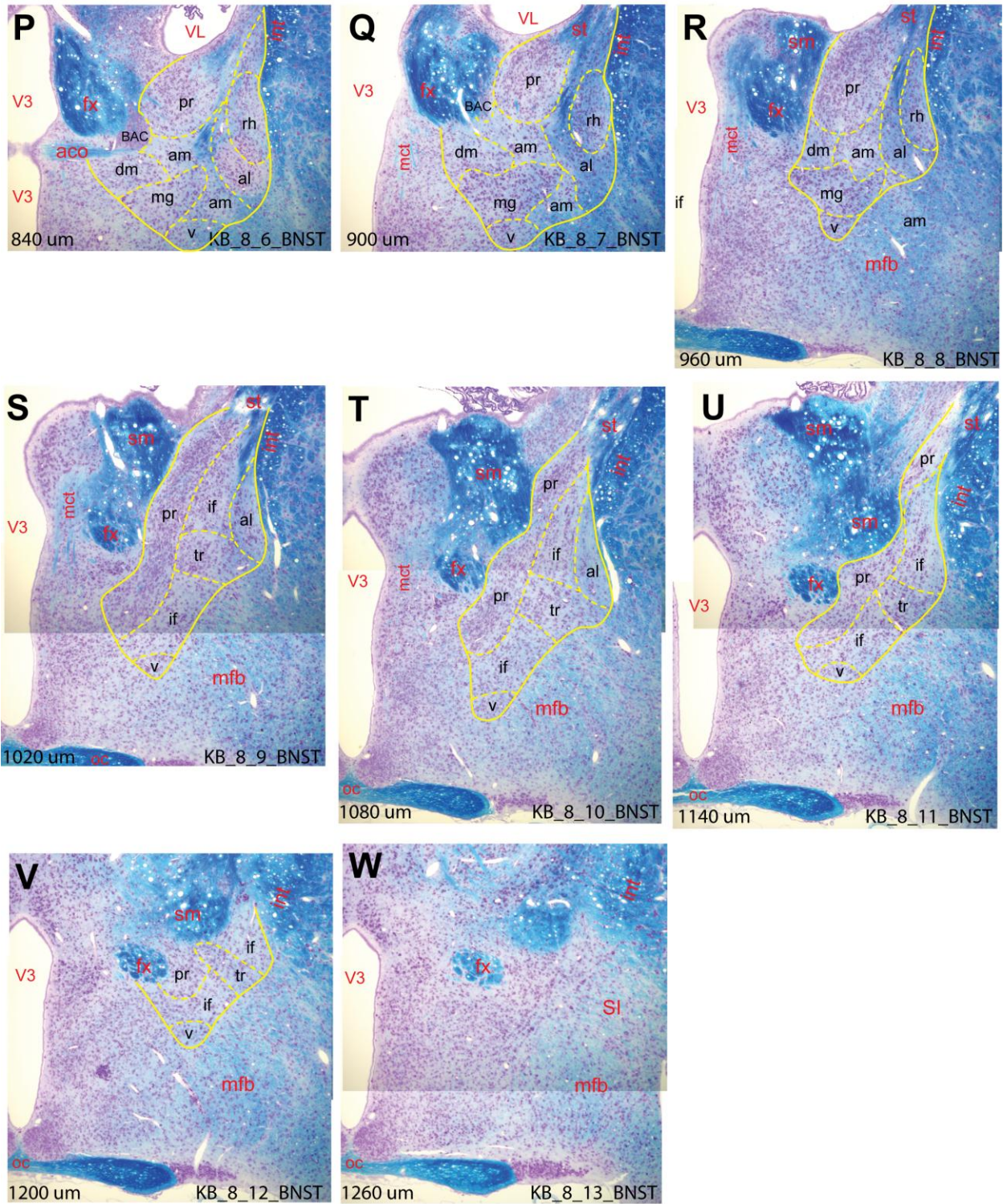


Figure 18. Rostral sections from Klüver-Barrera-stained BST reference atlas. Klüver-Barrera staining reveals BST cytoarchitecture in pink and myelinated fiber tracts in blue. Tissue sections are 20 μm thick, with a represented sectioning frequency of 60 μm . Rostrocaudal levels (lower left corner in each image) are in reference to the most rostral BST level (B, 0 μm). The location of BST subnuclei, as well as the parastriate nucleus (ps) and bed nucleus of the anterior commissure (BAC), are labeled in black while fiber tracts and ventricles are labeled in red (see abbreviations list).



(continued from Figure 18.) Caudal sections from Klüver-Barrera stained BST reference atlas.

Table 2. Experimental animals divided into groups based on injection site and tracing approach. Case numbers are listed in the columns. 21 rats were injected with PRV/CTB mixture, generating both monosynaptic and viral labeling data. These cases (shaded cells) are listed in both the mono labeling group and one of the PRV groups (see Results). Final group sizes for each tracer group and injection site are indicated at the bottom of each column. Results from 45 rats produced 66 sets of data that were analyzed in this study.

Mono			48 hr			60 hr			<u>Total</u>
CEAm	MEAad	MEApd	CEAm	MEAad	MEApd	CEAm	MEAad	MEApd	
11-449	11-450	12-34	11-291	11-314	11-313	12-15	12-46	12-48	n = 66
11-473	11-537	12-35	11-293	12-168	11-108	12-16	12-47	12-234	
12-170	12-168	12-37	11-311	12-169	12-171	12-17	12-195	12-290	
12-240	12-169	12-171	11-185	12-324	12-172	12-240	12-252		
12-289	12-324	12-172	11-186		12-173	12-289	12-253		
12-291	12-195	12-173	11-187			12-291	12-254		
12-292	12-252	12-234	11-188			12-292	12-255		
12-294	12-253	12-290	11-312			12-294	12-256		
	12-254		12-170				12-235		
	12-255								
	12-235								
	12-256								
n = 8	n = 12	n = 8	n = 9	n = 4	n = 5	n = 8	n = 9	n = 3	

3.3 RESULTS

Iontophoretic injections of FG/BDA tracer cocktail into amygdalar subnuclei generated retrogradely-labeled (i.e., FG-positive) neurons overlapping anterogradely-labeled (i.e., BDA-positive) terminal fields within the BST (Figs. 19, 20, 21). BST labeling was topographically distributed after tracer cocktail delivery into the CEAm, MEAad, and MEApd. CEAm-targeted delivery sites generated dense anterograde and retrograde labeling within the algBST (Fig. 19), while MEAad- and MEApd-targeted sites generated varying densities of anterograde and retrograde labeling within specific subregions of the amgBST and pBST (Figs. 20 and 21). In cases with MEAad tracer delivery, anterograde and retrograde labeling was localized within more lateral regions of the BSTpr, and also was distributed within the BSTif, BSTtr, and BSTam (Fig. 20). Conversely, in cases with MEApd tracer delivery, retrograde and anterograde labeling was concentrated within the most medial aspect of the BSTpr that contains calbindin-positive neurons, with additional light labeling observed within the BSTam (Fig. 21).

Statistical analyses were performed to quantitatively compare retrograde labeling patterns among the three amygdalar tracer delivery sites (i.e., CEAm vs. MEAad vs. MEApd). First, we examined whether mixing CTB with PRV altered the pattern of first-order CTB retrograde labeling achieved within the BST compared to retrograde FG labeling achieved after iontophoretic delivery of FG mixed with BDA. An independent samples t-test revealed that iontophoretic delivery of FG/BDA ($n = 7$) resulted in significantly more first-order FG-positive BST neurons compared to the number of first-order CTB-positive neurons labeled after co-injection of PRV/CTB ($n = 21$; 577 ± 62 FG-labeled neurons vs. 117 ± 27 PRV/CTB dual-labeled neurons, $P < 0.001$). However, the distribution of retrogradely-labeled BST neurons in both tracer groups was similar. There were no significant tracer group differences in the

proportion of total BST neurons that occupied the amgBST ($P = 0.06$), algBST ($P = 0.83$), or pBST ($P = 0.30$). Thus, proportional labeling data from both tracer groups were combined into a single monosynaptic tracer group (Table 2; Fig. 22). There also were no significant differences in the total number of PRV-positive BST neurons counted in rats that received amygdalar injections of PRV/CTB cocktail vs. those injected with PRV alone ($P = 0.98$ for the 48 hr post-inoculation group; $P = 0.26$ for the 60 hr post-inoculation group).



Figure 19. Retrograde and anterograde labeling in the BST after monosynaptic FG/BDA iontophoresis or PRV/CTB co-injection into the CEAm. Sections representing six rostrocaudal levels were used to quantify retrograde labeling. Calbindin 28k (green) was used as a neuroanatomical marker due to its unique distribution within the BST. Top row: Iontophoretic delivery of FG/BDA cocktail into the CEAm produced dense BDA anterograde labeling (red) and FG retrograde labeling (blue) in the algBST. Middle row: Co-injection of PRV/CTB into the mCEA after 48 hr survival time revealed a similar distribution of CTB monosynaptic retrograde labeling (red) and PRV-labeling (blue). Bottom row: The proportion of PRV labeling after 60 hr survival time was significantly increased within the amgBST and pBST (for quantification, see Figs. 22, 23). Scale bars = 100 μ m.



Figure 20. Retrograde and anterograde BST labeling after monosynaptic FG/BDA iontophoresis or PRV/CTB co-injection into the MEAad. Sections representing six rostrocaudal levels were used to quantify retrograde labeling. Calbindin 28k (green) was used as a neuroanatomical marker to help delineate BST subnuclear boundaries. Top row: Iontophoretic delivery of FG/BDA cocktail into the MEAad produced dense BDA anterograde labeling (red) and FG retrograde labeling (blue) in the amgBST and pBST. Anterograde and retrograde algBST labeling was sparse, especially within the BSTov. A similar distribution of CTB monosynaptic retrograde labeling (red) and PRV-labeling (blue) was observed after co-injection of PRV/CTB into the MEAad at 48 hr (middle row) and 60 hr (bottom row) survival times (for quantification, see Figs. 22, 23). Scale bars = 100 μ m.



Figure 21. Retrograde and anterograde BST labeling after monosynaptic FG/BDA iontophoresis or PRV/CTB co-injection into the MEApd. Sections representing six rostrocaudal levels were used to quantify retrograde labeling. Calbindin 28k (green) was used as a neuroanatomical marker to help delineate BST subnuclear boundaries. Top row: Iontophoretic delivery of FG/BDA cocktail into the MEApd produced dense BDA anterograde labeling (red) and FG retrograde labeling (blue) in the pBST, specifically the BSTpr, with lighter labeling in the BSTam. This labeling distribution was distinct from labeling in more lateral aspects of the BSTpr and BSTam after MEAad injections (see Fig. 20). Middle row: Co-injection of PRV/CTB into the MEApd after 48 hr survival time revealed a similar distribution of CTB monosynaptic retrograde labeling (red) and PRV-labeling (blue). Bottom row: After 60 hr survival, the proportion of PRV-labeling was significantly increased within the amBST, specifically the BSTam (for quantification, see Figs. 22, 23). Scale bars = 100 μ m.

Retrograde BST labeling after tracer delivery into the CEAm

Quantification of monosynaptic retrograde labeling across BST subnuclear groups after CEAm tracer delivery revealed that approximately 20% of retrogradely-labeled BST neurons were located within the pBST, ~16% were located within the amgBST, and ~64% were located within the algBST (Fig. 23). One-way ANOVA confirmed that these BST subnuclear labeling distribution patterns were significantly different than patterns achieved in rats after tracer delivery into the MEAad or MEApd, as described below [pBST: $F(2,25) = 53.37, P < 0.001$; amgBST: $F(2,25) = 15.60, P < 0.001$; algBST: $F(2,25) = 131.15, P < 0.001$].

More BST neurons were labeled 48 and 60 hr after PRV injections into the CEAm compared to the number of neurons labeled after monosynaptic CEAm tracer delivery, with more PRV labeling present at 60 hr vs. 48 hr post-inoculation (Fig. 22). One-way ANOVA confirmed a significant effect of tracer group (i.e., monosynaptic vs. 48 hr PRV vs. 60 hr PRV) on the total number of labeled BST neurons [$F(2,22) = 18.02, P < 0.001$] (see Fig.22 for post-hoc comparisons). However, despite increased numbers of PRV-positive BST neurons in the 48 hr post-inoculation group compared to the number of retrogradely-labeled neurons in rats with monosynaptic tracer delivery, the subnuclear distribution of labeled BST neurons was similar between groups (pBST: $26\% \pm 3$ vs. $20\% \pm 3$; amgBST: $15\% \pm 1$ vs. $16\% \pm 2$; algBST: $59\% \pm 2$ vs. $64\% \pm 4$; $P > 0.05$ for each subnuclear comparison). The proportion of total PRV retrograde labeling located within the pBST ($32\% \pm 3$) and amgBST ($22\% \pm 1$) was significantly increased in rats killed 60 hr post-PRV ($P < 0.05$ for between-group comparisons in both regions), whereas the proportion of total retrograde labeling located within the algBST was significantly decreased 60 hr post-PRV ($46\% \pm 3, P < 0.05$ for both between-group comparisons).

To identify which subnuclei were responsible for driving the altered distribution patterns of BST labeling observed in PRV 60 hr cases, separate one-way ANOVAs were performed to assess the proportion of total BST labeling present within each of 12 individual BST subnuclei (Figs. 24, 25, 26). Tracer group (i.e., monosynaptic vs. PRV 48 hr vs. PRV 60 hr) had a significant effect on the proportion of labeled neurons within just 3 of the 12 BST subnuclei, i.e., the BSTpr [$F(2,22) = 8.70, P = 0.02$], the BSTal [$F(2,22) = 14.39, P < 0.001$], and the BSTam [$F(2,22) = 16.46, P < 0.001$]. Post-hoc tests determined that the proportion of retrograde labeling within the BSTpr and BSTam of PRV 60 hr cases ($19\% \pm 3$ and $18\% \pm 1$, respectively) was significantly increased compared to both monosynaptic ($8\% \pm 1$ and $12\% \pm 1$) and PRV 48 hr cases ($13\% \pm 2$ and $11\% \pm 1, P < 0.03$). Conversely, significantly smaller proportions of total retrograde labeling were present within the BSTal of PRV 48 and 60 hr cases ($27\% \pm 2, 24\% \pm 2$) compared to labeling in monosynaptic cases ($38\% \pm 2; P < 0.001$ for monosynaptic vs. PRV 48 hr and vs. PRV 60 hr). Although the one-way ANOVA result for the BSTov did not reach significance, t-comparisons revealed a significant decrease in the proportion of total retrograde labeling within the BSTov of PRV 60 hr cases compared to PRV 48 hr cases ($25\% \pm 3$ vs. $15\% \pm 2, P < 0.05$).

Correlation analyses were performed to determine whether the proportion of BST labeling present within individual BST subnuclei was associated with the proportion of labeling present within other BST subnuclei in CEAm-injected cases (Table 3). BSTpr and BSTam labeling proportions were not significantly correlated with each other, but labeling proportions within both the BSTpr and BSTam were negatively correlated with labeling proportions in the BSTal and BSTov. Labeling proportions within the BSTov also were negatively correlated with

labeling proportions in the BSTif and BSTtr, but were positively correlated with labeling proportions within the BSTfu (Table 3).

Retrograde BST labeling after tracer delivery into the MEAad

Quantification of monosynaptic retrograde labeling within BST subnuclear groups in rats after MEAad-targeted tracer delivery revealed that approximately 56%, ~33%, and ~11% of retrogradely-labeled neurons were located within the pBST, amgBST, and algBST, respectively (Fig. 23). One-way ANOVA revealed no significant effect of tracer group on the proportion of retrograde labeling within the pBST [$F(2,22) = 0.29, P = 0.75$], amgBST [$F(2,22) = 1.41, P = 0.27$], algBST [$F(2,22) = 0.20, P = 0.82$].

Similar to results in CEAm-injected rats, one-way ANOVA confirmed a significant effect of tracer group on the total number of retrogradely-labeled BST neurons in rats after MEAad injection [$F(2,22) = 36.39, P < 0.001$] (Fig. 22). Post-hoc tests revealed significantly greater numbers of retrogradely-labeled BST neurons within the 48 hr (1288 ± 440 PRV-labeled neurons) and 60 hr PRV groups (3500 ± 458 PRV-labeled neurons) compared to BST labeling in the monosynaptic tracer group (see Fig. 22). The number of PRV-labeled BST neurons 60 hrs post-inoculation was also significantly greater than in 48 hr PRV cases ($P < 0.001$).

Despite no significant differences in the overall pattern of labeling across BST subnuclear groups, separate one-way ANOVAs revealed a small but significant effect of tracer group on the proportion of retrograde labeling within the BSTrh [$F(2,22) = 3.51, P < 0.05$], and a nonsignificant trend for an effect of tracer group within the BSTov [$F(2,22) = 3.451, P = 0.05$] (Fig. 24). Post-hoc tests determined that the small proportion of retrograde labeling within the BSTrh was significantly increased in PRV 48 hr cases ($2\% \pm 1$) compared to the smaller proportion of labeling in monosynaptic cases ($1\% \pm 0, P = 0.03$), and the proportion of labeling

in PRV 60 hr cases ($1\% \pm 0$) was significantly decreased compared to PRV 48 hr labeling ($2\% \pm 1$, $P = 0.02$). Correlation analyses of proportional labeling within the BST subnuclei revealed no significant associations between labeling within the BSTrh and labeling within any other BST subnucleus (Table 4).

Retrograde BST labeling after tracer delivery into the MEApd

Quantification of monosynaptic BST retrograde labeling in rats that received tracer delivery into the MEApd revealed that approximately 84%, ~13%, and ~4% of retrogradely-labeled neurons were located within the pBST, amgBST, and algBST, respectively (Fig. 23). Separate one-way ANOVAs confirmed a significant effect of tracer group on the proportion of retrogradely labeled neurons within the pBST [$F(2,13) = 4.08$, $P = 0.04$] and amgBST [$F(2,13) = 5.08$, $P = 0.02$]. Post-hoc tests revealed significantly decreased proportions of retrograde labeling within the pBST of PRV 60 hr cases ($59\% \pm 6$) compared to PRV 48 hr ($84\% \pm 4$) and monosynaptic labeling cases ($84\% \pm 6$; see Fig. 23). Additionally, a significantly increased proportion of labeling was present within the amgBST in PRV 60 hr cases ($32\% \pm 4$) compared to PRV 48 hr ($13\% \pm 3$, $P = 0.02$) and monosynaptic labeling ($13\% \pm 4$, $P = 0.01$) cases.

Similar to results in CEAm- and MEAad-injected cases, PRV injections into the MEApd resulted in more total BST labeling at 48 and 60 hr post-inoculation times compared to BST labeling in rats injected with monosynaptic tracer (Fig. 22). One-way ANOVA confirmed a significant effect of tracer group on the total number of retrogradely-labeled BST neurons after MEApd injection [$F(2,13) = 9.54$, $P = 0.003$]. Post-hoc tests revealed significantly larger numbers of retrogradely-labeled BST neurons in the PRV 48 hr (2316 ± 904 PRV-labeled neurons) and 60 hr groups (4160 ± 1261 PRV-labeled neurons) compared to monosynaptic retrograde labeling (191 ± 4 retrogradely-labeled neurons, $P < 0.05$). Despite the trend towards

increased PRV labeling within the BST in PRV 60 hr cases compared to PRV 48 hr cases, the difference was not significant ($P = 0.10$).

Separate one-way ANOVAs within individual BST subnuclei revealed a significant effect of tracer group on the proportion of retrograde labeling within the BSTdm [$F(2,13) = 4.17$, $P = 0.04$], and a nonsignificant trend within the BSTpr [$F(2,13) = 3.40$, $P = 0.07$] and BSTam [$F(2,13) = 3.60$, $P = 0.06$] (Fig. 25, 26). Post-hoc tests determined that the low proportion of retrograde labeling within the BSTdm in PRV 60 hr cases ($2\% \pm 1$) was significantly increased compared to the proportion of labeling within the BSTdm in monosynaptic cases ($0\% \pm 0$, $P = 0.01$).

Correlation analyses of the proportional retrograde labeling within individual BST subnuclei in MEApd-injected cases were performed to determine whether labeling in other subnuclei was correlated with the decreased BSTpr labeling and/or the increased BSTam and BSTdm labeling (Table 5). Retrograde labeling within the BSTdm was positively correlated with labeling in the BSTv and BSTfu, and was negatively correlated with labeling in the BSTpr. The proportion of retrograde labeling within the BSTpr was negatively correlated with labeling in the BSTif, BSTrh, BSTal, BSTov, BSTfu, BSTam, and BSTdm. In contrast, BSTam labeling was negatively correlated with labeling within the BSTpr, and was positively correlated with labeling in the BSTrh, BSTov, BSTfu, and BSTal.

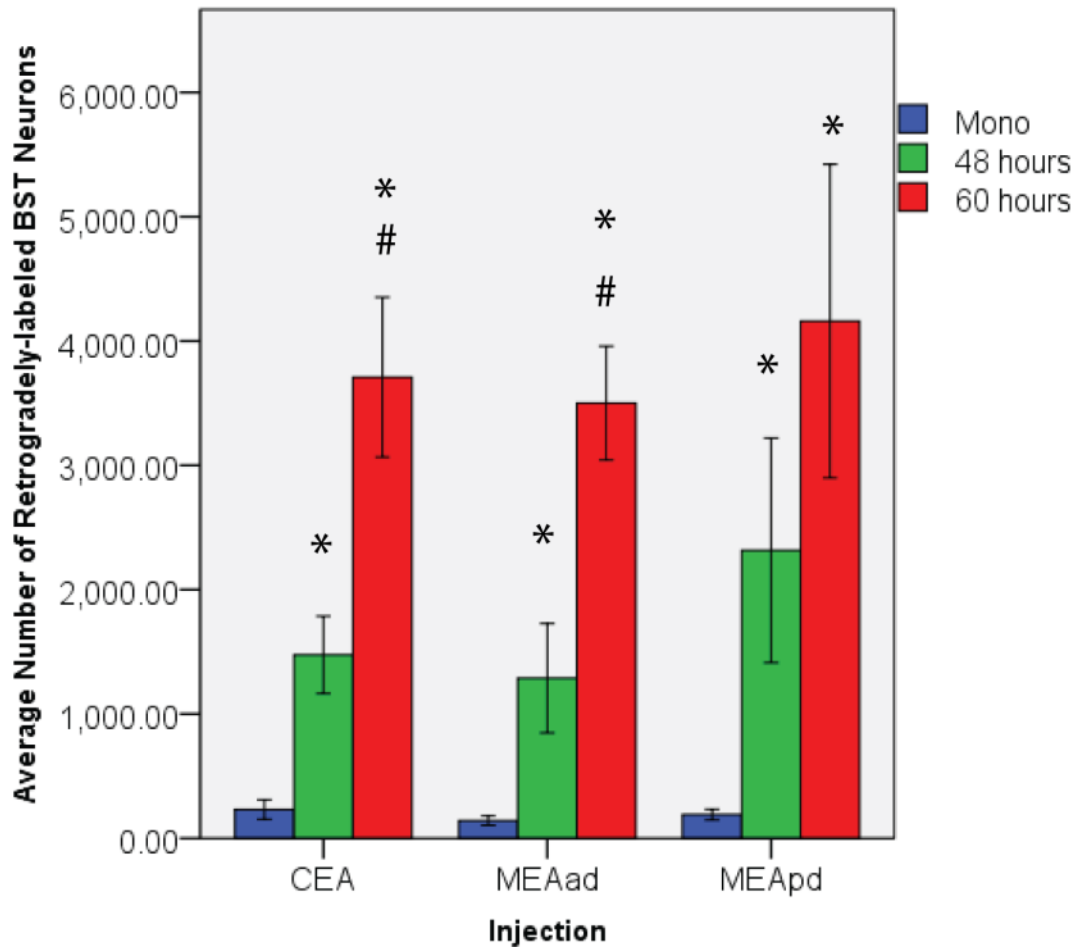


Figure 22. Average number of retrogradely-labeled BST neurons following tracer delivery into the CEAm, MEAad, and MEApd. ANOVA revealed a significant effect of tracer group on the number of retrogradely-labeled BST neurons (see Results). In CEAm and MEAad cases, post-hoc tests revealed significantly greater numbers of retrogradely-labeled BST neurons within the 48 hr and 60 hr PRV groups compared to the monosynaptic tracer group. Labeling in PRV 60 hr cases was significantly greater than in PRV 48 hr cases. Within the MEApd injection group, the number of retrogradely-labeled neurons in PRV 60 hr cases was significantly greater than in monosynaptic cases, whereas the difference between PRV 48 hr cases and PRV 60 hr was not significant. *, $P < 0.05$ compared to monosynaptic; #, $P < 0.05$ compared to PRV 48 hr cases.

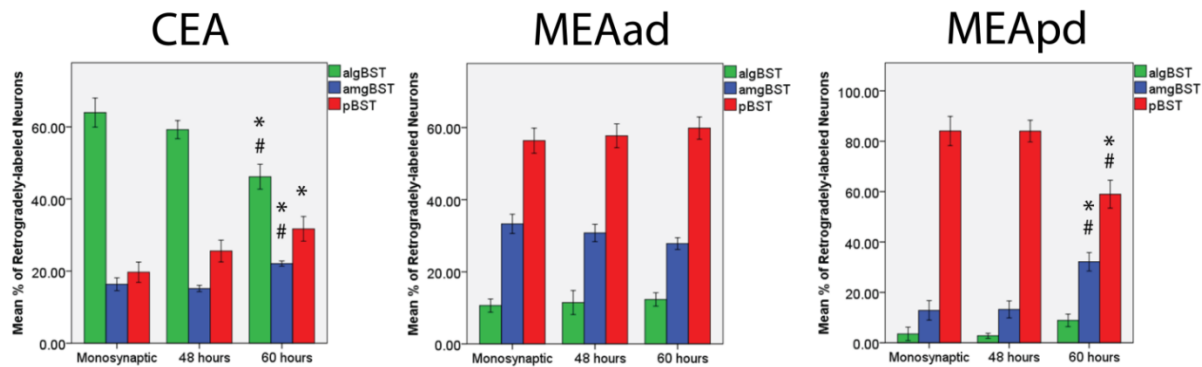


Figure 23. Distribution of retrograde labeling within BST subnuclear groups. Iontophoretic delivery of monosynaptic tracers into the CEAm, MEAad, and MEApd produced 3 distinct patterns of retrograde labeling within BST subnuclear groups. ANOVA revealed a significant effect of tracer group on the distribution of retrograde labeling in rats with CEAm- and MEApd-targeted injections, but not in rats with MEAad-targeted injections (see Results). Post-hoc tests determined that the proportional distribution of labeling was not significantly different between monosynaptic and PRV 48 hr cases ($P > 0.05$ for each subnuclear comparison), despite the almost 10-fold higher number of retrogradely labeled neurons in PRV 48 hr cases (see Fig. 22 for total counts). In CEAm-targeted cases, the proportions of retrograde labeling present within the amgBST and pBST were significantly increased, and proportions within the algBST decreased, in PRV 60 hr vs. 48 hr cases. In MEApd-targeted cases, the proportion of labeling was significantly increased within the amgBST and decreased within the pBST compared to labeling in PRV 48 hr and monosynaptic cases. No distribution differences were observed as a function of tracer group in MEAad-targeted cases. * = $P < 0.05$ compared to monosynaptic, # = $P < 0.05$ compared to PRV 48 hr cases.

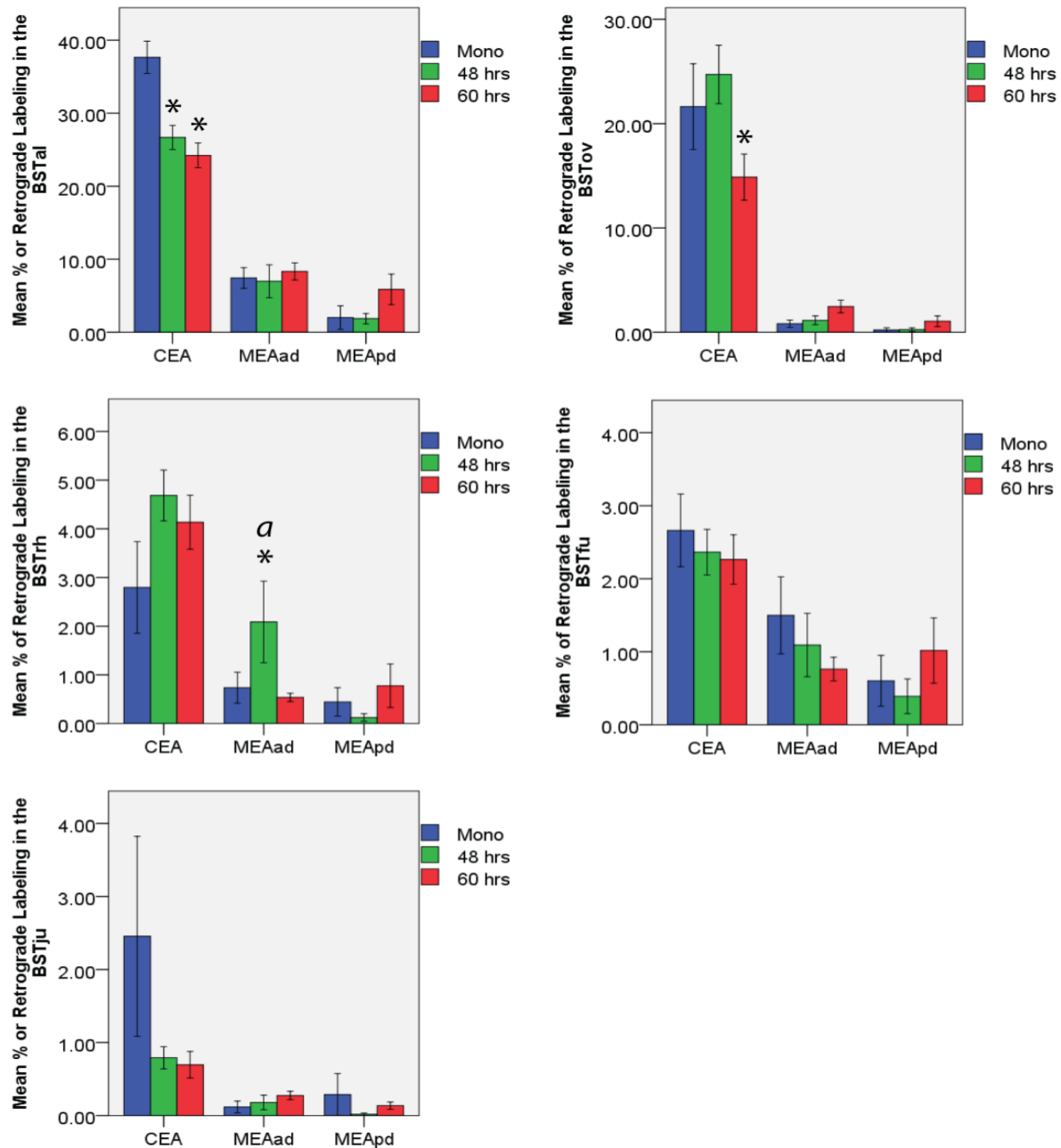


Figure 24. Distribution of retrograde labeling within individual subnuclei of the algBST. Generally, higher proportions of retrograde labeling within algBST subnuclei were observed in CEA cases than in MEAad- or MEApd-injected cases. In CEA-injected cases, one-way ANOVA revealed a significant effect of tracer group on labeling within the BSTal and BSTov. ANOVA analysis of retrograde labeling in MEAad cases determined a significant effect of tracer group on the proportion of labeling within the BSTRh. Post-hoc tests confirmed that in CEA-injected cases the proportion of retrograde labeling in the BSTal was significantly decreased in PRV 48 and 60 hr cases compared to monosynaptic cases. CEA-injected PRV 60 hr cases also contained decreased proportion of labeling within the BSTov. In MEAad-injected cases, post-hoc tests determined minor, yet significant, changes in the proportion of retrograde labeling in the BSTRh following PRV 48 and 60 hr post-inoculation times, respectively. * = $P < 0.05$ compared to monosynaptic, # = $P < 0.05$ compared to PRV 48 hr cases, a = $P < 0.05$ compared to PRV 60 hr cases.

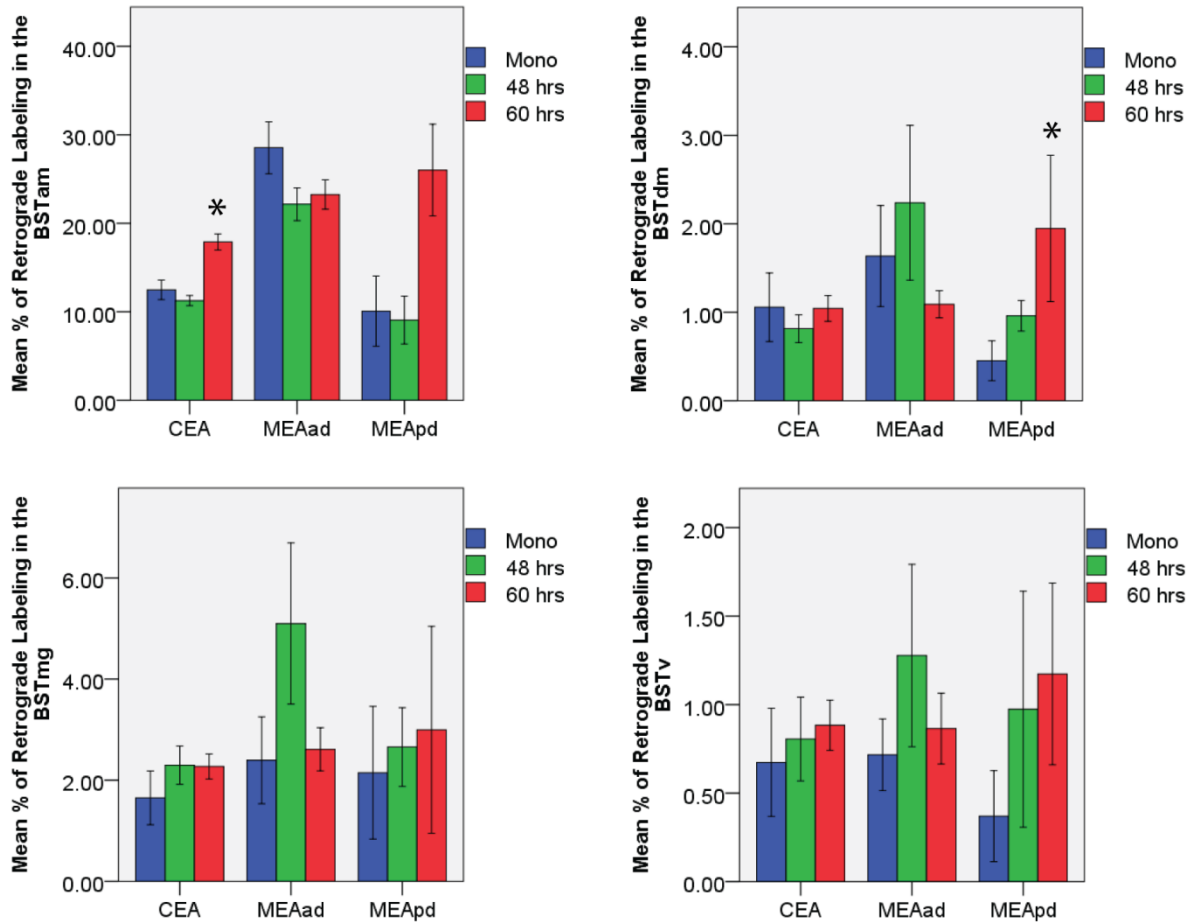


Figure. 25 Distribution of retrograde labeling within individual subnuclei of the amgBST. In CEA-injected cases, one-way ANOVA revealed a significant effect of tracer group on the proportion of retrograde labeling in the BSTpr. Post-hoc tests confirmed that PRV 60 hr cases contained a significantly greater proportion of retrograde labeling in the BSTam compared to monosynaptic cases. ANOVA analysis of MEApd-injected cases found a significant effect of tracer group on the proportion of labeling in the BSTdm and a nonsignificant trend on labeling within the BSTam. Post-hoc tests revealed a significantly greater proportion of labeling in the BSTdm after 60 hr post-inoculation time compared to monosynaptic cases. * = $P < 0.05$ compared to monosynaptic, # = $P < 0.05$ compared to PRV 48 hr cases.

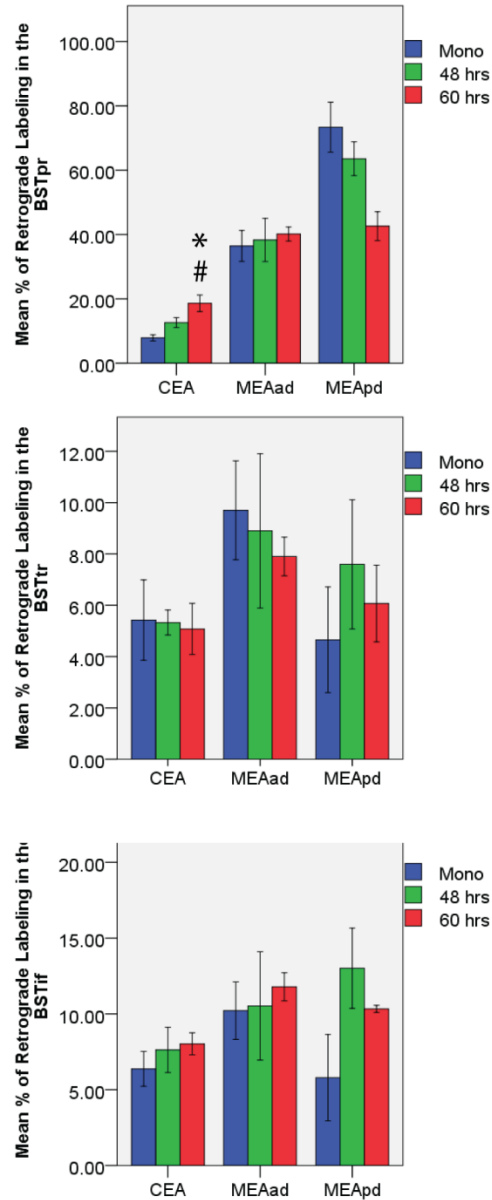


Figure 26. Distribution of retrograde labeling within individual pBST subnuclei. ANOVA analysis of CEA-injected cases revealed a significant effect of tracer group on the proportion of retrograde labeling within the BSTpr. Post-hoc tests confirmed that PRV 60 hr cases contained a significantly greater proportion of retrograde labeling in the BSTpr compared to both PRV 48 hr and monosynaptic cases. In MEApd cases, one-way ANOVA revealed a nonsignificant trend for an effect on the proportion of retrograde labeling within the BSTpr. * = $P < 0.05$ compared to monosynaptic, # = $P < 0.05$ compared to PRV 48 hr cases.

Table 3. Correlations in retrograde labeling between individual BST subnuclei in CEAm-injected cases. Correlation analyses were performed to determine if the proportion of BST labeling observed within individual BST subnuclei was associated with the changes observed within the BSTpr, BSTam, BSTal, and BSTov. BSTpr and BSTam labeling proportions were negatively correlated with labeling proportions in both the BSTal and BSTov. However, labeling within the BSTpr and BSTam was not correlated. Labeling proportions within the BSTov were negatively correlated with labeling in the BSTif and BSTtr, and were positively correlated with labeling within the BSTfu.

Correlations within CEAm-injected Cases

		BSTif	BSTv	BSTpr	BSTtr	BSTth	BSTal	BSTju	BSTov	BSTfu	BSTam	BSTdm	BSTmg
BSTif	Pearson Correlation	1	.093	.330	.391	.393	-.195	-.392	-.565**	-.379	.113	.053	-.236
	Sig. (2-tailed)		.660	.107	.054	.052	.349	.052	.003	.062	.589	.801	.255
	N	25	25	25	25	25	25	25	25	25	25	25	25
BSTv	Pearson Correlation	.093	1	.212	.484*	-.102	-.320	-.323	-.175	-.139	.143	.134	-.197
	Sig. (2-tailed)	.660		.309	.014	.628	.118	.116	.402	.509	.496	.524	.346
	N	25	25	25	25	25	25	25	25	25	25	25	25
BSTpr	Pearson Correlation	.330	.212	1	.265	.157	-.577**	-.206	-.533**	-.289	.233	-.068	-.046
	Sig. (2-tailed)	.107	.309		.201	.455	.003	.322	.006	.161	.262	.748	.829
	N	25	25	25	25	25	25	25	25	25	25	25	25
BSTtr	Pearson Correlation	.391	.484*	.265	1	.095	-.148	-.539**	-.511**	-.311	.148	-.165	-.372
	Sig. (2-tailed)	.054	.014	.201		.651	.482	.005	.009	.131	.481	.430	.067
	N	25	25	25	25	25	25	25	25	25	25	25	25
BSTth	Pearson Correlation	.393	-.102	.157	.095	1	-.185	-.360	-.186	-.126	-.080	-.226	.235
	Sig. (2-tailed)	.052	.628	.455	.651		.376	.077	.372	.549	.702	.278	.258
	N	25	25	25	25	25	25	25	25	25	25	25	25
BSTal	Pearson Correlation	-.195	-.320	-.577**	-.148	-.185	1	.084	.165	.006	-.412*	.040	-.103
	Sig. (2-tailed)	.349	.118	.003	.482	.376		.691	.432	.975	.040	.848	.626
	N	25	25	25	25	25	25	25	25	25	25	25	25
BSTju	Pearson Correlation	-.392	-.323	-.206	-.539**	-.360	.084	1	.300	.386	-.221	-.007	-.066
	Sig. (2-tailed)	.052	.116	.322	.005	.077	.691		.146	.056	.289	.973	.755
	N	25	25	25	25	25	25	25	25	25	25	25	25
BSTov	Pearson Correlation	-.565**	-.175	-.533**	-.511**	-.186	.165	.300	1	.406*	-.470*	-.180	.158
	Sig. (2-tailed)	.003	.402	.006	.009	.372	.432	.146		.044	.018	.390	.450
	N	25	25	25	25	25	25	25	25	25	25	25	25
BSTfu	Pearson Correlation	-.379	-.139	-.289	-.311	-.126	.006	.386	.406*	1	-.070	-.460*	-.058
	Sig. (2-tailed)	.062	.509	.161	.131	.549	.975	.056	.044		.738	.021	.781
	N	25	25	25	25	25	25	25	25	25	25	25	25
BSTam	Pearson Correlation	.113	.143	.233	.148	-.080	-.412*	-.221	-.470*	-.070	1	.160	-.025
	Sig. (2-tailed)	.589	.496	.262	.481	.702	.040	.289	.018	.738		.445	.906
	N	25	25	25	25	25	25	25	25	25	25	25	25
BSTdm	Pearson Correlation	.053	.134	-.068	-.165	-.226	.040	-.007	-.180	-.460*	.160	1	.352
	Sig. (2-tailed)	.801	.524	.748	.430	.278	.848	.973	.390	.021	.445		.084
	N	25	25	25	25	25	25	25	25	25	25	25	25
BSTmg	Pearson Correlation	-.236	-.197	-.046	-.372	.235	-.103	-.066	.158	-.058	-.025	.352	1
	Sig. (2-tailed)	.255	.346	.829	.067	.258	.626	.755	.450	.781	.906	.084	
	N	25	25	25	25	25	25	25	25	25	25	25	25

** Correlation is significant at the 0.01 level (2-tailed).

* Correlation is significant at the 0.05 level (2-tailed).

Table 4. Correlation of retrograde labeling between individual BST subnuclei in MEAad-injected cases. Correlation analyses were performed to determine if the proportion of BST labeling observed within individual BST subnuclei was associated with the changes observed within the BSTrh. BSTrh labeling was not significantly correlated to labeling within any other BST subnucleus.

Correlations within MEAad-injected Cases

	BSTif	BSTv	BSTpr	BSTtr	BSTrh	BSTal	BSTju	BSTov	BSTfu	BSTam	BSTdm	BSTmg	
BSTif	Pearson Correlation	1	.375	-.481	.643**	.013	.078	.062	.000	-.042	-.294	.186	-.376
	Sig. (2-tailed)		.065	.015	.001	.951	.712	.770	1.000	.842	.153	.373	.064
	N	25	25	25	25	25	25	25	25	25	25	25	25
BSTv	Pearson Correlation	.375	1	-.175	.105	.199	.072	-.089	-.177	-.238	-.213	.309	.050
	Sig. (2-tailed)	.065		.401	.617	.340	.731	.673	.398	.253	.306	.133	.811
	N	25	25	25	25	25	25	25	25	25	25	25	25
BSTpr	Pearson Correlation	-.481*	-.175	1	-.667**	-.077	-.589**	-.147	-.332	-.451*	-.519**	-.098	.539**
	Sig. (2-tailed)	.015	.401		.000	.714	.002	.482	.105	.024	.008	.642	.005
	N	25	25	25	25	25	25	25	25	25	25	25	25
BSTtr	Pearson Correlation	.643**	.105	-.667**	1	-.006	.188	-.043	-.072	.387	-.075	.353	-.457*
	Sig. (2-tailed)	.001	.617	.000		.977	.369	.840	.732	.056	.722	.083	.022
	N	25	25	25	25	25	25	25	25	25	25	25	25
BSTrh	Pearson Correlation	.013	.199	-.077	-.006	1	-.041	.202	.049	-.218	.022	.013	.083
	Sig. (2-tailed)	.951	.340	.714	.977		.846	.332	.816	.294	.918	.953	.692
	N	25	25	25	25	25	25	25	25	25	25	25	25
BSTal	Pearson Correlation	.078	.072	-.589**	.188	-.041	1	.537**	.566**	.310	.249	-.221	-.505*
	Sig. (2-tailed)	.712	.731	.002	.369	.846		.006	.003	.132	.230	.288	.010
	N	25	25	25	25	25	25	25	25	25	25	25	25
BSTju	Pearson Correlation	.062	-.089	-.147	-.043	.202	.537**	1	.487*	-.010	-.088	-.260	-.230
	Sig. (2-tailed)	.770	.673	.482	.840	.332	.006		.014	.964	.677	.209	.269
	N	25	25	25	25	25	25	25	25	25	25	25	25
BSTov	Pearson Correlation	.000	-.177	-.332	-.072	.049	.566**	.487*	1	-.049	.186	-.255	-.176
	Sig. (2-tailed)	1.000	.398	.105	.732	.816	.003	.014		.816	.374	.218	.400
	N	25	25	25	25	25	25	25	25	25	25	25	25
BSTfu	Pearson Correlation	-.042	-.238	-.451*	.387	-.218	.310	-.010	-.049	1	.349	-.208	-.290
	Sig. (2-tailed)	.842	.253	.024	.056	.294	.132	.964	.816		.088	.319	.160
	N	25	25	25	25	25	25	25	25	25	25	25	25
BSTam	Pearson Correlation	-.294	-.213	-.519**	-.075	.022	.249	-.088	.186	.349	1	-.174	-.281
	Sig. (2-tailed)	.153	.306	.008	.722	.918	.230	.677	.374	.088		.406	.173
	N	25	25	25	25	25	25	25	25	25	25	25	25
BSTdm	Pearson Correlation	.186	.309	-.098	.353	.013	-.221	-.260	-.255	-.208	-.174	1	-.116
	Sig. (2-tailed)	.373	.133	.642	.083	.953	.288	.209	.218	.319	.406		.579
	N	25	25	25	25	25	25	25	25	25	25	25	25
BSTmg	Pearson Correlation	-.376	.050	.539**	-.457*	.083	-.505*	-.230	-.176	-.290	-.281	-.116	1
	Sig. (2-tailed)	.064	.811	.005	.022	.692	.010	.269	.400	.160	.173	.579	
	N	25	25	25	25	25	25	25	25	25	25	25	25

*. Correlation is significant at the 0.05 level (2-tailed).

** Correlation is significant at the 0.01 level (2-tailed).

Table 5. Correlation of retrograde labeling between individual BST subnuclei in MEApd-injected cases. Correlation analyses were performed to determine if the proportion of BST labeling observed within individual BST subnuclei was associated with the significant increases observed within the BSTdm and nonsignificant trends within the BSTpr and BSTam. Labeling within the BSTam and BSTdm was negatively correlated with labeling proportions in the BSTpr. BSTpr labeling was found to be negative correlated to labeling within most algBST subnuclei and BSTif. In contrast, labeling within the BSTam was positively correlated to labeling within many of the algBST subnuclei. BSTdm labeling was found to be positively correlated to labeling within the BSTfu.

Correlations within MEApd-injected Cases

		BSTif	BSTv	BSTpr	BSTtr	BSTrh	BSTal	BSTju	BSTov	BSTfu	BSTam	BSTdm	BSTmg
BSTif	Pearson Correlation	1	.655**	-.571*	.571*	.049	.167	.064	.123	.079	.020	.473	-.265
	Sig. (2-tailed)		.006	.021	.021	.857	.538	.815	.650	.771	.943	.064	.320
	N	16	16	16	16	16	16	16	16	16	16	16	16
BSTv	Pearson Correlation	.655**	1	-.430	.092	-.028	-.006	-.147	-.142	.402	.157	.651**	-.044
	Sig. (2-tailed)	.006		.096	.733	.918	.983	.587	.600	.123	.562	.006	.871
	N	16	16	16	16	16	16	16	16	16	16	16	16
BSTpr	Pearson Correlation	-.571*	-.430	1	-.462	-.685**	-.754**	-.462	-.733**	-.593*	-.769**	-.644**	.109
	Sig. (2-tailed)	.021	.096		.072	.003	.001	.072	.001	.015	.001	.007	.687
	N	16	16	16	16	16	16	16	16	16	16	16	16
BSTtr	Pearson Correlation	.571*	.092	-.462	1	.003	.056	.039	.152	-.169	-.075	.178	.185
	Sig. (2-tailed)	.021	.733	.072		.992	.837	.886	.575	.531	.782	.510	.493
	N	16	16	16	16	16	16	16	16	16	16	16	16
BSTrh	Pearson Correlation	.049	-.028	-.685**	.003	1	.848**	.774**	.748**	.690**	.817**	.271	-.305
	Sig. (2-tailed)	.857	.918	.003	.992		.000	.000	.001	.003	.000	.310	.250
	N	16	16	16	16	16	16	16	16	16	16	16	16
BSTal	Pearson Correlation	.167	-.006	-.754**	.056	.848**	1	.769**	.931**	.555*	.789**	.243	-.298
	Sig. (2-tailed)	.538	.983	.001	.837	.000		.000	.000	.026	.000	.365	.263
	N	16	16	16	16	16	16	16	16	16	16	16	16
BSTju	Pearson Correlation	.064	-.147	-.462	.039	.774**	.769**	1	.584*	.604	.430	.162	-.187
	Sig. (2-tailed)	.815	.587	.072	.886	.000	.000		.018	.013	.096	.548	.489
	N	16	16	16	16	16	16	16	16	16	16	16	16
BSTov	Pearson Correlation	.123	-.142	-.733**	.152	.748**	.931**	.584*	1	.359	.785**	.169	-.269
	Sig. (2-tailed)	.650	.600	.001	.575	.001	.000	.018		.172	.000	.531	.314
	N	16	16	16	16	16	16	16	16	16	16	16	16
BSTfu	Pearson Correlation	.079	.402	-.593*	-.169	.690**	.555*	.604	.359	1	.712**	.614	-.112
	Sig. (2-tailed)	.771	.123	.015	.531	.003	.026	.013	.172		.002	.011	.680
	N	16	16	16	16	16	16	16	16	16	16	16	16
BSTam	Pearson Correlation	.020	.157	-.769**	-.075	.817**	.789**	.430	.785**	.712**	1	.438	-.242
	Sig. (2-tailed)	.943	.562	.001	.782	.000	.000	.096	.000	.002		.090	.366
	N	16	16	16	16	16	16	16	16	16	16	16	16
BSTdm	Pearson Correlation	.473	.651**	-.644**	.178	.271	.243	.162	.169	.614	.438	1	.122
	Sig. (2-tailed)	.064	.006	.007	.510	.310	.365	.548	.531	.011	.090		.653
	N	16	16	16	16	16	16	16	16	16	16	16	16
BSTmg	Pearson Correlation	-.265	-.044	.109	.185	-.305	-.298	-.187	-.269	-.112	-.242	.122	1
	Sig. (2-tailed)	.320	.871	.687	.493	.250	.263	.489	.314	.680	.366	.653	
	N	16	16	16	16	16	16	16	16	16	16	16	16

** . Correlation is significant at the 0.01 level (2-tailed).

* . Correlation is significant at the 0.05 level (2-tailed).

3.4 DISCUSSION

Iontophoretic delivery of FG/BDA tracer cocktail revealed that the majority of FG-labeled BST neurons were located within BDA-labeled amygdala terminal fields, confirming the interpretation of several anterograde tracing studies in rat (Canteras, Simerly et al. 1995, Dong, Petrovich et al. 2000, Dong, Petrovich et al. 2001, Dong and Swanson 2003, Dong and Swanson 2004, Dong and Swanson 2004, Dong and Swanson 2006, Dong and Swanson 2006) and cocktail tracer injections in hamster (Coolen and Wood 1998) that amygdala subnuclei are connected to BST subnuclei via topographically-organized bidirectional projection systems. Quantification of monosynaptic and transsynaptic retrograde labeling in FG/BDA-, PRV-, and PRV/CTB-injected cases provide the first quantitative analysis of the distribution of CEAm-, MEAad-, and MEApd-projecting BST circuits. As expected, CEAm-projecting BST neurons were located primarily within the algBST, while MEAad- and MEApd-projecting BST neurons were distributed within complementary regions of the pBST and amgBST. Analysis of labeling data from rats that were sacrificed 48 hours after receiving PRV injections into amygdalar subnuclei revealed no change in the distribution of retrograde labeling compared to monosynaptic labeling patterns, despite an approximately 10-fold increase in the number of retrogradely-labeled, PRV-positive BST neurons. The similar distribution of retrograde labeling suggests that 2nd-order PRV-infected neurons are located locally within the same BST subnuclei and/or subnuclear groups as 1st-order projection neurons.

In contrast to the similar subnuclear distribution of BST labeling observed in both monosynaptic and 48 hr PRV cases, different labeling distribution patterns were observed in rats 60 hrs after CEAm- and MEApd-targeted viral injections, whereas the distribution of BST labeling 60 hr after MEAad-targeted PRV injections remained similar to that observed in 48 hr

MEAad-targeted cases. In CEAm 60 hr cases, a significantly greater proportion of retrograde labeling was present within amgBST and pBST (specifically the BSTam and BSTpr subnuclei) compared to monosynaptic retrograde tracer-injected CEAm cases, evidence that the CEAm receives multisynaptic input from BST subnuclei beyond those that directly innervate (and receive input from) the CEA. MEApd 60 hr cases displayed a significantly greater proportion of retrograde labeling in the amgBST, including increased labeling within the BSTdm and a non-significant but strong trend towards increased labeling within the BSTam. In both MEAad and MEApd injection cases, retrograde labeling within the algBST was relatively light, particularly within the BSTov. These findings support the view that both monosynaptic and polysynaptic inputs to the MEA from the BST are confined to the amgBST and pBST.

Methodological considerations

Although differences were observed in the number of FG- and CTB-labeled BST neurons in rats that received FG/BDA or PRV/CTB tracer injections, there were no significant tracer-related differences in the proportional distribution of retrograde labeling across BST subnuclear groups. Differences in the total number of FG- vs. CTB-labeled neurons are likely due to differences in tracer concentration, uptake affinity, and local diffusion at the injection site. There were no significant differences in the number of PRV-positive BST neurons in rats injected with a 3:1 mixture of PRV/CTB compared to labeling in rats injected with PRV alone, consistent with previous reports indicating that CTB does not reduce PRV invasiveness, transport, or replication (Chen, Yang et al. 1999, Aston-Jones and Card 2000).

Interestingly, the total number of retrogradely-labeled BST neurons in monosynaptic, PRV 48 hr, and PRV 60 hr cases was similar regardless of amygdala injection site (Fig. 21). Monosynaptic retrograde tracers typically labeled an average of 100-200 neurons, while viral labeling in PRV 48 hr and 60 hr cases totaled approximately 1000-2000 and 3000-4000 neurons, respectively. While these consistent labeling results are partially explained by the use of consistent injection parameters for each amygdala subnucleus, they suggest similarity in the architecture of amygdala-projecting BST circuits. Previous studies indicate that PRV retrograde transport and infection of neurons in multisynaptic circuits depends on the number and variety of axonal inputs received by each neuron in the circuit (Card, Enquist et al. 1999). In the present study, the similar total numbers of BST neurons infected, regardless of amygdalar injection site, suggests similarities in the synaptic wiring of BST neurons within CEAm-, MEAad-, and MEApd-projecting circuits. In other words, first- and second-order BST projection neurons may receive a similar number of axonal inputs from second- and third-order BST neurons, respectively, regardless of whether the multisynaptic BST circuits are targeting the CEA or the MEA.

The BSTpr and BSTam provide multisynaptic input to the CEAm

A major finding of our study is evidence that the BSTpr provides multisynaptic input to the CEA. The MEAad, MEApd, and BSTpr have been identified as constituent members of the brain's social and reproductive behavior network in rodent species (Newman 1999). Electrolytic lesions of the BSTpr in male hamsters cause increased ejaculation latency, and decreased chemoinvestigatory behavior towards females (Newman 1999). Studies analyzing neuronal Fos expression have identified specific neuronal subpopulations within the BSTpr and MEApd that

are activated in response to discrete chemosensory stimuli and mating events (Veening and Coolen 1998). Our finding that the BSTpr provides multisynaptic input to the CEAm provides a potential anatomical substrate through which anxiety-related behaviors mediated by the CEA could be modulated by inputs from the BSTpr that are sensitive to the animal's current reproductive context. The BSTpr and MEApd have each been shown to display sexually dimorphism with regards to nuclear volume (Mizukami, Nishizuka et al. 1983, Hines, Allen et al. 1992), synaptic organization (Nishizuka and Arai 1981, Nishizuka and Arai 1983), and neurotransmitter phenotype (Malsbury and McKay 1987, Miller, Vician et al. 1989), effects that are mediated by circulating androgens (Cooke, Tabibnia et al. 1999). Whether the BSTpr provides multisynaptic input to the CEAm in female rats remains to be determined. However, the BST is proposed to participate in sex-specific stress/learning circuits based on evidence that a masculinized, but not a feminized, BST is necessary for stress to enhance classical eyeblink conditioning [87-89]. In addition, sex differences have been observed in fear conditioning paradigms [90, 91], in which the CEAm plays a critical role (Duvarci, Popa et al. 2011). While most studies on sex differences have focused on the direct effects of circulating sex hormones, a multisynaptic circuit from the BSTpr to the CEAm may provide the anatomical substrate through which these differences become manifest.

Relatively little is known about the functional role of the BSTam, perhaps because its potential functions are so broad. The BSTam maintains diverse and relatively diffuse anatomical connections, including direct connections with regions implicated in controlling neuroendocrine, autonomic, and somatomotor behavioral outputs. In addition, the BSTam is the only BST subnucleus to receive input from all other BST subnuclei (Fig. 17). Based on its diverse and widespread connectivity, Dong and Swanson hypothesized that the BSTam has an integrative

role within a differentiated striatopallidal circuit that regulates energy homeostasis (Dong and Swanson 2006). Our viral tracing results demonstrate that the BSTam participates directly or indirectly in CEAm-, MEAad-, and MEApd-projecting circuits, providing further evidence that the BSTam serves an integrative function with multiple BST circuits.

Neuroendocrine vs. Autonomic Circuits within the BST

Previous studies have suggested that MEA/BST circuits are more likely to be involved in the regulation of neuroendocrine function than CEA/BST circuits, based on comparisons of the overlap of CEA and MEA projections and neuroendocrine-projecting BNST neurons (Prewitt and Herman 1998) and evidence that the MEA and pBNST/amgBNST also directly innervate brain regions of the hypothalamic visceromotor pattern generator network that regulated neuroendocrine output (Thompson and Swanson 2003). Viral tracing experiments have revealed the distribution of multisynaptic circuits that project to autonomic and neuroendocrine motoneurons. After PRV injections into visceral organs, retrogradely labeled neurons eventually appear within the algBST (Rinaman, Levitt et al. 2000). In contrast, after PRV injections into the paraventricular nucleus of the hypothalamus (PVN), where most neuroendocrine neurons are located, retrogradely labeled neurons appear within the amgBST and pBST (JP Card, unpublished observations). Considering the distribution of pre-autonomic and pre-neuroendocrine BST circuits as compared to the distribution of amygdala-projecting BST circuits, the pattern of viral labeling observed after PRV injections into the MEApd and MEAad is similar to the distribution of pre-neuroendocrine BST circuits. The CEAm appears to receive direct projections from BST subnuclei with pre-autonomic connections, which may be modulated by inputs from BST subnuclei that regulate neuroendocrine output.

Conclusions

While previous studies have defined the efferent projections of amygdalar and BST subnuclei, the interconnected nature of BST subnuclei has complicated our understanding of how multisynaptic amygdala-projecting BST circuits are organized. Results from the present study reveal several organizational principles for multisynaptic BST circuit outputs to specific amygdala subnuclei. The results also indicate that the BSTpr and BSTam provide multisynaptic input to the CEAm, suggesting that the CEAm receives multimodal inputs related to the reproductive, autonomic, and neuroendocrine functions of the BST.

4.0 GENERAL DISCUSSION

4.1 SUMMARY AND INTERPRETATION OF EXPERIMENTAL FINDINGS

The concept of the extended amygdala suggests that the central and medial nuclei of the amygdala and the BST are parts of a contiguous cellular column of neurons with similar anatomical connectivity and functional output. In support of the extended amygdala concept, amygdala and BST regions appear to receive input and send projections to similar brain regions and results from several studies indicate that lesions of the amygdala often produce experimental results that are quite similar to results obtained after lesions in associated BST regions (Zardetto-Smith, Beltz et al. 1994, Newman 1999, Tanimoto, Nakagawa et al. 2003, Nakagawa, Yamamoto et al. 2005, Deyama, Nakagawa et al. 2007). On the other hand, the concept of the central extended amygdala has been challenged by results from behavioral studies that suggest a dissociation of CEA and BST functions (Walker and Davis 1997, Fendt, Endres et al. 2003, Walker, Toufexis et al. 2003, Jasnow, Davis et al. 2004, Funk, O'Dell et al. 2006, Walker, Miles et al. 2009). For example, the CEA and lateral BST have been reported to play unique roles in mediating behavioral processes associated with fear, anxiety (Walker and Davis 1997, Fendt, Endres et al. 2003, Walker, Toufexis et al. 2003, Sullivan, Apergis et al. 2004), social defeat (Jasnow, Davis et al. 2004), social interaction (Cecchi, Khoshbouei et al. 2002) and ethanol self-administration (Funk, O'Dell et al. 2006). These differences in amygdala vs. BST function are

likely to be mediated by distinct anatomical circuits.

The studies in this dissertation were designed to more closely examine the anatomical relationship of the amygdala and BST and test some of the assumptions proposed by the extended amygdala concept. In the first study, we tested the hypothesis proposed by de Olmos and Heimer that “all or most of the central extended amygdala would share similar inputs” (de Olmos and Heimer 1999). Dual retrograde tracing of inputs to the CEAm and BSTvl revealed overlapping distributions of retrograde labeling from both injection sites. However, compared to distinct CEAm and BSTvl inputs, collateralization of input to the CEAm and BSTvl was relatively minor among most extended amygdala-projecting brain regions. Additionally, brain regions associated with cortical or sensory systems contained larger numbers of neurons projecting to the CEAm vs. the BSTvl (Fig. 14) while striatal-like regions and areas associated with Swanson’s behavioral control columns contained larger numbers of neurons projecting to the BSTvl vs. the CEAm. In light of these new findings, we proposed an organizational hypothesis for two primary pathways through which behaviorally-relevant information is processed by the CEA and BST. Our organizational model suggests that top-down information processing of the extended amygdala is similar to the striatopallidal circuits proposed by Swanson (Dong, Petrovich et al. 2000, Swanson 2000, Dong, Petrovich et al. 2001, Dong and Swanson 2003, Dong and Swanson 2004). In contrast, the extended amygdala receives dense bottom-up feedback signaling from the motor system. We suggest that increased density of feedback circuitry could be the specialization that makes the extended amygdala unique for mediating subconscious behavioral responses (discussed further in section 4.2).

The second study examines the anatomical circuits between the amygdala and BST subnuclei, particularly multisynaptic BST circuits along the proposed feedback pathway that

provide input to the amygdala subnuclei. Qualitative interpretations from several anterograde tracing studies indicated that connections between amygdala and BST subnuclei are topographically-organized reciprocal projection systems, in agreement with the concept of central and medial divisions of the extended amygdala. We hypothesized that multisynaptic amygdala-projecting BST circuits would be limited to BST subnuclei within the topographic boundaries suggested by the direct amygdala/BST connectivity, despite evidence that BST subnuclei are highly interconnected. The results of this study indicate that the CEAm receives multisynaptic input from the BSTam and BSTpr, two subnuclei that are associated with the medial extended amygdala. In contrast, multisynaptic MEA-projecting BST circuits were primarily confined to amgBST and pBST subnuclear groups. These findings suggest that the CEAm receives a variety of behavioral feedback signals associated with autonomic and neuroendocrine output, whereas the MEAad and MEApd receive more specific feedback information from BST subnuclei regulating neuroendocrine output and reproductive behavior. The variety of multisynaptic BST circuits to the CEAm suggests a number of pathways that could alter CEAm-mediated stress responses (discussed further in section 4.3).

4.2 EXTENDED AMYGDALA VS. STRIATOPALLIDAL MODEL OF THE ANATOMICAL RELATIONSHIP BETWEEN THE AMYGDALA AND BST

Lennart Heimer, Larry Swanson, and their colleagues have made compelling arguments for their respective models describing the anatomical relationship between the amygdala and BST (Alheid and Heimer 1988, Swanson and Petrovich 1998, de Olmos and Heimer 1999, Swanson 2000, Swanson 2003). Clearly, both similarities and differences exist between

striatopallidal and amygdala/BST circuitry. The findings presented here provide additional evidence for a distinction between the amygdala and BST. Our finding that the CEAm and BSTvl receive preferential input from cortical, sensory, and motor systems suggests that amygdala and BST neurons are involved in processing different aspects of behaviorally-relevant information. We suggest that the primary difference between amygdala/BST and striatopallidal circuits is the enhanced bottom-up feedback pathway in amygdala/BST circuits. Compared to striatopallidal circuits controlling voluntary somatomotor behavior, motor feedback is likely more important for amygdala/BST circuits regulating subconscious homeostatic behaviors. This hypothesis is consistent with evidence that changes in visceral and endocrine outflow can occur with little or no ongoing control by cortical structures.

The topographically-organized projection systems of the amygdala and BST would suggest that each amygdala subnucleus and respective BST counterpart may mediate distinct striatopallidal channels with little integration between channels. In this comparison, BST projections to the amygdala would be similar to pallidostriatal circuits (Walker, Arbuthnott et al. 1989, Rajakumar, Elisevich et al. 1994, Kita and Kita 2001). Our study of multisynaptic amygdala-projecting BST circuits revealed several general principles for information processing within the amygdala and BST. First, the similarity among amygdala injection sites in generating progressively greater numbers of retrogradely-labeled BST neurons after monosynaptic tracer or PRV indicates that amygdala-projecting BST circuits have similar synaptology. Second, 1st - and 2nd-order amygdala-projecting BST neurons are located within the same BST subnuclear groups, suggesting that information is integrated within BST subnuclear groups before being sent to the amygdala, consistent with a closed pallidostriatal circuit. However, third-order CEAm-projecting BST neurons were identified within the amgBST and pBST, indicating that the CEAm

receives input from BST regions outside its topographic boundaries. In contrast, 3rd-order MEA-projecting BST neurons were located within the MEA topographic boundary in the BST. Considering the distinct functions of CEA and MEA circuits, these findings suggest that the CEAm receives feedback information regarding a variety of BST-mediated homeostatic behaviors, whereas the MEA may be more dedicated to reproductive-related feedback (discussed further in section 4.3). It is currently unknown whether striatal input from multisynaptic pallidostriatal circuits are maintained within topographic pallidal boundaries, however, the experimental design used to delineate amygdala-projecting BST circuits could be applied in future studies of multisynaptic pallidostriatal circuits.

Overall, the amygdala and BST are connected to many of the neural networks which regulate motivational behavior. Indeed, the amygdala and BST have been implicated in reproductive, stress-induced anorexic, rewarding, and aggressive behavioral responses (Veening and Coolen 1998, Ciccocioppo, Fedeli et al. 2003, Trainor, Bird et al. 2004, Consiglio, Borsoi et al. 2005, Harris and Aston-Jones 2007) in addition to modulating neuroendocrine and autonomic responses (Herman, Cullinan et al. 1994). Swanson has suggested that the caudorostral striatopallidal circuit influences motivated behavior such that the MEA/BST relays pheromonal information to the hypothalamic motor system while the CEA/BST relays cortical information to the autonomic system (Swanson 2000). However, our study indicates that the CEAm receives input from BST regions involved in both autonomic and neuroendocrine circuits. In addition to the prominent role of the extended amygdala in a variety of complex behaviors, the amygdala and BST do not seem to be limited to one type of motor function. The variety of behavioral roles for the amygdala and BST suggests that these regions have a vast influence over how an animal will respond to any stimulus, threatening or non-threatening.

4.3 THE AMYGDALA AND BST CIRCUITS IN BEHAVIORAL RESPONSES

The following section will discuss the major functional roles of the extended amygdala circuitry. Anatomical connectivity determines the functional role of a brain region and changes in neurocircuitry can often predict the dysfunction which occurs in neurobiological diseases such as Parkinson's and Huntington's disease. After describing the involvement of the extended amygdala in behavior, I will speculate how the findings described in this dissertation impact our understanding of how amygdala and BST circuits might influence behavior.

4.3.1 Fear and anxiety

While the similarity between amygdala and BST anatomical circuitry is debatable, a strong functional relationship between the amygdala and BST clearly exists. In the rat, studies using the acoustic startle and fear conditioning paradigms have revealed a critical role for the CEA and BST in the behavioral response to fear and anxiety (Walker, Toufexis et al. 2003). However, several studies have demonstrated subtle differences in how these areas are recruited by threatening stimuli. Initially, the concept of the fear circuitry in the brain was centered on the amygdala. The BLA processed multimodal sensory information for threatening cues and, if a threat was present in the environment, activate the CEA to generate the behavioral freezing response. This freezing response to a tone could be enhanced by pairing the tone with a shock over a training period (fear-potentiated startle). The discovery that led researchers to the BST was the finding that infusion of corticotrophin-releasing hormone (CRH) into the lateral ventricles and well lit conditions also enhanced the startle response (CRH-enhanced startle, light-enhanced startle) (Lee and Davis 1997, Walker, Miles et al. 2009). Lesions of the BST, but not

the CEA, blocked CRH- and light-enhanced startle while lesions of the CEA, but not the BST, blocked fear-potentiated startle. These findings led Davis and colleagues to conclude that there was a double dissociation between the involvement of the BST and CEA in CRH-enhanced/light-enhanced versus fear-potentiated startle (Walker and Davis 1997). This functional disparity was puzzling, given the strong reciprocal connections between the CEA and BST. Two theories have arisen to account for this result. The first theory posits that the CEA is involved in conditioned fear responses, while the BST mediates innate unconditioned fear responses through the CRH system. The second theory proposes that it is equally likely that the CEA may mediate acute fear responses to short duration cues while the BST mediates sustained fear in response to diffuse long-duration threatening cues (ex. light, predator odor (Fendt, Siegl et al. 2005)). Regardless of which theory is correct, the BST plays a critical role for behavioral fear responses, perhaps mediating differences in anxiety between individuals (Sullivan, Apergis et al. 2004, Duvarci, Bauer et al. 2009). More recent evidence suggests that the BST can respond to differences in contextual environment (which are not innate), but not specific cues, has increased support of the acute vs. sustained fear theory (Sullivan, Apergis et al. 2004).

4.3.2 Addiction-related behaviors

Drug addiction is a relapsing disorder that can be characterized by distinct behavioral phases that progress from impulsive to compulsive behavioral disorders (Koob 2003, Koob 2009). The development of addiction begins with an animal's urge to partake in a rewarding substance. The feeling of reward that follows intake leads to positive reinforcement of the drug-seeking behavior, believed to be mediated by the mesolimbic dopamine system. As an animal develops tolerance and the rewarding effects of the drug are attenuated, negative emotional states

and withdrawal become the primary motivation for the animal to continue drug intake. The relief from anxiety and stress caused by withdrawal is called negative reinforcement. Together, the combination of a drug's positive reinforcing effects with the reduction of negative affect following abstinence provides the powerful motivational drive for drug addiction.

The amygdala and BST are well-situated to provide an anatomical substrate for the interaction between reward and stress that characterize positive and negative reinforcement following drug intake (Koob and Le Moal 2001). The BST is connected to two brain regions that have been implicated in reward processing: dopaminergic neurons in the ventral tegmental area (VTA) and orexin neurons in the lateral hypothalamic area (LHA) (Harris, Wimmer et al. 2005, Aston-Jones, Smith et al. 2009). Robust dopaminergic inputs from the VTA primarily innervate the lateral subnucleus of the CEA (CEAl) and oval subnucleus of the BST (BSTov), where many stress-responsive CRH-expressing neurons are located (Freedman and Cassell 1994). Interactions between the dopamine and CRH neurotransmitters systems have been proposed as a mechanism for altered allostasis during addiction (George, Le Moal et al. 2012). In addition, BST neurons project to and directly influence the activity of VTA neurons (Jalabert, Aston-Jones et al. 2009). Electrical or low dose chemical stimulation (10-50 mM glutamate) of anteroventral BST neurons increases activity of VTA dopamine neurons via a glutamatergic BST projection to the VTA (Georges and Aston-Jones 2001, Georges and Aston-Jones 2002). These experiments also found that low dose chemical stimulation can cause long-lasting oscillatory activity in VTA dopamine neurons. However, stronger chemical stimulation (100 mM glutamate) completely inactivated VTA neurons. Additional evidence has shown that a non-glutamatergic BST projection to the VTA is critical for the expression of cocaine place preference (Sartor and Aston-Jones 2012). Further anatomical studies of discrete glutamatergic

vs. non-glutamatergic BST-VTA circuits are needed, but the functional evidence for the BST and VTA in reward processing is overwhelming.

A variety of studies have implicated LHA orexin neurons in circuits generating arousal (Hagan, Leslie et al. 1999, Huang, Qu et al. 2001, Yamanaka, Beuckmann et al. 2003) and feeding behavior (Haynes, Jackson et al. 1999, Willie, Chemelli et al. 2001, Zhu, Yamanaka et al. 2002). Recently, orexin neurons have been shown to modulate stimulus-reward associations via activation of VTA dopamine neurons (Harris and Aston-Jones 2006, Aston-Jones, Smith et al. 2009). Stimulation of orexin neurons or microinjection of orexin into the VTA can reinstate a previously extinguished morphine preference in rats (Aston-Jones, Smith et al. 2009). Orexin fibers innervate BST subnuclei in a variety of species, although the distribution of orexin fibers appears different between rodents (Peyron, Tighe et al. 1998, Nixon and Smale 2007). In the rat, orexin fibers are primarily distributed within the anterior and ventral BST regions and injection of orexin-A directly into the BST induces anxiety-like behavior (Lungwitz, Molosh et al.). In addition, BST neurons have been shown to project to orexin neurons [58]. This evidence indicates that orexin may enhance positive reinforcement through its actions in the VTA while modulating negative reinforcement through its anxiogenic properties in the BST.

Furthermore, the BST receives input from anxiety-related brain regions such as the noradrenergic neurons in the nucleus of the solitary tract (NTS), ventrolateral medulla (VLM), and to a lesser extent, the locus coeruleus (LC). The ventral BST contains the densest noradrenergic terminal field in the brain and norepinephrine produces inhibitory responses in ventral BST neurons via modulation of glutamatergic and GABA-ergic inputs (Casada and Dafny 1993, Egli, Kash et al. 2004, McElligott and Winder 2009). Behavioral experiments have revealed that norepinephrine in the BST is critical for opiate-withdrawal-induced aversion and

blockade of noradrenergic signaling in the CEA or BST prevents stress-induced reinstatement, suggesting a role for norepinephrine actions in the extended amygdala in mediating negative-reinforcement following drug-intake (Delfs, Zhu et al. 2000, Leri, Flores et al. 2002, Smith and Aston-Jones 2008).

Taken together, functional evidence suggests bidirectional interactions of the BST with VTA dopamine, LHA orexin, and brainstem norepinephrine in reward-related behaviors. However, the BST's complex neuroanatomy prevents a clear understanding of how these functional interactions translate into anatomical circuits, particularly with the VTA and BST where VTA-projecting BST neurons are largely segregated from areas of the BST with the densest dopaminergic innervation.

4.3.3 Social and reproductive behaviors

The role of the medial amygdala subnuclei and posterior BST in reproductive behavior has been well established in rodents, particularly in the hamster (Newman 1999). The posterodorsal subnucleus of the MEA (MEApd) and principal subnucleus of the BST (BSTpr) are sexually dimorphic in relation to nuclear volume (Mizukami, Nishizuka et al. 1983, Hines, Allen et al. 1992), synaptic organization (Nishizuka and Arai 1981, Nishizuka and Arai 1983), and neurotransmitter phenotype (Malsbury and McKay 1987, Miller, Vician et al. 1989), effects that are mediated by circulating androgens (Cooke, Tabibnia et al. 1999). The MEApd and BSTpr system is characterized by substance P and enkephalin neurons in both rat and hamster. In rat, vasopressin and cholecystokinin (CCK) are also abundant. By contrast, hamsters have populations of prodynorphin neurons and dopamine neurons (75% of which contain androgen receptors). Neurons within the MEApd and BSTpr express androgen and estrogen receptors that

suggest neuronal activity in the MEApd and BSTpr are sensitive to hormone fluctuations over diurnal, estrous, and seasonal breeding cycles (Simerly, Chang et al. 1990, Wood and Newman 1995, Wood and Newman 1995). In support of hormone-mediated influences, an implant of testosterone or its metabolite estradiol delivered unilaterally to the MEApd or BSTpr can restore mounting behavior in castrated male hamsters, whereas implants in MEAad are ineffective (Wood and Newman 1995, Wood 1996, Wood 1996).

Lesion studies of the anterodorsal subnucleus of the MEA (MEAad), MEApd, BSTpr, and posterior intermediate BST (BSTpi, corresponding to the BSTtr and BSTif in the Swanson nomenclature) have revealed roles for these regions in distinct aspects of reproductive behavior (Powers, Newman et al. 1987, Newman 1999). Males with MEAad lesions essentially failed to engage in any chemoinvestigatory or copulatory activities whereas those with lesions including MEApd showed decreased chemoinvestigation and a lengthening of the copulatory sequence. Similar to the MEApd, lesions of the BSTpr increased ejaculation latencies and attenuated chemoinvestigatory behavior. In contrast, lesions which included both BSTpi and BSTpr either prevented copulatory behavior or only occasional mounting behavior occurred in male hamsters.

Studies that have examined Fos expression patterns in the hamster brain after mating events have provided additional evidence for the involvement of the MEA and BST in reproductive behavior. Fos protein is widely used as a marker for neuronal activity and Fos expression has been shown to be transiently elevated approximately one hour after a behavioral stimulus (Sagar, Sharp et al. 1988). Following mating, neuronal subpopulations within the MEAad /BSTpi and MEApd/BSTpr contain elevated expression of Fos (Veening and Coolen 1998). However, while MEApd/BSTpr neurons are selectively activated by mating or discrete sexual stimuli, MEAad/BSTpi neurons in both males and females contain elevated Fos

expression after either mating or intrasexual aggressive encounters (Joppa, Meisel et al. 1995, Kollack-Walker and Newman 1995, Potegal, Ferris et al. 1996, Kollack-Walker and Newman 1997). Additionally, specific clusters of Fos-activated neurons within the MEApd and BSTpr have been observed following ejaculation, providing further support for these subnuclei in mating-specific behaviors (Veening and Coolen 1998).

4.3.4 Impact of the dissertation studies on our understanding of extended amygdala-mediated behavior

Based on the experiments conducted in section 2.0, we hypothesized that differential input from the cortical, sensory, and motor systems account for the distinct roles of the CEAm and BSTvl in certain behaviors. Indeed, several studies have revealed that noradrenergic viscerosensory input to the BST is critical for anxiety responses to predator odor (Fendt, Siegl et al. 2005), opiate withdrawal-induced aversion (Delfs, Zhu et al. 2000), conditioned place aversion to painful stimuli (Deyama, Nakagawa et al. 2007, Deyama, Katayama et al. 2009), and the suppression of pulsatile luteinizing hormone in female rats (Yamada, Uenoyama et al. 2006). Another major source of motor system input comes from hypothalamic nuclei of the behavioral control columns although no studies have examined the functional role of hypothalamic input to the BST.

The finding that the BSTpr projects multisynaptically to the CEAm in male rats reveals an anatomical circuit through which amygdala stress reactivity could be influenced by sex or reproductive behavior. As discussed above, the BSTpr is sexually dimorphic and has a clearly defined role in reproductive behavior. In contrast, the CEAm has been implicated in the behavioral responses of fear conditioning (Duvarci, Popa et al. 2011). Recently, Bangasser and

Shors suggested that the BST may be involved in a sex-specific stress/learning circuit based on evidence that a masculinized, but not feminized, BST is required for stress to enhance classical eyeblink conditioning (Bangasser, Santollo et al. 2005, Bangasser and Shors 2008, Bangasser and Shors 2010) and other studies have demonstrated sex-related differences in fear conditioning (Pryce, Lehmann et al. 1999, Baran, Armstrong et al. 2009). Furthermore, sex differences are apparent in several neurobiological stress-related diseases such as post-traumatic stress disorder (Tolin and Foa 2006), depression (Nolen-Hoeksema 2001), and autonomic disorders such as irritable bowel syndrome (Naliboff, Berman et al. 2003). Most studies on sex differences have focused on direct effects of circulating sex hormones, however a multisynaptic circuit from the BSTpr to the CEAm may serve as an anatomical substrate for sex differences in stress reactivity. Further studies will need to determine if the BSTpr input to the CEAm exists in female rats.

4.4 CONCLUSIONS AND FUTURE DIRECTIONS

The studies in this dissertation have increased our understanding of the anatomical organization of extended amygdala circuits and pathways for information processing by amygdala and BST subnuclei. We have provided evidence for the amygdala and BST as a differentiated striatopallidal circuit. Differences between amygdala/BST circuits and more established striatopallidal circuits may be due to enhanced behavioral feedback pathways from the hypothalamus and other motor system regions. Increased feedback may be a specialization that allows the amygdala/BST to regulate homeostatic behavior with little or no cortical involvement. To examine multisynaptic amygdala-projecting BST circuits along this feedback pathway, we performed transsynaptic viral tracer injections into the CEAm, MEAad, and

MEApd. In contrast to the topographically-organized channels suggested by anterograde tracing studies, we found that the CEAm receives multisynaptic input from the BSTpr and BSTam. While we were unable to determine the exact circuit in which the BSTpr multisynaptically projects to the CEAm, future experiments applying the Cre-recombinant properties of PRV-263 can address this issue.

Genetic engineering of the PRV-Bartha strain has created a new class of recombinant PRV strains whose expression of specific genes are dependent upon a Cre-recombination event (DeFalco, Tomishima et al. 2001). The first recombinant virus was PRV-Ba2001 which has a *Lox-Stop-Lox* cassette inserted upstream from a Tau-GFP reporter gene and the gene that encodes the thymidine kinase viral protein. Thymidine kinase is necessary for the synthesis of viral DNA and the *Lox-Stop-Lox* cassette prevents the transcription of downstream sequences unless it is removed by Cre-mediated recombination. Therefore, viral replication and GFP translation is restricted to neurons which express the exogenous bacterial protein Cre. However, several issues make viral tracing with PRV-Ba2001 difficult. The restriction of viral replication makes it difficult to grow high-titer stocks of PRV-Ba2001 and adds an evolutionary selection pressure for faster growing revertants (Card, Kobiler et al. 2011). More recently, a Brainbow PRV strain (PRV-263, used in section 3.0 experiments) has been developed which can identify multisynaptic circuits from Cre-expressing neurons without the difficulties associated with PRV-Ba2001. Under normal circumstances, PRV-263 expresses a red fluorescent reporter gene. In the event of recombination with Cre, PRV-263 will express a blue or yellow fluorescent reporter gene. Furthermore, the blue or yellow fluorophor profile is replicated and expressed upstream in multisynaptic circuits. Recombinant viral strains provide a powerful new approach to examining specific multisynaptic pathways through manipulations of neuronal Cre expression. To

determine the pathways by which BSTpr and BSTam neurons became infected following injection into the CEAm, the experiments in section 3.0 can be repeated using animals that have previously been injected with a Cre-expressing lentivirus into a BST subnucleus hypothesized to be an intermediary between the CEAm and BSTpr or BSTam. Alternatively, Cre-expressing transgenic animals could be used to determine if BSTpr or BSTam neurons became infected by transsynaptic passage through a phenotypic BST neuronal subpopulation.

Future studies of experimental brain tissue from section 3.0 could be used to determine the phenotypic characteristics of multisynaptic amygdala-projecting BST circuits. The BST contains a variety of phenotypic neurochemical subpopulations including calbindin- , calretinin- , somatostatin- , and CRH-expressing neurons. By comparing the colocalization of monosynaptic retrograde tracer or PRV with phenotypic neurochemical markers, we can determine whether certain neurochemicals are expressed in BST projection neurons or interneurons. These experiments could provide further insight into the anatomical organization of extended amygdala circuits and allow for new strategies for the functional dissection of specific BST circuits.

BIBLIOGRAPHY

- Alexander, G. E. and M. D. Crutcher (1990). "Functional architecture of basal ganglia circuits: neural substrates of parallel processing." Trends in Neurosciences **13**(7): 266-271.
- Alexander, G. E., M. R. DeLong and P. L. Strick (1986). "Parallel organization of functionally segregated circuits linking basal ganglia and cortex." Annual Review of Neuroscience **9**(1): 357-381.
- Alheid, G. and L. Heimer (1988). "New perspectives in basal forebrain organization of special relevance for neuropsychiatric disorders: the striatopallidal, amygdaloid, and corticopetal components of substantia innominata." Neuroscience **1**: 1-39.
- Altschuler, S. M., X. Bao, D. Bieger, D. A. Hopkins and R. R. Miselis (1989). "Viscerotopic representation of the upper alimentary tract in the rat: Sensory ganglia and nuclei of the solitary and spinal trigeminal tracts." The Journal of Comparative Neurology **283**(2): 248-268.
- Aston-Jones, G. and J. P. Card (2000). "Use of pseudorabies virus to delineate multisynaptic circuits in brain: opportunities and limitations." Journal of Neuroscience Methods **103**(1): 51-61.
- Aston-Jones, G., S. Chen, Y. Zhu and M. L. Oshinsky (2001). "A neural circuit for circadian regulation of arousal." Nat Neurosci **4**(7): 732-738.
- Aston-Jones, G., R. J. Smith, D. E. Moorman and K. A. Richardson (2009). "Role of lateral hypothalamic orexin neurons in reward processing and addiction." Neuropharmacology **56**, **Supplement 1**(0): 112-121.
- Aston-Jones, G., Y. Zhu and J. P. Card (2004). "Numerous GABAergic afferents to locus coeruleus in the pericerulear dendritic zone: possible interneuronal pool." The Journal of Neuroscience **24**(9): 2313-2321.
- Bangasser, D. A., J. Santollo and T. J. Shors (2005). "The bed nucleus of the stria terminalis is critically involved in enhancing associative learning after stressful experience." Behavioral Neuroscience **119**(6): 1459-1466.
- Bangasser, D. A. and T. J. Shors (2008). "The bed nucleus of the stria terminalis modulates learning after stress in masculinized but not cycling females." The Journal of Neuroscience **28**(25): 6383-6387.

- Bangasser, D. A. and T. J. Shors (2010). "Critical brain circuits at the intersection between stress and learning." Neuroscience & Biobehavioral Reviews **34**(8): 1223-1233.
- Baran, S. E., C. E. Armstrong, D. C. Niren, J. J. Hanna and C. D. Conrad (2009). "Chronic stress and sex differences on the recall of fear conditioning and extinction." Neurobiology of learning and memory **91**(3): 323.
- Bhatnagar, S. and M. Dallman (1998). "Neuroanatomical basis for facilitation of hypothalamic-pituitary-adrenal responses to a novel stressor after chronic stress." Neuroscience **84**(4): 1025-1039.
- Bhatnagar, S., R. Huber, E. Lazar, L. Pych and C. Vining (2003). "Chronic stress alters behavior in the conditioned defensive burying test: role of the posterior paraventricular thalamus." Pharmacology Biochemistry and Behavior **76**(2): 343-349.
- Bhatnagar, S., R. Huber, N. Nowak and P. Trotter (2002). "Lesions of the posterior paraventricular thalamus block habituation of hypothalamic-pituitary-adrenal responses to repeated restraint." Journal of Neuroendocrinology **14**(5): 403-410.
- Canteras, N. S., R. B. Simerly and L. W. Swanson (1995). "Organization of projections from the medial nucleus of the amygdala: A PHAL study in the rat." The Journal of Comparative Neurology **360**(2): 213-245.
- Card, J., L. Rinaman, R. Lynn, B. Lee, R. Meade, R. Miselis and L. Enquist (1993). "Pseudorabies virus infection of the rat central nervous system: ultrastructural characterization of viral replication, transport, and pathogenesis." The Journal of Neuroscience **13**(6): 2515-2539.
- Card, J. P. (1998). "Exploring brain circuitry with neurotropic viruses: New horizons in neuroanatomy." The Anatomical Record **253**(6): 176-185.
- Card, J. P. (1998). "Practical considerations for the use of pseudorabies virus in transneuronal studies of neural circuitry." Neuroscience & Biobehavioral Reviews **22**(6): 685-694.
- Card, J. P. and L. W. Enquist (2001). Transneuronal circuit analysis with pseudorabies viruses. Current Protocols in Neuroscience, John Wiley & Sons, Inc.
- Card, J. P. and L. W. Enquist (2012). Use and visualization of neuroanatomical viral transneuronal tracers Visualization Techniques. **70**: 225-268.
- Card, J. P., L. W. Enquist and R. Y. Moore (1999). "Neuroinvasiveness of pseudorabies virus injected intracerebrally is dependent on viral concentration and terminal field density." The Journal of Comparative Neurology **407**(3): 438-452.
- Card, J. P., O. Kobiler, E. B. Ludmir, V. Desai, A. F. Sved and L. W. Enquist (2011). "A dual infection pseudorabies virus conditional reporter approach to identify projections to collateralized neurons in complex neural circuits." PLoS ONE **6**(6): e21141.

- Card, J. P., O. Kobiler, J. McCambridge, S. Ebdlahad, Z. Shan, M. K. Raizada, A. F. Sved and L. W. Enquist (2011). "Microdissection of neural networks by conditional reporter expression from a Brainbow herpesvirus." Proceedings of the National Academy of Sciences.
- Card, J. P., P. Levitt and L. W. Enquist (1998). "Different patterns of neuronal infection after intracerebral injection of two strains of pseudorabies virus." J. Virol. **72**(5): 4434-4441.
- Casada, J. H. and N. Dafny (1993). "Responses of neurons in bed nucleus of the stria terminalis to microiontophoretically applied morphine, norepinephrine and acetylcholine." Neuropharmacology **32**(3): 279-284.
- Cecchi, M., H. Khoshbouei, M. Javors and D. A. Morilak (2002). "Modulatory effects of norepinephrine in the lateral bed nucleus of the stria terminalis on behavioral and neuroendocrine responses to acute stress." Neuroscience **112**(1): 13-21.
- Chen, S., M. Yang, R. R. Miselis and G. Aston-Jones (1999). "Characterization of transsynaptic tracing with central application of pseudorabies virus." Brain Research **838**(1-2): 171-183.
- Chiba, T., T. Kayahara and K. Nakano (2001). "Efferent projections of infralimbic and prelimbic areas of the medial prefrontal cortex in the Japanese monkey, *Macaca fuscata*." Brain Research **888**(1): 83-101.
- Ciccocioppo, R., A. Fedeli, D. Economidou, F. Policani, F. Weiss and M. Massi (2003). "The bed nucleus is a neuroanatomical substrate for the anorectic effect of corticotropin-releasing factor and for its reversal by nociceptin/orphanin FQ." J. Neurosci. **23**(28): 9445-9451.
- Ciriello, J., C. G. Schultz and S. Roder (1994). "Collateral axonal projections from ventrolateral medullary non-catecholaminergic neurons to central nucleus of the amygdala." Brain Research **663**(2): 346-351.
- Ciriello, J., L. P. Solano-Flores, M. P. Rosas-Arellano, G. J. Kirouac and T. Babic (2008). "Medullary pathways mediating the parasubthalamic nucleus depressor response." American Journal of Physiology - Regulatory, Integrative and Comparative Physiology **294**(4): R1276-R1284.
- Consiglio, A. R., A. Borsoi, G. A. M. Pereira and A. B. Lucion (2005). "Effects of oxytocin microinjected into the central amygdaloid nucleus and bed nucleus of stria terminalis on maternal aggressive behavior in rats." Physiology & Behavior **85**(3): 354-362.
- Cooke, B. M., G. Tabibnia and S. M. Breedlove (1999). "A brain sexual dimorphism controlled by adult circulating androgens." Proceedings of the National Academy of Sciences **96**(13): 7538-7540.
- Coolen, L. M. and R. I. Wood (1998). "Bidirectional connections of the medial amygdaloid nucleus in the Syrian hamster brain: Simultaneous anterograde and retrograde tract tracing." The Journal of Comparative Neurology **399**(2): 189-209.

Cullinan, W., D. Ziegler and J. Herman (2008). "Functional role of local GABAergic influences on the HPA axis." Brain Structure and Function **213**(1): 63-72.

Cullinan, W. E., J. P. Herman and S. J. Watson (1993). "Ventral subicular interaction with the hypothalamic paraventricular nucleus: Evidence for a relay in the bed nucleus of the stria terminalis." The Journal of Comparative Neurology **332**(1): 1-20.

de Olmos, J. S. and L. Heimer (1999). "The concepts of the ventral striatopallidal system and extended amygdala." Annals of the New York Academy of Sciences **877**(Advancing from the Ventral Striatum to the Extended Amygdala: Implications for Neuropsychiatry and Drug Abuse): 1-32.

de Olmos, J. S. and W. R. Ingram (1972). "The projection field of the stria terminalis in the rat brain. An experimental study." The Journal of Comparative Neurology **146**(3): 303-333.

DeFalco, J., M. Tomishima, H. Liu, C. Zhao, X. Cai, J. D. Marth, L. Enquist and J. M. Friedman (2001). "Virus-assisted mapping of neural inputs to a feeding center in the hypothalamus." Science **291**(5513): 2608-2613.

Delfs, J. M., Y. Zhu, J. P. Druhan and G. Aston-Jones (2000). "Noradrenaline in the ventral forebrain is critical for opiate withdrawal-induced aversion." Nature **403**(6768): 430-434.

DeVito, J. L., M. E. Anderson and K. E. Walsh (1980). "A horseradish peroxidase study of afferent connections of the globus pallidus in *Macaca mulatta*." Experimental Brain Research **38**(1): 65-73.

Deyama, S., T. Katayama, N. Kondoh, T. Nakagawa, S. Kaneko, T. Yamaguchi, M. Yoshioka and M. Minami (2009). "Role of enhanced noradrenergic transmission within the ventral bed nucleus of the stria terminalis in visceral pain-induced aversion in rats." Behavioural Brain Research **197**(2): 279-283.

Deyama, S., T. Nakagawa, S. Kaneko, T. Uehara and M. Minami (2007). "Involvement of the bed nucleus of the stria terminalis in the negative affective component of visceral and somatic pain in rats." Behavioural Brain Research **176**: 367-371.

Dong, H. W., G. D. Petrovich and L. W. Swanson (2000). "Organization of projections from the juxtacapsular nucleus of the BST: a PHAL study in the rat." Brain Research **859**(1): 1-14.

Dong, H. W., G. D. Petrovich and L. W. Swanson (2001). "Topography of projections from amygdala to bed nuclei of the stria terminalis." Brain Research Reviews **38**(1-2): 192-246.

Dong, H. W. and L. W. Swanson (2003). "Projections from the rhomboid nucleus of the bed nuclei of the stria terminalis: Implications for cerebral hemisphere regulation of ingestive behaviors." The Journal of Comparative Neurology **463**(4): 434-472.

Dong, H. W. and L. W. Swanson (2004). "Organization of axonal projections from the anterolateral area of the bed nuclei of the stria terminalis." The Journal of Comparative Neurology **468**(2): 277-298.

- Dong, H. W. and L. W. Swanson (2004). "Projections from bed nuclei of the stria terminalis, posterior division: Implications for cerebral hemisphere regulation of defensive and reproductive behaviors." The Journal of Comparative Neurology **471**(4): 396-433.
- Dong, H. W. and L. W. Swanson (2006). "Projections from bed nuclei of the stria terminalis, dorsomedial nucleus: Implications for cerebral hemisphere integration of neuroendocrine, autonomic, and drinking responses." The Journal of Comparative Neurology **494**(1): 75-107.
- Dong, H. W. and L. W. Swanson (2006). "Projections from bed nuclei of the stria terminalis, magnocellular nucleus: Implications for cerebral hemisphere regulation of micturition, defecation, and penile erection." The Journal of Comparative Neurology **494**(1): 108-141.
- Duvarci, S., E. P. Bauer and D. Pare (2009). "The Bed Nucleus of the Stria Terminalis Mediates Inter-individual Variations in Anxiety and Fear." J. Neurosci. **29**(33): 10357-10361.
- Duvarci, S., D. Popa and D. Paré (2011). "Central Amygdala Activity during Fear Conditioning." The Journal of Neuroscience **31**(1): 289-294.
- Egli, R. E., T. L. Kash, K. Choo, V. Savchenko, R. T. Matthews, R. D. Blakely and D. G. Winder (2004). "Norepinephrine Modulates Glutamatergic Transmission in the Bed Nucleus of the Stria Terminalis." Neuropsychopharmacology **30**(4): 657-668.
- Enquist, L. W. and J. P. Card (2003). "Recent advances in the use of neurotropic viruses for circuit analysis." Current Opinion in Neurobiology **13**(5): 603-606.
- Fanselow, M. S. and J. E. LeDoux (1999). "Why We Think Plasticity Underlying Pavlovian Fear Conditioning Occurs in the Basolateral Amygdala." Neuron **23**(2): 229-232.
- Favoreel, H. W., G. Van Minnebruggen, H. J. Nauwynck, L. W. Enquist and M. B. Pensaert (2002). "A Tyrosine-Based Motif in the Cytoplasmic Tail of Pseudorabies Virus Glycoprotein B Is Important for both Antibody-Induced Internalization of Viral Glycoproteins and Efficient Cell-to-Cell Spread." Journal of Virology **76**(13): 6845-6851.
- Fendt, M., T. Endres and R. Apfelbach (2003). "Temporary inactivation of the bed nucleus of the stria terminalis but not of the amygdala blocks freezing induced by trimethylthiazoline, a component of fox feces." The Journal of Neuroscience **23**(1): 23-28.
- Fendt, M. and M. S. Fanselow (1999). "The neuroanatomical and neurochemical basis of conditioned fear." Neuroscience & Biobehavioral Reviews **23**(5): 743-760.
- Fendt, M., S. Siegl and B. Steiniger-Brach (2005). "Noradrenaline Transmission within the Ventral Bed Nucleus of the Stria Terminalis Is Critical for Fear Behavior Induced by Trimethylthiazoline, a Component of Fox Odor." J. Neurosci. **25**(25): 5998-6004.
- Fisk, G. D. and J. M. Wyss (2000). "Descending projections of infralimbic cortex that mediate stimulation-evoked changes in arterial pressure." Brain Research **859**(1): 83-95.

- Flint, S. J., L. W. Enquist, V. R. Racaniello and A. M. Skalka (2008). Principles of virology, ASM Press.
- Freedman, L. J. and M. D. Cassell (1994). "Distribution of dopaminergic fibers in the central division of the extended amygdala of the rat." Brain Research **633**(1-2): 243-252.
- Funk, C. K., L. E. O'Dell, E. F. Crawford and G. F. Koob (2006). "Corticotropin-Releasing Factor within the Central Nucleus of the Amygdala Mediates Enhanced Ethanol Self-Administration in Withdrawn, Ethanol-Dependent Rats." The Journal of Neuroscience **26**(44): 11324-11332.
- García-López, M., A. Abellán, I. Legaz, J. L. R. Rubenstein, L. Puelles and L. Medina (2008). "Histogenetic compartments of the mouse centromedial and extended amygdala based on gene expression patterns during development." The Journal of Comparative Neurology **506**(1): 46-74.
- Gauriau, C. and J.-F. Bernard (2002). "Pain pathways and parabrachial circuits in the rat." Experimental Physiology **87**(02): 251-258.
- Gaykema, R. P. A., C.-C. Chen and L. E. Goehler (2007). "Organization of immune-responsive medullary projections to the bed nucleus of the stria terminalis, central amygdala, and paraventricular nucleus of the hypothalamus: Evidence for parallel viscerosensory pathways in the rat brain." Brain Research **1130**: 130-145.
- Geerling, J. C. and A. D. Loewy (2006). "Aldosterone-sensitive neurons in the nucleus of the solitary tract: Bidirectional connections with the central nucleus of the amygdala." The Journal of Comparative Neurology **497**(4): 646-657.
- George, O., M. Le Moal and G. F. Koob (2012). "Allostasis and addiction: Role of the dopamine and corticotropin-releasing factor systems." Physiology & Behavior **106**(1): 58-64.
- Georges, F. and G. Aston-Jones (2001). "Potent Regulation of Midbrain Dopamine Neurons by the Bed Nucleus of the Stria Terminalis." The Journal of Neuroscience **21**(16): RC160.
- Georges, F. and G. Aston-Jones (2002). "Activation of Ventral Tegmental Area Cells by the Bed Nucleus of the Stria Terminalis: A Novel Excitatory Amino Acid Input to Midbrain Dopamine Neurons." J. Neurosci. **22**(12): 5173-5187.
- Gerfen, C. R. and P. E. Sawchenko (1984). "An anterograde neuroanatomical tracing method that shows the detailed morphology of neurons, their axons and terminals: immunohistochemical localization of an axonally transported plant lectin, Phaseolus vulgaris leucoagglutinin (PHA-L)." Brain Res **290**(2): 219-238.
- Goto, M. and L. W. Swanson (2004). "Axonal projections from the parasubthalamic nucleus." The Journal of Comparative Neurology **469**(4): 581-607.
- Groenewegen, H. J., H. W. Berendse and S. N. Haber (1993). "Organization of the output of the ventral striatopallidal system in the rat: Ventral pallidal efferents." Neuroscience **57**(1): 113-142.

Groenewegen, H. J., C. I. Wright and H. B. M. Uylings (1997). "The anatomical relationships of the prefrontal cortex with limbic structures and the basal ganglia." J Psychopharmacol **11**(2): 99-106.

Haber, S. N. (2003). "The primate basal ganglia: parallel and integrative networks." Journal of Chemical Neuroanatomy **26**(4): 317-330.

Hagan, J. J., R. A. Leslie, S. Patel, M. L. Evans, T. A. Wattam, S. Holmes, C. D. Benham, S. G. Taylor, C. Routledge, P. Hemmati, R. P. Munton, T. E. Ashmeade, A. S. Shah, J. P. Hatcher, P. D. Hatcher, D. N. C. Jones, M. I. Smith, D. C. Piper, A. J. Hunter, R. A. Porter and N. Upton (1999). "Orexin A activates locus coeruleus cell firing and increases arousal in the rat." Proceedings of the National Academy of Sciences **96**(19): 10911-10916.

Hammack, S. E., J.-D. Guo, R. Hazra, J. Dabrowska, K. M. Myers and D. G. Rainnie (2009). "The response of neurons in the bed nucleus of the stria terminalis to serotonin: Implications for anxiety." Progress in Neuro-Psychopharmacology and Biological Psychiatry **33**(8): 1309-1320.

Harris, G. C. and G. Aston-Jones (2006). "Arousal and reward: a dichotomy in orexin function." Trends in Neurosciences **29**(10): 571-577.

Harris, G. C. and G. Aston-Jones (2007). "Activation in extended amygdala corresponds to altered hedonic processing during protracted morphine withdrawal." Behavioural Brain Research **176**(2): 251-258.

Harris, G. C., M. Wimmer and G. Aston-Jones (2005). "A role for lateral hypothalamic orexin neurons in reward seeking." Nature **437**(7058): 556-559.

Haynes, A. C., B. Jackson, P. Overend, R. E. Buckingham, S. Wilson, M. Tadayyon and J. R. S. Arch (1999). "Effects of single and chronic intracerebroventricular administration of the orexins on feeding in the rat." Peptides **20**(9): 1099-1105.

Heidbreder, C. A. and H. J. Groenewegen (2003). "The medial prefrontal cortex in the rat: evidence for a dorso-ventral distinction based upon functional and anatomical characteristics." Neuroscience & Biobehavioral Reviews **27**(6): 555-579.

Heimer, L. (2003). "A New Anatomical Framework for Neuropsychiatric Disorders and Drug Abuse." Am J Psychiatry **160**(10): 1726-1739.

Heimer, L. and G. W. Van Hoesen (2006). "The limbic lobe and its output channels: Implications for emotional functions and adaptive behavior." Neuroscience & Biobehavioral Reviews **30**(2): 126-147.

Herkenham, M. (1980). "Laminar organization of thalamic projections to the rat neocortex." Science **207**(4430): 532-535.

Herman, J. P., W. E. Cullinan and S. J. Watson (1994). "Involvement of the Bed Nucleus of the Stria Terminalis in Tonic Regulation of Paraventricular Hypothalamic CRH and AVP mRNA Expression." Journal of Neuroendocrinology **6**(4): 433-442.

- Hines, M., L. S. Allen and R. A. Gorski (1992). "Sex differences in subregions of the medial nucleus of the amygdala and the bed nucleus of the stria terminalis of the rat." Brain Research **579**(2): 321-326.
- Hoover, J. and P. Strick (1993). "Multiple output channels in the basal ganglia." Science **259**(5096): 819-821.
- Huang, Z.-L., W.-M. Qu, W.-D. Li, T. Mochizuki, N. Eguchi, T. Watanabe, Y. Urade and O. Hayaishi (2001). "Arousal effect of orexin A depends on activation of the histaminergic system." Proceedings of the National Academy of Sciences **98**(17): 9965-9970.
- Hurley, K. M., H. Herbert, M. M. Moga and C. B. Saper (1991). "Efferent projections of the infralimbic cortex of the rat." The Journal of Comparative Neurology **308**(2): 249-276.
- Jaferi, A., N. Nowak and S. Bhatnagar (2003). "Negative feedback functions in chronically stressed rats: role of the posterior paraventricular thalamus." Physiology & Behavior **78**(3): 365-373.
- Jalabert, M., G. Aston-Jones, E. Herzog, O. Manzoni and F. Georges (2009). "Role of the bed nucleus of the stria terminalis in the control of ventral tegmental area dopamine neurons." Progress in Neuro-Psychopharmacology and Biological Psychiatry **33**(8): 1336-1346.
- Jasnow, A. M., M. Davis and K. L. Huhman (2004). "Involvement of Central Amygdalar and Bed Nucleus of the Stria Terminalis Corticotropin-Releasing Factor in Behavioral Responses to Social Defeat." Behavioral Neuroscience **118**(5): 1052-1061.
- Johnston, J. B. (1923). "Further contributions to the study of the evolution of the forebrain." The Journal of Comparative Neurology **35**(5): 337-481.
- Joppa, M. A., R. L. Meisel and M. A. Garber (1995). "-Fos expression in female hamster brain following sexual and aggressive behaviors." Neuroscience **68**(3): 783-792.
- Ju, G. and L. W. Swanson (1989). "Studies on the cellular architecture of the bed nuclei of the stria terminalis in the rat: I. Cytoarchitecture." J Comp Neurol **280**(4): 587-602.
- Ju, G., L. W. Swanson and R. B. Simerly (1989). "Studies on the cellular architecture of the bed nuclei of the stria terminalis in the rat: II. Chemoarchitecture." J Comp Neurol **280**(4): 603-621.
- Kalia, M. and J. M. Sullivan (1982). "Brainstem projections of sensory and motor components of the vagus nerve in the rat." The Journal of Comparative Neurology **211**(3): 248-264.
- Kincaid, A. E., J. B. Penney Jr, A. B. Young and S. W. Newman (1991). "Evidence for a projection from the globus pallidus to the entopeduncular nucleus in the rat." Neuroscience Letters **128**(1): 121-125.
- Kita, H. and T. Kita (2001). "Number, origins, and chemical types of rat pallidostriatal projection neurons." The Journal of Comparative Neurology **437**(4): 438-448.

- Kollack-Walker, S. and S. W. Newman (1995). "Mating and agonistic behavior produce different patterns of Fos immunolabeling in the male Syrian hamster brain." Neuroscience **66**(3): 721-736.
- Kollack-Walker, S. and S. W. Newman (1997). "Mating-induced expression of c-fos in the male Syrian hamster brain: role of experience, pheromones, and ejaculations." J Neurobiol **32**(5): 481-501.
- Koob, G. F. (2003). "Neuroadaptive mechanisms of addiction: studies on the extended amygdala." European Neuropsychopharmacology **13**(6): 442-452.
- Koob, G. F. (2009). "Neurobiological substrates for the dark side of compulsivity in addiction." Neuropharmacology **56, Supplement 1**(0): 18-31.
- Koob, G. F. and M. Le Moal (2001). "Drug Addiction, Dysregulation of Reward, and Allostasis." Neuropsychopharmacology **24**(2): 32.
- Lasek, R., B. S. Joseph and D. G. Whitlock (1968). "Evaluation of a radioautographic neuroanatomical tracing method." Brain Res **8**(2): 319-336.
- Lee, Y. and M. Davis (1997). "Role of the Hippocampus, the Bed Nucleus of the Stria Terminalis, and the Amygdala in the Excitatory Effect of Corticotropin-Releasing Hormone on the Acoustic Startle Reflex." J. Neurosci. **17**(16): 6434-6446.
- Leri, F., J. Flores, D. Rodaros and J. Stewart (2002). "Blockade of Stress-Induced But Not Cocaine-Induced Reinstatement by Infusion of Noradrenergic Antagonists into the Bed Nucleus of the Stria Terminalis or the Central Nucleus of the Amygdala." The Journal of Neuroscience **22**(13): 5713-5718.
- Li, S. and G. J. Kirouac (2008). "Projections from the paraventricular nucleus of the thalamus to the forebrain, with special emphasis on the extended amygdala." The Journal of Comparative Neurology **506**(2): 263-287.
- Lungwitz, E. A., A. Molosh, P. L. Johnson, B. P. Harvey, R. C. Dirks, A. Dietrich, P. Minick, A. Shekhar and W. A. Truitt "Orexin-A induces anxiety-like behavior through interactions with glutamatergic receptors in the bed nucleus of the stria terminalis of rats." Physiology & Behavior(0).
- Malsbury, C. W. and K. McKay (1987). "A sex difference in the pattern of substance P-like immunoreactivity in the bed nucleus of the stria terminalis." Brain Research **420**(2): 365-370.
- Maurice, N., J. M. Deniau, A. Menetrey, J. Glowinski and A. M. Thierry (1997). "Position of the ventral pallidum in the rat prefrontal cortex-basal ganglia circuit." Neuroscience **80**(2): 523-534.
- McDonald, A. J., S. J. Shammah-Lagnado, C. Shi and M. Davis (1999). "Cortical afferents to the extended amygdala." Annals of the New York Academy of Sciences **877**(Advancing from the Ventral Striatum to the Extended Amygdala: Implications for Neuropsychiatry and Drug Abuse): 309-338.

McElligott, Z. A. and D. G. Winder (2009). "Modulation of glutamatergic synaptic transmission in the bed nucleus of the stria terminalis." Progress in Neuro-Psychopharmacology and Biological Psychiatry **33**(8): 1329-1335.

McGinty, J. F. (1999). "Introduction." Annals of the New York Academy of Sciences **877**(Advancing from the Ventral Striatum to the Extended Amygdala: Implication for Neuropsychiatry and Drug Abuse): xii-xvi.

Medina, L., I. Legaz, G. González, F. De Castro, J. L. R. Rubenstein and L. Puelles (2004). "Expression of Dbx1, Neurogenin 2, Semaphorin 5A, Cadherin 8, and Emx1 distinguish ventral and lateral pallial histogenetic divisions in the developing mouse claustramygdaloid complex." The Journal of Comparative Neurology **474**(4): 504-523.

Miller, M. A., L. Vician, D. K. Clifton and D. M. Dorsa (1989). "Sex differences in vasopressin neurons in the bed nucleus of the stria terminalis by in situ hybridization." Peptides **10**(3): 615-619.

Mizukami, S., M. Nishizuka and Y. Arai (1983). "Sexual difference in nuclear volume and its ontogeny in the rat amygdala." Experimental Neurology **79**(2): 569-575.

Myers, E. A. and L. Rinaman (2002). "Viscerosensory activation of noradrenergic inputs to the amygdala in rats." Physiology and Behavior **77**: 723-729.

Nagy, F. Z. and D. Pare (2008). "Timing of Impulses From the Central Amygdala and Bed Nucleus of the Stria Terminalis to the Brain Stem." J Neurophysiol **100**(6): 3429-3436.

Nakagawa, T., R. Yamamoto, M. Fujio, Y. Suzuki, M. Minami, M. Satoh and S. Kaneko (2005). "Involvement of the bed nucleus of the stria terminalis activated by the central nucleus of the amygdala in the negative affective component of morphine withdrawal in rats." Neuroscience **134**: 9-19.

Naliboff, B. D., S. Berman, L. Chang, S. W. G. Derbyshire, B. Suyenobu, B. A. Vogt, M. Mandelkern and E. A. Mayer (2003). "Sex-related differences in IBS patients: central processing of visceral stimuli." Gastroenterology **124**(7): 1738-1747.

Nauta, W. (1993). "Some early travails of tracing axonal pathways in the brain." The Journal of Neuroscience **13**(4): 1337-1345.

Newman, S. W. (1999). "The medial extended amygdala in male reproductive behavior: A node in the mammalian social behavior network." Annals of the New York Academy of Sciences **877**(1): 242-257.

Nishizuka, M. and Y. Arai (1981). "Sexual dimorphism in synaptic organization in the amygdala and its dependence on neonatal hormone environment." Brain Research **212**(1): 31-38.

Nishizuka, M. and Y. Arai (1983). "Male-female differences in the intra-amygdaloid input to the medial amygdala." Experimental Brain Research **52**(3): 328-332.

- Nixon, J. and L. Smale (2007). "A comparative analysis of the distribution of immunoreactive orexin A and B in the brains of nocturnal and diurnal rodents." Behavioral and Brain Functions **3**(1): 28.
- Nolen-Hoeksema, S. (2001). "Gender Differences in Depression." Current Directions in Psychological Science **10**(5): 173-176.
- Paxinos, G. and C. Watson (2007). The rat brain in stereotaxic coordinates. San Diego, Elsevier Academic Press.
- Petrovich, G. D. and L. W. Swanson (1997). "Projections from the lateral part of the central amygdalar nucleus to the postulated fear conditioning circuit." Brain Research **763**(2): 247-254.
- Peyron, C., D. K. Tighe, A. N. van den Pol, L. de Lecea, H. C. Heller, J. G. Sutcliffe and T. S. Kilduff (1998). "Neurons Containing Hypocretin (Orexin) Project to Multiple Neuronal Systems." The Journal of Neuroscience **18**(23): 9996-10015.
- Potegal, M., C. F. Ferris, M. Hebert, J. Meyerhoff and L. Skaredoff (1996). "Attack priming in female Syrian golden hamsters is associated with a c-fos-coupled process within the corticomедial amygdala." Neuroscience **75**(3): 869-880.
- Powers, J. B., S. W. Newman and M. L. Bergondy (1987). "MPOA and BNST lesions in male Syrian hamsters: Differential effects on copulatory and chemoinvestigatory behaviors." Behavioural Brain Research **23**(3): 181-195.
- Prewitt, C. M. F. and J. P. Herman (1998). "Anatomical interactions between the central amygdaloid nucleus and the hypothalamic paraventricular nucleus of the rat: a dual tract-tracing analysis." Journal of Chemical Neuroanatomy **15**(3): 173-186.
- Pryce, C. R., J. Lehmann and J. Feldon (1999). "Effect of Sex on Fear Conditioning is Similar for Context and Discrete CS in Wistar, Lewis and Fischer Rat Strains." Pharmacology Biochemistry and Behavior **64**(4): 753-759.
- Radley, J. J., C. M. Arias and P. E. Sawchenko (2006). "Regional Differentiation of the Medial Prefrontal Cortex in Regulating Adaptive Responses to Acute Emotional Stress." The Journal of Neuroscience **26**(50): 12967-12976.
- Radley, J. J., K. L. Gosselink and P. E. Sawchenko (2009). "A Discrete GABAergic Relay Mediates Medial Prefrontal Cortical Inhibition of the Neuroendocrine Stress Response." The Journal of Neuroscience **29**(22): 7330-7340.
- Radley, J. J. and P. E. Sawchenko (2011). "A Common Substrate for Prefrontal and Hippocampal Inhibition of the Neuroendocrine Stress Response." The Journal of Neuroscience **31**(26): 9683-9695.
- Rajakumar, N., K. Elisevich and B. A. Flumerfelt (1994). "The pallidostriatal projection in the rat: a recurrent inhibitory loop?" Brain Research **651**(1-2): 332-336.

- Reilly, S. (1999). "The parabrachial nucleus and conditioned taste aversion." Brain Research Bulletin **48**(3): 239-254.
- Reynolds, S. M. and D. S. Zahm (2005). "Specificity in the Projections of Prefrontal and Insular Cortex to Ventral Striatopallidum and the Extended Amygdala." J. Neurosci. **25**(50): 11757-11767.
- Rinaman, L., P. Levitt and J. P. Card (2000). "Progressive Postnatal Assembly of Limbic–Autonomic Circuits Revealed by Central Transneuronal Transport of Pseudorabies Virus." The Journal of Neuroscience **20**(7): 2731-2741.
- Roder, S. and J. Ciriello (1994). "Collateral axonal projections to limbic structures from ventrolateral medullary A1 noradrenergic neurons." Brain Research **638**(1-2): 182-188.
- Sagar, S. M., F. R. Sharp and T. Curran (1988). "Expression of c-fos protein in brain: metabolic mapping at the cellular level." Science (New York, N.Y.) **240**(4857): 1328-1331.
- Sakai, N. and T. Yamamoto (1998). "Role of the medial and lateral parabrachial nucleus in acquisition and retention of conditioned taste aversion in rats." Behavioural Brain Research **93**(1-2): 63-70.
- Salazar-Juárez, A., C. Escobar and R. Aguilar-Roblero (2002). "Anterior paraventricular thalamus modulates light-induced phase shifts in circadian rhythmicity in rats." American Journal of Physiology - Regulatory, Integrative and Comparative Physiology **283**(4): R897-R904.
- Santiago, A. C. and S. J. Shammah-Lagnado (2004). "Efferent connections of the nucleus of the lateral olfactory tract in the rat." The Journal of Comparative Neurology **471**(3): 314-332.
- Sartor, G. C. and G. Aston-Jones (2012). "Regulation of the ventral tegmental area by the bed nucleus of the stria terminalis is required for expression of cocaine preference." European Journal of Neuroscience: n/a-n/a.
- Sesack, S. R., A. Y. Deutch, R. H. Roth and B. S. Bunney (1989). "Topographical organization of the efferent projections of the medial prefrontal cortex in the rat: An anterograde tract-tracing study with Phaseolus vulgaris leucoagglutinin." The Journal of Comparative Neurology **290**(2): 213-242.
- Shammah-Lagnado, S. J., G. F. Alheid and L. Heimer (1999). "Afferent connections of the interstitial nucleus of the posterior limb of the anterior commissure and adjacent amygdalostriatal transition area in the rat." Neuroscience **94**(4): 1097-1123.
- Shammah-Lagnado, S. J., G. F. Alheid and L. Heimer (2001). "Striatal and central extended amygdala parts of the interstitial nucleus of the posterior limb of the anterior commissure: Evidence from tract-tracing techniques in the rat." The Journal of Comparative Neurology **439**(1): 104-126.

- Shin, J.-W., J. C. Geerling and A. D. Loewy (2008). "Inputs to the ventrolateral bed nucleus of the stria terminalis." The Journal of Comparative Neurology **511**(5): 628-657.
- Simerly, R. B., C. Chang, M. Muramatsu and L. W. Swanson (1990). "Distribution of androgen and estrogen receptor mRNA-containing cells in the rat brain: an in situ hybridization study." J Comp Neurol **294**(1): 76-95.
- Sink, K. S., D. L. Walker, S. M. Freeman, E. I. Flandreau, K. J. Ressler and M. Davis (2012). "Effects of continuously enhanced corticotropin releasing factor expression within the bed nucleus of the stria terminalis on conditioned and unconditioned anxiety." Mol Psychiatry.
- Sink, K. S., D. L. Walker, Y. Yang and M. Davis (2011). "Calcitonin Gene-Related Peptide in the Bed Nucleus of the Stria Terminalis Produces an Anxiety-Like Pattern of Behavior and Increases Neural Activation in Anxiety-Related Structures." The Journal of Neuroscience **31**(5): 1802-1810.
- Smith, R. and G. Aston-Jones (2008). "Noradrenergic transmission in the extended amygdala: role in increased drug-seeking and relapse during protracted drug abstinence." Brain Structure and Function **213**(1): 43-61.
- Soma, M., H. Aizawa, Y. Ito, M. Maekawa, N. Osumi, E. Nakahira, H. Okamoto, K. Tanaka and S. Yuasa (2009). "Development of the mouse amygdala as revealed by enhanced green fluorescent protein gene transfer by means of in utero electroporation." The Journal of Comparative Neurology **513**(1): 113-128.
- Sullivan, G. M., J. Apergis, D. E. A. Bush, L. R. Johnson, M. Hou and J. E. Ledoux (2004). "Lesions in the bed nucleus of the stria terminalis disrupt corticosterone and freezing responses elicited by a contextual but not by a specific cue-conditioned fear stimulus." Neuroscience **128**(1): 7-14.
- Sun, N., L. Roberts and M. D. Cassell (1991). "Rat central amygdaloid nucleus projections to the bed nucleus of the stria terminalis." Brain Research Bulletin **27**(5): 651-662.
- Sved, A. F., G. Cano and J. P. Card (2001). "Neuroanatomical specificity of the circuits controlling sympathetic outflow to different targets." Clin Exp Pharmacol Physiol **28**(1-2): 115-119.
- Swanson, L. (2004). Brain Maps: Structure of the Rat Brain. San Diego, CA, Elsevier.
- Swanson, L. W. (2000). "Cerebral hemisphere regulation of motivated behavior." Brain Research **886**(1-2): 113-164.
- Swanson, L. W. (2003). "The Amygdala and Its Place in the Cerebral Hemisphere." Annals of the New York Academy of Sciences **985**(The Amygdala in Brain Function: Basic and Clinical Approaches): 174-184.
- Swanson, L. W. (2004). Brain Maps: Structure of the Rat Brain. San Diego, CA, Elsevier.

Swanson, L. W. and G. D. Petrovich (1998). "What is the amygdala?" Trends in Neurosciences **21**(8): 323-331.

Takada, M., H. Tokuno, Y. Ikai and N. Mizuno (1994). "Direct projections from the entopeduncular nucleus to the lower brainstem in the rat." The Journal of Comparative Neurology **342**(3): 409-429.

Tanimoto, S., T. Nakagawa, Y. Yamauchi, M. Minami and M. Satoh (2003). "Differential contributions of the basolateral and central nuclei of the amygdala in the negative affective component of chemical somatic and visceral pain in rats." European Journal of Neuroscience **18**(8): 2343-2350.

Thompson, R. H. and L. W. Swanson (2003). "Structural characterization of a hypothalamic visceromotor pattern generator network." Brain Research Reviews **41**(2-3): 153-202.

Thompson, R. H. and L. W. Swanson (2010). "Hypothesis-driven structural connectivity analysis supports network over hierarchical model of brain architecture." Proc Natl Acad Sci U S A **107**(34): 15235-15239.

Tkacs, N. C. and J. Li (1999). "Immune stimulation induces Fos expression in brainstem amygdala afferents." Brain Research Bulletin **48**(2): 223-231.

Tolin, D. F. and E. B. Foa (2006). "Sex Differences in Trauma and Posttraumatic Stress Disorder: A Quantitative Review of 25 Years of Research." Psychological Bulletin **132**(6): 959-959.

Trainor, B. C., I. M. Bird and C. A. Marler (2004). "Opposing hormonal mechanisms of aggression revealed through short-lived testosterone manipulations and multiple winning experiences." Hormones and Behavior **45**(2): 115-121.

Van der Werf, Y. D., M. P. Witter and H. J. Groenewegen (2002). "The intralaminar and midline nuclei of the thalamus. Anatomical and functional evidence for participation in processes of arousal and awareness." Brain Research Reviews **39**(2-3): 107-140.

Veening, J. G. and L. M. Coolen (1998). "Neural activation following sexual behavior in the male and female rat brain." Behavioural Brain Research **92**(2): 181-193.

Vertes, R. P. (2004). "Differential projections of the infralimbic and prelimbic cortex in the rat." Synapse **51**(1): 32-58.

Walker, D. L. and M. Davis (1997). "Double Dissociation between the Involvement of the Bed Nucleus of the Stria Terminalis and the Central Nucleus of the Amygdala in Startle Increases Produced by Conditioned versus Unconditioned Fear." J. Neurosci. **17**(23): 9375-9383.

Walker, D. L., L. A. Miles and M. Davis (2009). "Selective participation of the bed nucleus of the stria terminalis and CRF in sustained anxiety-like versus phasic fear-like responses." Progress in Neuro-Psychopharmacology and Biological Psychiatry **33**(8): 1291-1308.

- Walker, D. L., D. J. Toufexis and M. Davis (2003). "Role of the bed nucleus of the stria terminalis versus the amygdala in fear, stress, and anxiety." European Journal of Pharmacology **463**(1-3): 199-216.
- Walker, R. H., G. W. Arbuthnott and A. K. Wright (1989). "Electrophysiological and anatomical observations concerning the pallidostriatal pathway in the rat." Experimental Brain Research **74**(2): 303-310.
- Watson, R. E., S. J. Wiegand, R. W. Clough and G. E. Hoffman (1986). "Use of cryoprotectant to maintain long-term peptide immunoreactivity and tissue morphology." Peptides **7**(1): 155-159.
- Willie, J. T., R. M. Chemelli, C. M. Sinton and M. Yanagisawa (2001). "To eat or to sleep? Orexin in the regulation of feeding and wakefulness." Annual Review of Neuroscience **24**(1): 429-458.
- Wood, R. I. (1996). "Estradiol, but not dihydrotestosterone, in the medial amygdala facilitates male hamster sex behavior." Physiol Behav **59**(4-5): 833-841.
- Wood, R. I. (1996). "Functions of the steroid-responsive neural network in the control of male hamster sexual behavior." Trends Endocrinol Metab **7**(9): 338-344.
- Wood, R. I. and S. W. Newman (1995). "Androgen and estrogen receptors coexist within individual neurons in the brain of the Syrian hamster." Neuroendocrinology **62**(5): 487-497.
- Wood, R. I. and S. W. Newman (1995). "The medial amygdaloid nucleus and medial preoptic area mediate steroidal control of sexual behavior in the male Syrian hamster." Horm Behav **29**(3): 338-353.
- Wouterlood, J. L. L. a. F. G. (2006). Multiple Neuroanatomical Tract Tracing: Approaches for Multiple Tract-Tracing. Neuroanatomical Tract Tracing: Molecule, Neurons, and Systems. F. G. W. Laszlo Zaborszky, J.L. Lanciego. New York, Springer.
- Yamada, S., Y. Uenoyama, K. Maeda and H. Tsukamura (2006). "Role of noradrenergic receptors in the bed nucleus of the stria terminalis in regulating pulsatile luteinizing hormone secretion in female rats." The Journal of reproduction and development **52**(1): 115-121.
- Yamanaka, A., C. T. Beuckmann, J. T. Willie, J. Hara, N. Tsujino, M. Mieda, M. Tominaga, K.-i. Yagami, F. Sugiyama, K. Goto, M. Yanagisawa and T. Sakurai (2003). "Hypothalamic Orexin Neurons Regulate Arousal According to Energy Balance in Mice." Neuron **38**(5): 701-713.
- Yassa, M. A., R. L. Hazlett, C. E. L. Stark and R. Hoehn-Saric (2012). "Functional MRI of the amygdala and bed nucleus of the stria terminalis during conditions of uncertainty in generalized anxiety disorder." Journal of Psychiatric Research **46**(8): 1045-1052.
- Zahm, D. S. (2006). "The evolving theory of basal forebrain functional--anatomical 'macro-systems'." Neuroscience & Biobehavioral Reviews **30**(2): 148-172.

Zahm, D. S., S. L. Jensen, E. S. Williams and J. R. Martin III (1999). "Direct comparison of projections from the central amygdaloid region and nucleus accumbens shell." European Journal of Neuroscience **11**(4): 1119-1126.

Zardetto-Smith, A. M., T. G. Beltz and A. K. Johnson (1994). "Role of the central nucleus of the amygdala and bed nucleus of the stria terminalis in experimentally-induced salt appetite." Brain Research **645**(1-2): 123-134.

Zhu, Y., A. Yamanaka, K. Kunii, N. Tsujino, K. Goto and T. Sakurai (2002). "Orexin-mediated feeding behavior involves both leptin-sensitive and -insensitive pathways." Physiology and Behavior **77**(2-3): 251-257.